DISSERTATION

THE FLAVIVIRUS NS3 HELICASE MOTIF V CONTROLS UNWINDING FUNCTION AND ALTERS VIRAL PATHOGENESIS IN MOSQUITOES

Submitted by

Kelly Elizabeth Du Pont

Department of Chemistry

In partial fulfillment of the requirements

For the Degree of Doctor of Philosophy

Colorado State University

Fort Collins, Colorado

Fall 2020

Doctoral Committee:

Advisor: Martin McCullagh
Co-Advisor: Brian J. Geiss

Grzegorz Szamel
Christopher Snow
Amber Krummel
Shing Ho

ABSTRACT

THE FLAVIVIRUS NS3 HELICASE MOTIF V CONTROLS UNWINDING FUNCTION AND ALTERS VIRAL PATHOGENESIS IN MOSQUITOES

Over half of the world's population is at risk of flavivirus (e.g. dengue virus, West Nile virus, Japanese Encephalitis virus, and Zika virus) infection making it a global health concern. These specific mosquito-borne flaviviruses are responsible for causing a variety of symptoms and outcomes including flu-like fevers, encephalitis, hemorrhagic fevers, microcephaly, Guillain-Barré syndrome, and death. Unfortunately, vaccines and anti-viral therapeutics are not always effective in protecting against and treating viral infections. Sometimes these therapies cause more severe symptoms through an antibody dependent enhancement. Therefore, there is a pressing need for the development of effective anti-viral therapies against each flavivirus. For the advancement of these interventional strategies, a fundamental understanding of how flaviviruses replicate within hosts, including the mosquito vector, is required. This dissertation investigates how flaviviruses regulate viral replication, pathogenesis and mosquito transmission through the nonstructural protein 3 (NS3) helicase structure and function. A combination of virology, biochemistry, and computational simulations will be utilized to address how NS3 plays a role in viral infection, viral replication, and viral protein structure.

An essential aspect of flaviviral genome replication is the unwinding of the double-stranded RNA intermediate via the C-terminal helicase domain of NS3. NS3 helicase translocates along and unwinds the double-stranded nucleic acids in an ATP-dependent manner. However, the mechanism of energy transduction between the ATP- and RNA-binding pockets is not well understood. Previous simulations in the group led us to hypothesize that Motif V is a critical component of the transduction mechanism. Here, we tested Motif V mutations in both sub-

genomic replicon and recombinant protein systems to examine viral genome replication, helicase unwinding activity, ATP hydrolysis activity, and RNA binding affinity activity. NS3 helicase mutants, T407A and S411A, indicated reduced viral genome replication and increased turnover rates of helicase unwinding activity by a factor of 1.7 and 3.5 respectively. Additionally, we simulated Motif V mutants to probe the structural changes within NS3 helicase caused by the mutations. These simulations indicate that Motif V controls communication between the ATP-binding pocket and the helical gate. Motif V mutations T407A and S411A exhibit a hyperactive helicase phenotype leading to the regulation of translocation and unwinding during viral genome replication.

Next, we utilized T407A and S411A West Nile virus (Kunjin subtype) mutants in cell culture and *in vivo* to probe the how these mutations play a role in pathogenesis and transmission of flaviviruses. Of the two Kunjin virus mutants, only S411A Kunjin virus was recovered. In cell culture, S411A Kunjin decreased viral infection and increased cytopathogenicity as compared to WT Kunjin. Similarly, in surviving *Culex quinquefasciatus* mosquitoes, S411A Kunjin decreased infection rates as compared to WT Kunjin, but S411A Kunjin infection increased mortality compared with that of WT Kunjin infection. Additionally, S411A Kunjin increased viral dissemination and saliva positivity rates in surviving mosquitoes compared to WT Kunjin. These data suggest that S411A Kunjin increases pathogenesis in mosquitoes. Overall, these computational simulation, biochemical assay, and virology data indicate that flavivirus NS3 helicase Motif V may play a role in the pathogenesis, dissemination, and transmission efficiency of Kunjin virus, not just regulation of translocation and unwinding during viral genome replication. The molecular level insights presented in this dissertation provide the fundamental research for understanding how to target specific regions of NS3 helicase for the advancement of anti-viral therapeutics.

ACKNOWLEDGEMENTS

The completion of this dissertation could not have been possible without the support and academic guidance of my two research advisors, Martin McCullagh and Brian Geiss. Having both Martin and Brian as my mentors enabled me to learn numerous scientific techniques ranging from computational chemistry to biochemistry and virology. Martin challenged me throughout my graduate career; and because of his support I developed the necessary skills and techniques to become an independent computational chemist. Similarly, Brian tested me to become a self-sufficient biochemist and virologist. Together, Martin and Brian allowed me to grow not only as a scientist, but also as a person. They taught me important lessons such as tenacity, confidence in public speaking, and how to communicate between collaborators. I am a better person and scientist today for having Martin and Brian as my co-mentors and am so grateful to them.

I would also like to thank my committee members Chris Snow, Amber Krummel, Grzegorg Szamel, and Shing Ho who have provided guidance in my scientific and professional development. They pushed me outside of my comfort zone and highlighted areas for improvement. Under their guidance, I improved my skill and knowledge in statistical mechanics, enzymology, and virology.

Additionally, I would like to thank my undergraduate research advisor, Christopher Berndsen. He taught me how to be productive in a laboratory before I attended to graduate school and I greatly appreciate his patience and encouragement as I developed as an undergraduate researcher. He continues to be an active mentor to me by always being a source of encouragement and expertise. For instance, Christopher, an enzymologist, guided me on how to analyze the biochemical data for NS3 helicase.

In addition to my faculty mentors, I want to thank my peer and post-doc mentors, members of the McCullagh and Geiss groups, whom I value not only as colleagues, but as great friends. They sat through scores of group meeting presentations that ranged from research updates to practice talks for my orals, research seminar, and several conferences. They provided constructive feedback and a conducive environment for bouncing ideas around on how to improve experiments that did not work.

In particular, Kristen Feibelman always made time to answer my questions and helped me become proficient with laboratory equipment and techniques including the FPLC and cell culture work. I am very grateful to have learned from Erin Lynch who showed me the ropes on how to work with virus in BSL2, as well as how to perform focus forming assays and plaque assays. Additionally, I appreciate the collaborative discussions between Nicole Sexton and I allowing for my exposure to mosquito studies. Russell Davidson initiated many in depth discussions about NS3 that were always interesting and informative. Rex Lake worked with me to improve my code. All of my mentors, faculty, peer and post-doc, have provided the individual experiences that formed my graduate career across the three disciplines of computational chemistry, biochemistry, and virology.

I am also extremely fortunate to have a loving and supportive family who has helped me throughout the past five years. Numerous calls were made to my parents, Ruth and David Du Pont, my brother, Henry, and my fiancé, Bryce Zuccaro. They all believed in me and have provided their love and support in various ways. My Mother was my emotional anchor throughout my PhD, let alone my life. Whenever I am going through an extremely stressful time, she is always there for support and to give me advice. My Father was always an amazing source of knowledge and encouragement: “Research Hard, Research Smart!” My brother was consistently supportive especially towards the end of my PhD as I began to search for jobs. He significantly improved my

resume as well as provided guidance on how to expand my professional network. My fiancé was a rock the past couple years of my PhD. He listened to my frustrations and insecurities, and reminded me to take time for myself. I am extremely grateful to have so many important people in my life and I thank you all.

TABLE OF CONTENTS

CHAPTER 1 – LITERATURE REVIEW

Diseases from Mosquito-borne Flavivirus Infections

Flaviviridae is one of the positive-sense single-stranded RNA genome virus families and consists of three genera: *Hepacivirus, Pestivirus,* and *Flavivirus* (1–3). The viruses within these genera all share similarities in virion morphology, genome organization, and replication strategies, but they exhibit diverse biological properties and lack serological cross-reactivity (1). Interestingly, hepaciviruses and flaviviruses are considered human pathogens, whereas pestiviruses are considered animal pathogens (1). Pestiviruses typically infect livestock, such as cows and pigs. Viruses within the pestivirus genus include Bovine viral diarrhea virus 1 (BVDV-1), Bovine viral diarrhea virus 2 (BVDV-2), and Classical swine fever virus (CSFV). Hepaciviruses and flaviviruses both infect humans, but they cause different diseases as a result of infection. Additionally, hepaciviruses and flaviviruses are transmitted differently. Hepaciviruses, like Hepatitis C virus (HCV), are transmitted primarily through exposure to infectious blood or bodily fluids that contain blood, whereas the majority of flaviviruses are transmitted by an arthropod vector (1, 4). Flaviviruses consist of more than 50 species of viruses, 35 of which are arthropod-borne human pathogens. These viruses can cause a variety of diseases including flu-like fevers, encephalitis, meningitis, hemorrhagic fevers, microcephaly, and Guillain-Barré syndrome (3, 5, 6). Flaviviruses are classified into three groups based on their vector: mosquito-borne, tick-borne, or viruses with no known vector (1). This literature review will focus on mosquito-borne flaviviruses including dengue virus (DENV), Yellow Fever virus (YFV), Zika virus (ZIKV), West Nile virus (WNV), Japanese Encephalitis virus (JEV), and St Louis encephalitis virus (SLEV). These mosquito-borne flaviviruses can be further categorized by not only the mosquito vector, but also the types of diseases that arise from infection. DENV and YFV are hemorrhagic flaviviruses transmitted by *Aedes* (*Ae.*) mosquitoes. ZIKV is also transmitted by *Ae.* mosquitoes, but ZIKV causes neurotropic diseases. Whereas,

WNV, JEV and SLEV are encephalitic flaviviruses transmitted by *Culex* (*Cx.*) mosquitoes (5, 7–11). Generally speaking, flaviviruses are a global health concern because over half of the world's population is at risk for infection (12–18).

Flaviviruses are present in over 129 countries in both tropical and subtropical regions of the world. The majority of people at risk for flavivirus infections are localized to high population areas with a high mosquito density (19). The *Ae.* and *Cx.* mosquitoes within those areas do not discriminate between people; they will bite and transmit to anyone, children and adults alike. However, specific groups of people are more susceptible to severe infection dependent on the flavivirus. In the case of JEV, children younger than 15 years of age in many South-East Asian and Western Pacific countries are primarily affected by the virus (20, 21). Adults can also become infected with JEV, but on rare occasion. Upon infection, JEV does not develop sufficient viremia in the infected child to infect a feeding *Cx. tritaeniorhynchus* mosquito. Thus, humans are dead-end hosts for JEV (22–25). Most people infected with JEV are asymptomatic or display mild symptoms such as fever and headache. Of those infected with JEV, approximately 1 in 250 people will develop severe illness from infection such as encephalitis. Adults and children share symptoms of high fever, headache, neck stiffness, disorientation, coma, seizures, paralysis, and, death. Symptoms that are specific to infections within children include gastrointestinal pain and vomiting. The fatality rate of those with severe disease is approximately 30% (22, 26).

Similar to JEV, ZIKV also affects specific groups of people including but not limited to pregnant women and very young children. These susceptible people are bitten by an *Ae. aegypti* mosquito carrying one of the three lineages of ZIKV: West African, Asian/American, and Brazilian (27–29). Typically, adults and children who are infected with ZIKV are asymptomatic. When symptoms do occur, they take the form of a mild, self-limiting illness with a low-grade

fever, rash, headache, conjunctivitis and myalgia (30–32). On occasion, symptoms in adults and young children can develop into more severe illnesses such as Guillain-Barré syndrome, meningoencephalitis, and myelitis. If a pregnant woman becomes infected with ZIKV, the fetus has a 5 – 15% probability of developing congenital Zika syndrome (33–38). Congenital Zika syndrome refers to an infant born with microcephaly and other congenital malformations such as limb contractures, high muscle tone, eye abnormalities, and hearing loss. The pregnancy may also result in other complications due to ZIKV infection such as stillbirth, preterm birth and fetal loss (38, 39). ZIKV is unique from the other flaviviruses because it can undergo vertical transmission between mother and fetus, as well as be sexually transmitted (40–44).

Other flaviviruses, WNV, SLEV, YFV, and DENV, affect the general population within high mosquito density areas of endemic countries. WNV and SLEV cause encephalitis-based illnesses and are transmitted by *Cx.* mosquitoes. Like JEV, humans are considered dead-end hosts for WNV and SLEV infections due to low viremia levels within the host resulting in the inability to transmit the viruses to new uninfected mosquito vectors (9). WNV is primarily vectored by *Cx. pipiens, quinquefasciatus,* and *australicus* mosquitoes (45–47). These mosquitoes are found in North America, Africa, Europe, the Middle East, and West Asia. Approximately 80% of people infected with WNV are asymptomatic (9, 48). The remaining 20% of people infected with WNV develop West Nile fever with symptoms of fever, headache, body aches, nausea, vomiting and swollen lymph glands. Approximately 1 in 150 persons infected with WNV will develop a more severe form of disease such as encephalitis, meningitis, or West Nile poliomyelitis (9, 46, 48, 49). Symptoms of these diseases include headache, high fever, coma, tremors, convulsions and flaccid paralysis (49).

Similar encephalitic symptoms are seen in patients with SLEV infections. SLEV is vectored and transmitted primarily by *Cx. pipiens, quinquefasciatus, tarsalis,* and *nigripalpus* mosquitoes

within the United States as well as Brazil and Argentina in South America (50, 51). The majority of people infected with SLEV are asymptomatic. When symptoms do occur, SLEV manifests into a mild illness of flu-like symptoms with nausea. On rare occasion, the flu-like symptoms will develop into a more severe illness that presents as meningitis, encephalitis, coma, and sometimes even death (52).

YFV and DENV, the last couple of flaviviruses that affect the general population, cause hemorrhagic fever-based illnesses and are transmitted by *Aedes* mosquitoes. YFV is primarily transmitted by *Ae. aegypti* and *Ae. albopictus* mosquitoes in Africa, Central America and South America (53, 54). Many people who become infected with YFV may not know they have the virus because no symptoms are present. When symptoms arise, they manifest commonly as a mild illness with fever, headache, muscle pain, loss of appetite, and nausea or vomiting that disappears after 3 to 4 days of onset (55, 56). A small subset of people recovered from the initial illness will have a second, more severe illness within 24 hours of recovering from initial symptoms. This second wave of illness typically consists of high fevers with affected liver and/or kidney functions. During this second phase of YFV illness, people are likely to develop abdominal pain with vomiting, dark urine, and jaundice that causes yellowing of the skin and eyes due to liver and kidney failure. Bleeding from the eyes, nose, mouth, and stomach can also occur occasionally. Half of the patients who enter this phase of infection will die within 7 – 10 days upon onset of symptoms (19, 55, 56). Severe YFV illness is difficult to diagnose because the symptoms can be confused with other severe viral diseases such as hepatitis and dengue hemorrhagic fever (DHF).

Similar to YFV, the primary arthropod vector of DENV is *Ae. aegypti* with secondary vectors of *Ae. albopictus* and *Ae. polynesiensis* (57–59). These mosquito vectors carry any of the four DENV serotypes, all of which cause the same set of symptoms initially (12, 14). Following a

primary infection with one of the four DENV serotypes, approximately 70 – 80% of people are asymptomatic (17, 60, 61). When symptoms do occur, they manifest as dengue fever, a flu-like illness with a high fever, headache, rash, swollen glands, nausea, muscle and joint pain, and vomiting. Upon the onset of symptoms, the patients' immune response initiates synthesis of serotype specific antibodies. These antibodies will neutralize the infection within 2 – 7 days after the onset of symptoms resulting in immunity against that specific serotype. However, exposure to one of the other serotypes in a secondary infection will lead to an antibody-dependent enhancement (ADE) of that infection (62, 63). During the secondary infection, the primary infection antibodies can bind to the secondary serotype with low affinity but cannot neutralize it. These non-neutralized virus-antibody complexes can be internalized by cells that the virus would not normally be able to infect increasing the overall viremia within the host (64, 65). Ultimately, ADE induces cell signaling that increases vascular permeability leading to plasma leakage, fluid accumulation in the surrounding tissues, severe bleeding, respiratory distress, and organ impairment as seen in patients with DHF and dengue shock syndrome (DSS) (66–68). Without proper medical care in endemic third world countries, DHF and DSS can result in death (69). ADE also extends to secondary infections with other flaviviruses leading to the more serious illnesses described above such as encephalitis, hemorrhagic fever, and congenital Zika syndrome (65, 70). Thus, ADE is a serious concern in endemic areas with more than one flavivirus in circulation.

Antiviral therapeutics including anti-viral drugs and vaccines are a large focus for research and development against flaviviral infection. Currently, there are no specific antiviral treatments for severe symptoms caused by any of the flaviviral infections (9, 38, 71). However, if the symptoms are caught early and the individual receives proper medical care, then fatality can be reduced significantly (69). As for vaccine development, three vaccines protecting against JEV, YFV, and DENV have been developed thus far. The JEV vaccine is extremely effective at

providing protection against infection and is manufactured in great numbers in China, one of the countries endemic with JEV. Due to the manufacturing in China, the JEV vaccine is widely available to many other endemic South-East Asia and Western Pacific countries. Many of these endemic countries require the vaccination against JEV in their respective national immunization schedules to protect against infection (22). The YFV vaccine is also extremely effective and provides a life-long protection against yellow fever disease similar to the JEV vaccine. However, YFV is endemic in tropical areas of Africa, Central and South America because the vaccine is manufactured elsewhere leading to a lack of vaccine accessibility in the areas that need it the most (19). In many countries free of YFV, vaccination is required before traveling to endemic countries to prevent potential outbreaks upon returning home (19, 72). As for the DENV vaccine, it is only effective if the person receiving the vaccine has already had a primary infection with one of the serotypes of DENV. Receiving the vaccine prior to a natural primary infection may result in an ADE of infection, and the individual may develop more severe symptoms upon infection (73, 74). Additionally, if an individual receives the DENV vaccine before exposure to any of the other flaviviruses, ADE can amplify those flavivirus symptoms as well. Therefore, the DENV vaccine is not widely distributed in endemic countries due to the higher risk for developing more severe diseases caused by flaviviruses. DENV is the most prevalent flavivirus, circulating in over 129 countries worldwide with approximately 390 million people at risk for infection every year (8, 60, 75, 76). Due to the large presence of DENV and the other flaviviruses in overlapping countries, there is a pressing need for the development of antiviral therapies against each flavivirus. For the development of these interventional strategies, a fundamental understanding of how flaviviruses replicate within hosts, including the mosquito vector, is required. The rest of this literature review will discuss what is currently known and not known about flaviviral replication in the mosquito vector and host.

Flavivirus Infection of a Competent Mosquito Vector

Aedes and *Culex* mosquitoes are the primary vectors for flaviviruses. Following a blood meal on a viremic human or animal, the virus must initially establish infection in the mosquito midgut. From there, the virus must disseminate throughout the rest of the mosquito body, ending in the salivary gland for further transmission and spread of the virus to new hosts (77–79). The mosquito's ability to transmit infectious viruses is known as vector competence. Not every mosquito will be able to transmit flaviviruses due to their ability to inhibit viral dissemination within their tissues (80, 81). The virus has to overcome four tissue barriers: 1) the midgut infection barrier (MIB), 2) the midgut escape barrier (MEB), 3) the salivary gland infection barrier, and 4) the salivary gland escape barrier (82, 83). To successfully overcome the MIB, the flavivirus envelope glycoprotein has to interact with the midgut epithelial receptors to initiate receptor-mediated endocytosis (84–87). Once the virus can establish infection in the midgut epithelial cells, the virus will replicate in the midgut. When flaviviruses replicate at high levels in the midgut, the virus has a higher probability of escaping the midgut and disseminating into the rest of the mosquito (83, 88). Following escape from the midgut, flaviviruses usually disseminate into fat body, hemocytes, nerve, and muscle tissues (77, 89). Previous studies have suggested that infection in hemocytes may be critical for flaviviruses to penetrate into the salivary gland (90, 91). Upon salivary gland infection, the virus will replicate and accumulate in the apical cavities of acinar cells, which are the cells that secrete the bulk of the saliva fluid (83). Virus accumulation in the saliva will enable the mosquito to transmit the virus to other hosts continuing the spread of flaviviruses (78, 92, 93).

Flavivirus Structural and Life Cycle Overview

Flaviviruses have a positive-sense single-stranded RNA genome of approximately 11-kb that contains a single open reading frame (ORF) flanked by highly structured 5' and 3' untranslated regions (UTRs) (94). The ORF encodes for a single polyprotein that is co- and post-

translationally cleaved by viral and host proteases into three structural proteins (envelope (E), pre-membrane (prM), and capsid (C)), and eight nonstructural proteins (NS1, NS2A, NS2B, NS3, NS4A, 2K, NS4B, and NS5) (95). The translated structural and nonstructural proteins are involved in virion formation and viral replication, respectively. Additionally, the 5' and 3' UTRs contain structural elements that are critical for viral translation, replication, and pathogenesis (96–101). These structural elements include but are not limited to the 5' type-1 cap, the 5' stem loop A (5'SLA), the 5' and 3' cyclization sequences, and the 3' stem loop (3'SL). Without these structural elements, the virus would be targeted for degradation by the host cell and would not be able to replicate (102–108).

Within the mature flavivirus virion, the genomic RNA is in complex with the C protein forming the nucleocapsid core. This nucleocapsid core is incased by a host-derived bilipid membrane with a glycoprotein outer shell composed of membrane (M) and E proteins (109–114). The M protein is a proteolytic fragment, produced from the cleavage of prM during virion maturation. The E protein is the major structural component of the outer shell forming 90 antiparallel dimers that lay flat against the surface covering the M protein (115–117). Three E protein dimers form a raft, and there are 30 rafts that cover the surface of one virion with a 50 nm diameter (112, 118, 119). The E protein is responsible for initial interactions with the host cell during infection (120–123).

Flaviviruses bind to protein receptors on the surface of host cells through E protein interactions, and are brought into cells via clathrin-mediated endocytosis (Figure 1.1) (116, 124–127). Normally endosomes are trafficked to the lysosome and undergo an acidification process that primes the endosome for lysosomal fusion and degradation. Flaviviruses have evolved to use this acidification step to induce a conformational change in their envelope proteins that results in a fusion between viral and endosomal membranes, releasing the nucleocapsid core into the

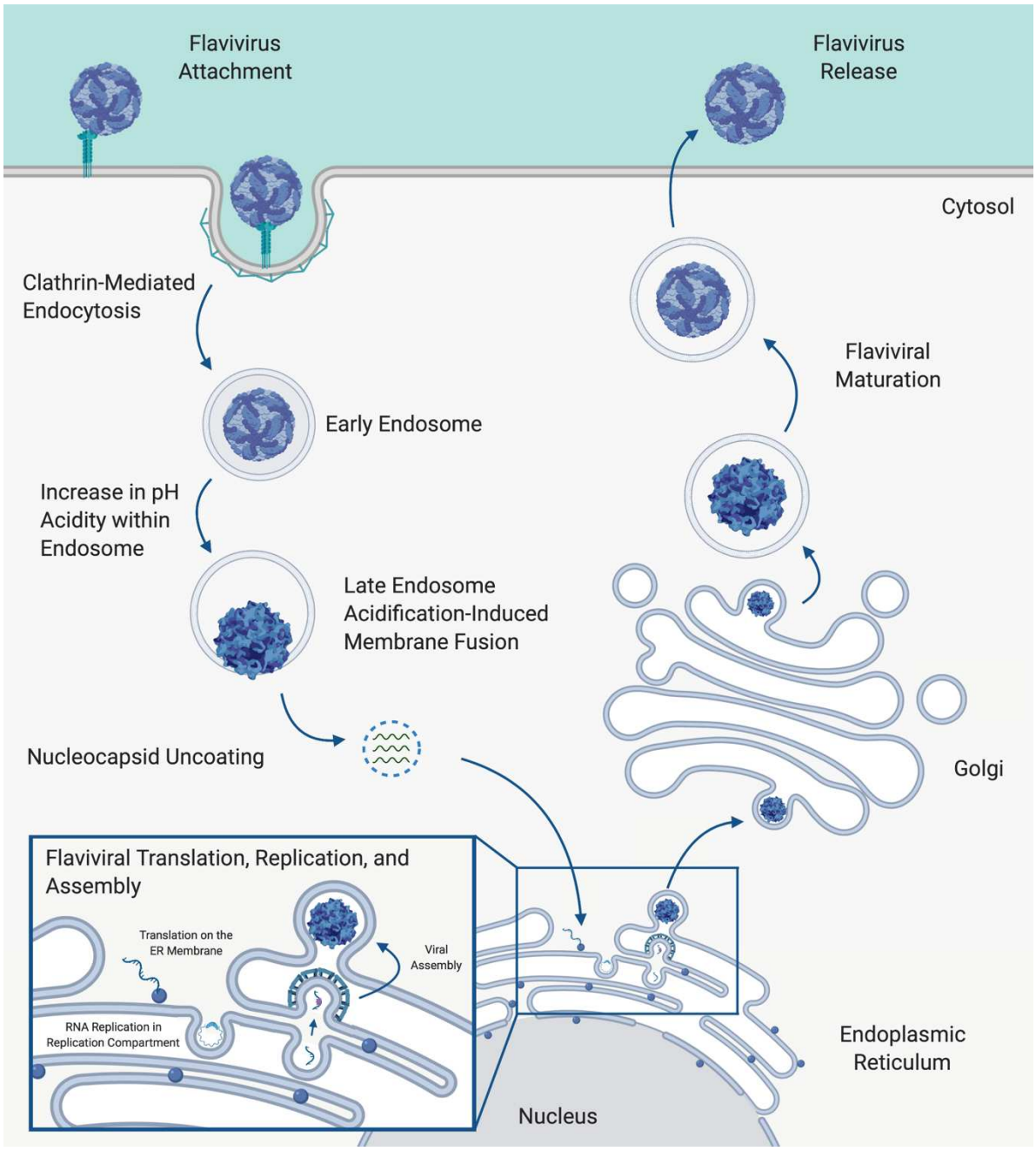

Figure 1.1. Flavivirus life cycle. The cycle begins with viral attachment and entry via clathrin-mediated endocytosis. Following entry, flaviviruses undergo endosomal fusion and genomic release into the cytoplasm. The viral RNA is trafficked to the endoplasmic reticulum for translation, replication and assembly. Viral maturation occurs as the virion travels through the Golgi leading to secretion of the mature virion from the cell via exocytosis. The inset focuses on the viral processes that occur at the endoplasmic reticulum membrane.

cytoplasm (115, 123). The nucleocapsid core is then uncoated; the C protein dissociates from the genomic RNA allowing the RNA to be trafficked to the endoplasmic reticulum (ER) (128). At the ER membrane, the genomic RNA is translated into the viral polyprotein and post-translationally processed into the structural and the nonstructural proteins via viral and host proteases. The nonstructural proteins are involved in the formation of the viral RNA replication compartments at the ER membrane as well as replication and capping of the viral RNA genome (129). These processes performed by the nonstructural proteins will be discussed in more detail in the next section. The viral structural proteins are used in the assembly and packaging of new immature virion particles that bud into the Golgi. As the immature virion travels through the Golgi, it undergoes a maturation process producing an infectious virion. The mature virion is then released from the host cell and is able to infect new host cells (130–132).

Viral Genome Replication

The nonstructural proteins are responsible for viral genome replication within replication compartments at the ER membrane (129, 133–135). Within these replication compartments, the nonstructural proteins associate together forming the flaviviral replication complex. The core of the replication complex is composed of NS3 and NS5. These two nonstructural proteins are the only viral proteins known to possess the enzymatic activities required for viral replication. NS3 and NS5 both contain two structurally distinct domains. NS3 consists of an N-terminal serine protease domain and a C-terminal helicase domain. NS3 serine protease activity is responsible for cleavage of the viral polyprotein (136–139). NS3 helicase domain possess RNA helicase, nucleotide triphosphatase (NTPase), and RNA triphosphatase (RTPase) enzymatic activities (140–144). NS3 helicase and NTPase activities carry out unwinding for the double-stranded RNA intermediate, while the RTPase activity is involved in priming the newly synthesized genomic RNA for 5’ RNA capping (145, 146). NS5 consists of an N-terminal RNA capping domain and a C-terminal RNA-dependent RNA polymerase (RdRP) domain. NS5 RNA capping

domain possess RNA guanylyltransferase (GTase) and methyltransferase (MTase) activities that are necessary for the addition of a type-1 cap structure ($^{m7}GpppN^{m}$) at the 5' end of the genomic RNA (147–149). NS5 RdRP activity is responsible for carrying out both negative-sense and positive-sense strand RNA synthesis (150–152).

The other nonstructural proteins (NS1, NS2A, NS2B, NS4A, 2K, and NS4B) are hypothesized to structurally support and regulate the core NS3:NS5 replication complex. NS1 is a glycoprotein located in the ER lumen, and NS2A, NS2B, NS4A, 2K, and NS4B are transmembrane proteins that span the ER membrane. NS1 associates with NS4A and NS4B stabilizing the membrane-spanning protein complex. NS2A, NS4A, 2K, and NS4B are likely involved in the formation of the replication compartment by altering the curvature of the ER membrane (153–156). NS2B interacts with the other transmembrane proteins forming a scaffold for the assembly of the replication complex (153). NS3 protease requires NS2B as a cofactor for active serine protease function (136, 138, 139, 157). Through this NS3 protease-NS2B interaction, the core replication complex is anchored to the ER membrane within the replication compartment. By creating the replication compartment, flaviviruses have evolved to protect the viral genomic RNA from being degraded by the host cell during viral genome replication.

Viral genome replication begins with the synthesis of a negative-sense antigenomic RNA strand. This negative-sense RNA strand serves as a template for synthesis of a new positive-sense genomic RNA strand. NS5 RdRP is responsible for the synthesis of this negative-sense template strand (2, 158–160). The 3' end of the positive-sense genomic RNA is the starting point for negative-sense antigenomic RNA synthesis. However, the highly structured nature of the 3'SL within the 3' UTR inhibits NS5 RdRP from initially binding to that region for the synthesis of the negative-sense antigenomic RNA strand (161). Therefore, NS5 RdRP initially binds the 5'SLA structural element found within the 5' UTR. This binding event causes the

genomic RNA to cyclize bringing the 5’ and 3’ UTRs together (162, 163). When the 5’ and 3’ UTRs are in close proximity, the 5’ and 3’ cyclization sequences hybridize inducing a conformation rearrangement within the 3’SL structural element. As a result of the conformation rearrangement, the 3’SL is in a single-stranded RNA structure optimal for NS5 RdRP to bind and begin synthesizing the negative-sense template strand in the 3’ to 5’ direction (164–166). As the negative-sense strand is synthesized, a double-stranded RNA intermediate is formed with the positive-sense RNA strand known as the replicative form (130, 152).

For the synthesis of a new positive-sense RNA strand, the replicative form must be unwound so that NS5 RdRP can bind the negative-sense RNA template strand (132, 167). This unwinding activity is performed by the NS3 helicase in an ATP-dependent manner. NS3 helicase binds the negative-sense RNA strand at the 3’ end as well as an ATP molecule. ATP hydrolysis powers translation along the negative-sense template strand unwinding the replicative form one base at a time (168, 169). NS3 is in complex with NS5 allowing for the newly unwound negative-sense template strand to be fed to NS5 RdRP for synthesis of the genomic RNA in the 5’ to 3’ direction (170, 171). As positive-sense synthesis begins, a replicative intermediate is formed. The replicative intermediate consists of the partially unwound positive-sense RNA, the newly synthesize positive-sense RNA, and the negative-sense template RNA. Once the original positive-sense RNA strand is completely unwound from the replicative intermediate, it can be packaged into an immature budding virion.

The newly synthesized positive-sense RNA strand is now in complex with the negative-sense RNA template strand and requires the addition of a 5’ type-1 cap structure (^{m7}GpppN^{m}) (144, 167). RNA capping utilizes four enzymatic activities of RTPase, N7-MTase, 2-O-MTase, and GTase activities. NS3 RTPase activity primes the newly synthesized positive-sense RNA strand by generating a 5’-diphosphorylated RNA (5’-ppRNA). The 5’-ppRNA binds NS5 RNA capping

domain and is then ligated with a GMP by GTase activity forming the base cap structure (GpppN) (147, 172). Next, N7-MTase transfers a methyl group onto the guanine N7 position from S-adenosyl-methionine (SAM) resulting in S-adenosyl-L-homocysteine (SAH) and the type-0 cap structure (^{m7}GpppN). A second methyl group from a new SAM is transferred onto the 2'-hydroxyl position of the first RNA nucleotide during 2'-O-MTase activity (148). This second MTase reaction results in the mature type-1 cap structure that is required for viral survival in the host cell. The capping of the positive-sense genomic RNA strand completes one cycle of genomic RNA synthesis. The newly capped genomic RNA is in complex with the negative-sense antigenomic RNA strand. Therefore NS3 must unwind the replicative form again for another round of viral genome replication. The negative-sense antigenomic RNA template strand is utilized repeatedly in this cycle for synthesizing many copies of the positive-sense RNA strand.

Ultimately, unwinding the replicative form during viral genome replication is essential for the survival of the virus. While NS3 is known to be critical for viral genome replication, it is not completely understood how NS3 functions within an infection. Being able to understand how NS3 functions during an infection will be critical for the advancement of vaccine and anti-viral therapeutic development. This dissertation will explore the fundamental mechanisms of NS3 during viral genome replication and infection.

Nonstructural Protein 3

NS3 is well conserved across all flaviviruses (WNV, JEV, DENV, ZIKV, YFV, and SLEV) with approximately 67% sequence identity. Structurally, the N-terminal serine protease domain and the C-terminal helicase domain are connected through a flexible linker of around 10 amino acids. The full length NS3 is approximately 70 kDa with 618 residues (160). The serine protease domain is a third of NS3 (residues 1-169), while the helicase domain is two-thirds of NS3

(residues 179-618). Serine protease activity is activated by the NS2B cofactor and is responsible for cleaving the viral polyprotein at specific sites between NS2A/NS2B, NS2B/NS3, NS3/NS4A, and NS4B/NS5 (173, 174). It is also through the NS3/NS2B interaction that localizes the NS3:NS5 core replication complex to the ER membrane within the replication compartment (138, 139). The helicase domain houses three enzymatic activities: RNA helicase unwinding activity, nucleotide triphosphatase (NTPase) activity, and RNA triphosphatase (RTPase) activity. The first two functions are involved in translation and unwinding of the replicative form during viral genome replication (140–143). The last function, RTPase activity, is responsible for priming the newly synthesized genomic RNA strand for RNA capping by NS5 (144, 145, 175). Because NS3 helicase unwinds the replicative form during viral replication, it is an excellent target for drug, vaccine, and anti-viral therapeutic development.

Helicases are ubiquitous enzymes within cells partaking in processes revolving around nucleic acids including replication and repair, transcription, translation, RNA maturation and splicing, and nuclear export processes (170, 176). Cellular and viral helicases are classified into six distinct superfamilies (SFs) based on their sequence, structure, and mechanistic features. Across all SFs, the base structural domain takes the form of tandem RecA-like folds either within the same polypeptide chain or between subunits. In the case of SF1 and SF2, the RecA-like domains are between subunits, whereas in SF3, SF4, SF5, and SF6, the RecA-like fold is the same polypeptide that repeats six (or twelve) times forming a hexameric ring structure (176). The majority of helicases belong to either SF1 or SF2, and the helicases within those SFs are further classified into subfamilies based off of their structural motifs. SF1 subfamilies include Upf1, RecD, UvrD/Rep; while SF2 subfamilies include Rad3, DEAD-box, RecQ, RecG, Ski2-like, RigI-like, T1R, DEAH/RHA, Viral/DEAH-like, Swi2/Snf2, Suv3, and T3R (170). These subfamilies all share seven “signature” motifs (I, Ia, II, III, IV, V, and VI) with the addition of several motifs that are specific to either the entire SF group or individual subfamilies within one

of the SFs (170, 176). These additional motifs are TxGx(177), Q-motif(178), Motif IVa(179), and TRG(180). In the case of Motif IVa, all SF2 helicases have this structural motif, while SF1 helicases do not. This is important to note because all *Flaviviridae* NS3 helicases are classified as SF2 helicases within the Viral/DEAH-like subfamily, and thus contain the seven signature motifs plus motif IVa (Figure 1.2). Additionally, recall that both flaviviruses (WNV, DENV, ZIKV, JEV, YFV, and SLEV) and hepaciviruses (HCV) are found within the *Flaviviridae* family. Therefore, NS3 helicases from both genera are found within the Viral/DEAH-like subfamily of SF2 helicases.

Within the viral/DEAH-like subfamily, there are three subdomains (1, 2, and 3); of those subdomains, 1 and 2 are RecA-like, while subdomain 3 is unique to the viral/DEAH-like subfamily. Subdomain 3 interacts with both subdomains 1 and 2 forming the RNA binding cleft seen in flavivirus NS3 helicases. The RNA binding cleft is one of two substrate binding pockets within NS3 helicase. A second substrate binding pocket is formed between subdomains 1 and 2 known as the ATP binding pocket (Figure 1.2) (168, 181). ATP binds to the ATP binding pocket and when initiated, ATP hydrolysis occurs here as well. During viral genome replication, NS3 helicase initially interacts with the double-stranded replicative form at the helical gate, a structural region that spans subdomains 2 and 3. The helical gate separates the double-stranded RNA intermediate allowing for the negative-sense antigenomic RNA strand to enter the RNA binding cleft at the 3'end (168, 182, 183). For translocation along the negative-sense RNA strand and further unwinding of the replicative form, NS3 helicase hydrolyzes ATP. One ATP molecule is hydrolyzed per nucleotide base pair (169, 184–187). As ATP is hydrolyzed, the negative-sense RNA strand will continue to enter the RNA binding cleft further splitting the replicative form at the helical gate. The highly conserved structural motifs are involved in the enzymatic activities of NS3 helicase. Motifs I, II, III, and VI are associated with ATP binding and hydrolysis, while Motifs Ia, IV, IVa, and V are associated with interdomain communication, RNA

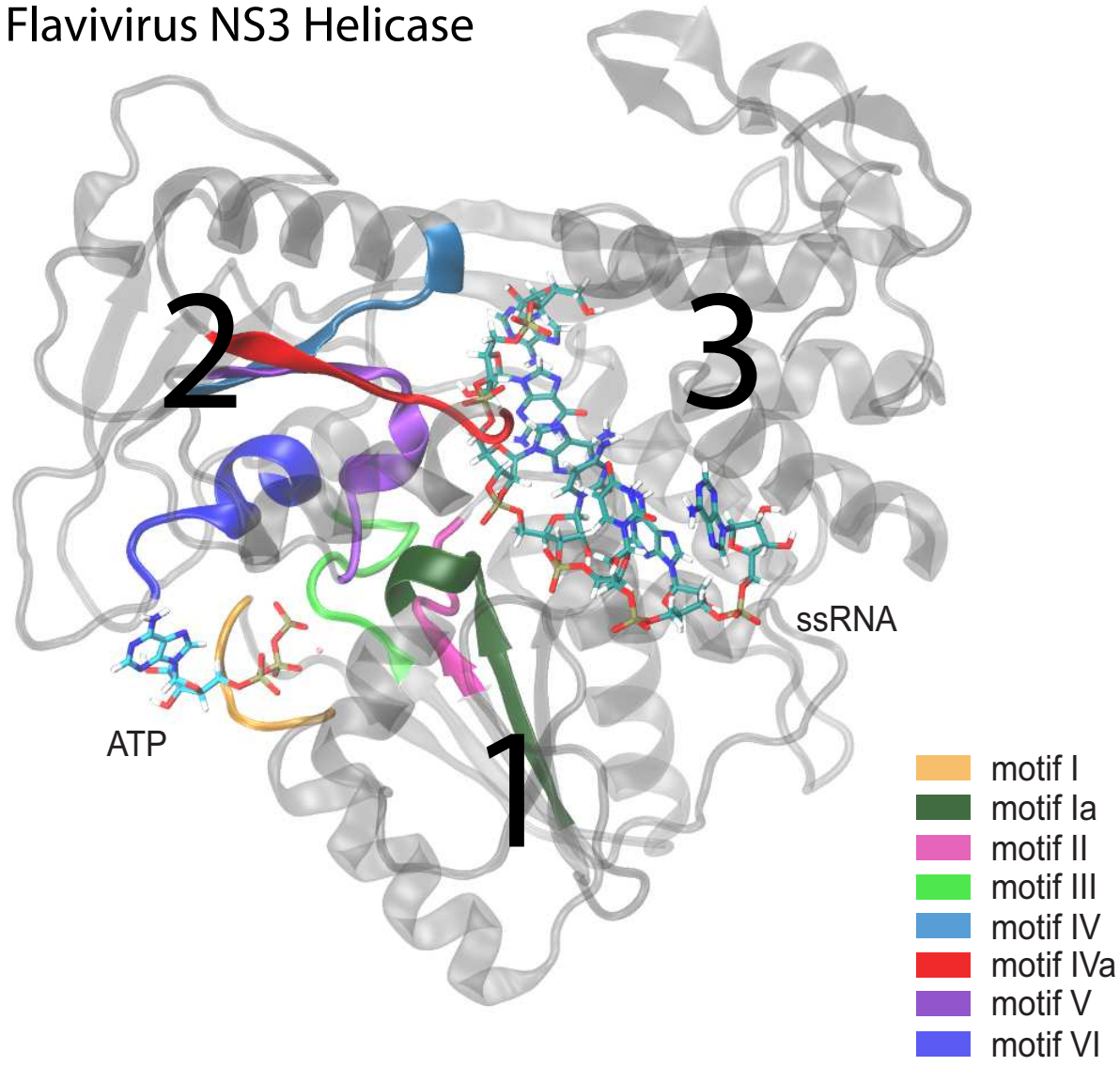

Figure 1.2. Flavivirus NS3 helicase structure (DENV4 NS3 helicase; Protein Data Bank code 2JLV). NS3 helicase consists of three subdomains (labeled as 1, 2, and 3). Within subdomains 1 and 2, there are eight highly conserved SF2 helicase structural motifs. These motifs are highlighted as follows: Motif I in orange; Motif Ia in dark green; Motif II in magenta; Motif III in lime green; Motif IV in blue; Motif IVa in red; Motif V in purple; and Motif VI in royal blue. Additionally, NS3 helicase substrates, ATP and ssRNA, are bound in their respective binding pockets. The ATP binding pocket is located between subdomains 1 and 2; and the RNA binding cleft is located between subdomain 3 and subdomains 1 and 2.

binding, and translocation. Interestingly, the motifs associated with ATP binding and the motifs associated with RNA binding are found between the two RecA-like subdomains. Motifs I, Ia, II, and III are in subdomain 1, and Motifs IV, IVa, V, and VI are in subdomain 2 (Figure 1.2). For the remainder of this literature review, we will discuss how each motif plays a role in the three enzymatic functions of NS3 helicase, and what residues within those motifs interact directly with either ssRNA or ATP. We will also elucidate how these motifs are still not well understood in relation to NS3 helicase function.

Motifs Responsible for ATPase Activity

Motifs I, II, III, and VI are associated with ATP binding and hydrolysis (Figure 1.3). Motifs I and II are considered hallmark motifs found in all phosphate binding loop (P-loop) proteins; they are also known as Walker A motif and Walker B motif, respectively. In flaviviruses, Motif I contains the conserved sequence of GAGKT; whereas in HCV, the conserved sequence is GSGKS. The secondary structure of Motif I forms a phosphate binding loop allowing for the residues within the motif to bind the β-phosphate of bound nucleotide triphosphate (188, 189). Motif II contains a DEAD box element that is involved in coordinating the magnesium ion within the ATP binding pocket. DEAD box elements comes in three variations: DEAD, DEAH, and DExH. For flavivirus NS3 helicases, the DEAD box element is DEAH; whereas for HCV the sequence is DECH. Motif III contains the conserved sequence of MTATP in flaviviruses; while in HCV, the conserved sequence is ATATP. Motif III is located near the ATP hydrolysis active site; however this motif does not directly interact with the bound ATP, so it will not be discussed further (190–193). The conserved sequence of flavivirus NS3 helicase Motif VI is QRRGRiGR; while in HCV, the conserved sequence is QRRGRTGR. Motif VI is thought to stabilize interactions between the residues within ATPase active site and the nucleic acid base of the bound nucleotide triphosphate molecule (191). When negative-sense RNA strand binds into the RNA binding cleft, the ATP binding pocket undergoes a conformation rearrangement moving from an “open”

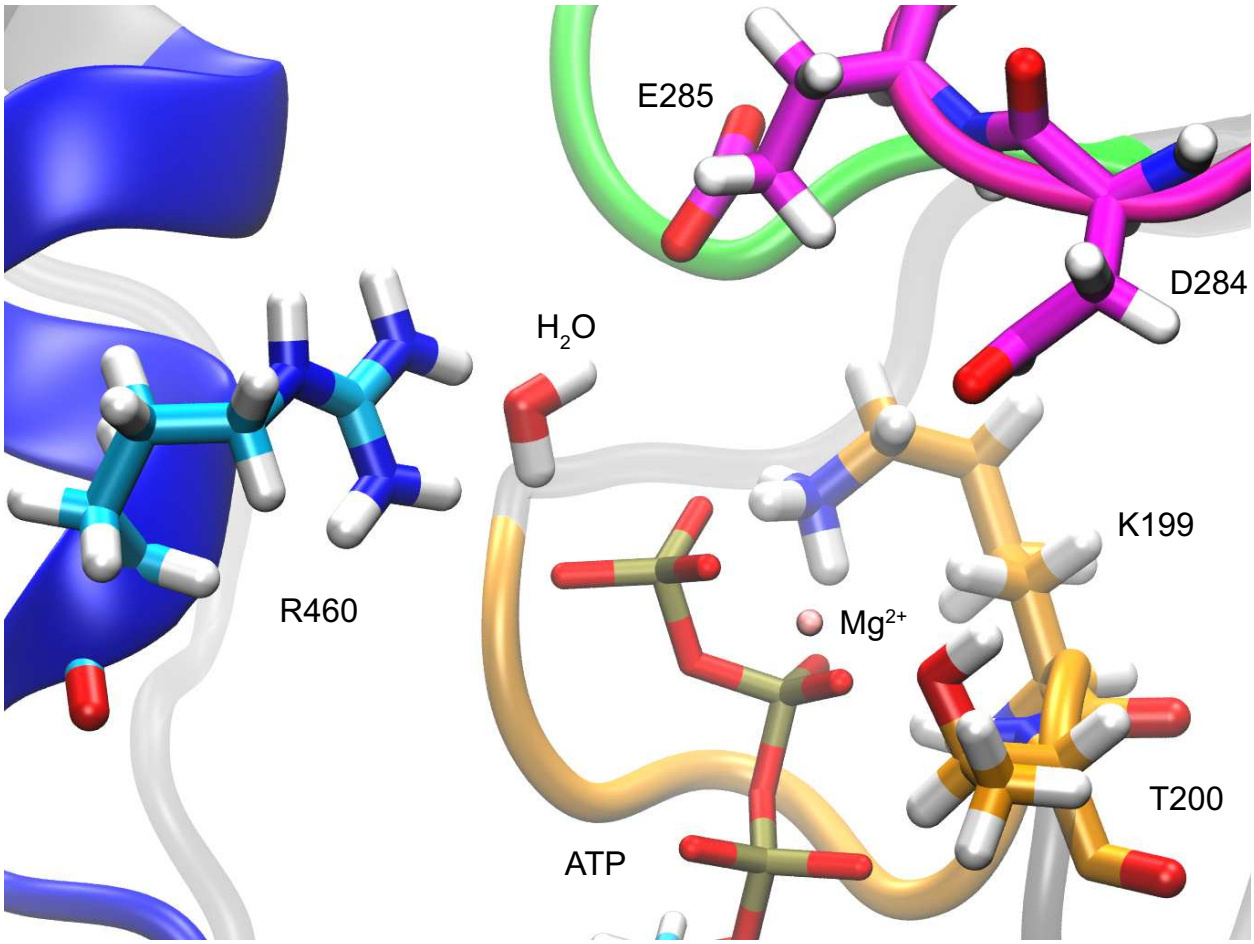

Figure 1.3. Flavivirus NS3 helicase interactions with ATP within the ATP binding pocket. Motif I (in orange), Motif II (in magenta), and Motif VI (in royal blue) form the ATP binding pocket within the NS3 helicase structure (PDB code 2JLV). Residue K199 from Motif I interacts with the ATP β-phosphate, while T200 from Motif I and D284 from Motif II coordinates with the Mg^{2+} ion. E285 from Motif II stabilizes interactions with the lytic water. R460 from Motif VI interacts with the lytic water and is also responsible for stabilizing the transition state during hydrolysis. Motif III (in lime green) is also near the ATP binding pocket, but specific interactions are not highlighted.

state that is less active to a “closed” state that is more catalytically active. The P- loop shifts towards the protein core allowing for optimal ATPase activity (168). Between Motif I, Motif II, and Motif VI, there are five residues that are essential for ATP binding and hydrolysis. In DENV2 NS3 helicase, residue K199 from Motif I coordinates with the β-phosphate of ATP; residue T200 from Motif I and residue D284 from Motif II coordinates with Mg^{2+}; residue E285 from Motif II coordinates with the lytic water; and residue R460 from Motif VI stabilizes the transition state during hydrolysis (Figure 1.3). We know these residues are directly involved in ATP hydrolysis due to DENV2 and HCV NS3 helicase mutational studies, which will be discussed in the remainder of this subsection.

Mutational analysis within Motif I, Motif II, and Motif VI not only verified the importance of each of those residues during ATPase activity, but also confirms that there is only one ATP binding pocket for NS3 helicase (Table 1.1). Motif I residues that were mutated include G198 and K199 from DENV2(140, 141, 143), as well as K210(194) from HCV (equivalent to residue K199 from DENV2). DENV2 NS3 helicase residues G198 and K199 were mutated to alanine(142, 143), as well as glutamic acid for K199 (140, 141). Residue K210 from HCV was mutated to alanine(195–198), asparagine(194), and glutamine (195). All of the Motif I mutations resulted in abolished ATPase activity suggesting that both residues, G198 and K199 (or K210 for HCV), are critical for ATP hydrolysis (140, 141, 143). These studies hypothesized that the loss of activity was due to a disruption of interactions with the b-phosphate of ATP. K199A and K199E were also tested for RTPase activity; these mutations led to a loss of RTPase activity suggesting that ATPase and RTPase activity occur in the same binding pocket (141). Additionally, helicase unwinding activity was tested for all DENV2 and HCV Motif I mutations except for K199E. Results indicated a loss of helicase unwinding activity suggesting that helicase unwinding activity is ATP-dependent (140, 143).

Table 1.1. *Flaviviridae* NS3 helicase mutations found within Motifs I, II, and VI. The mutations are characterized by *Flaviviridae* virus, either DENV2 or HCV. Previous mutational studies tested for various NS3 helicase functions including NTPase activity, helicase unwinding activity, and RTPase activity. Results from these mutational studies are reported as follows: the percentage as compared to WT (%), as active as WT (+++), increased activity (++++), decreased activity (++ or +), no activity (-), and not determined (nd).

Motif	Virus (Residue Range)	Mutation (Reference)	NTPase Activity	Helicase Activity	RTPase activity
I	DENV2 (aa193-202)	G198A (143)	+	-	nd
		K199A (142, 143)	-	-	-
		K199E (140, 141)	-	nd	-
	HCV (aa204-213)	K210A (195–198)	-	-	nd
		K210N (194)	-	-	nd
		K210Q (195)	-	-	nd
II	DENV2 (aa282-289)	M283F (143)	+	++++	nd
		D284A (142)	+	-	-
		E285A (142)	-	nd	-
	HCV (aa288-295)	D290N (194)	-	-	nd
		E291Q (194, 198)	-	-	nd
		C292A (194)	53% of wt	82% of wt	nd
		H293A (194)	6% of wt	75% of wt	nd
VI	DENV2 (aa456-467)	Q456N (199)	++	++++	++++
		R457A (143)	+++	-	nd
		R458A (143)	+++	-	nd
		R457A/R458A (143)	+	-	nd
		R460A (199)	+	++	+
		R463A (199)	+	++++	+
	HCV (aa460-471)	Q460H (200)	-	+	nd
		R461A (200)	27% of wt	-	nd
		R461Q (194)	7% of wt	-	nd
		R462L (200)	4% of wt	-	nd
		G463A (200)	8% of wt	+++	nd
		R464A (200)	-	-	nd
		T465N (200)	22% of wt	+++	nd
		G466A (200)	5% of wt	+	nd
		R467K (200)	-	-	nd

Motif II residues were mutated to the following: M283F(143), D284A, and E285A in DENV2(142), and D290N, E291Q, C292A, and H293A in HCV(194, 198). HCV residues D290, E291, C292, and H293 are equivalent (same positioning in Motif II) to residues D284, E285, A286, and H287 in DENV2. M283F was designed as a mutation in DENV2 because phenylalanine commonly occurs at this position in other positive-strand RNA based viruses. M283F resulted in a reduced ATPase activity with an increased helicase unwinding activity; however no rational was discussed for this observed difference in activity (143). In the case of D284A and E285A in DENV2, results indicated that ATPase, RTPase, and helicase unwinding activities exhibited decreased or loss of activity across the board suggesting that these two residues are critical for NS3 helicase function (142). HCV D290N and E291Q also exhibited a loss of ATPase and helicase unwinding activity suggesting that those residues are critical for NS3 function as well (194, 198). However, HCV mutations C292A and H293A either reduced ATPase activity by half or nearly abolish activity, respectively suggesting that C292 and H293 are important for ATP hydrolysis but they are not nearly as critical as D290 or E291 (194).

Mutations in Motif VI residues include Q456N, R457A, R458A, R457A/R578A, R460A, and R463A from DENV2(143, 199), and Q460H, R461A, R461Q (R457 in DENV2), R462L, G463A, R464A, T465N, G466A, R467K from HCV (194, 200). Residue Q456 being the first amino acid in DENV2 Motif VI was mutated to an asparagine to determine the importance of the length of the side chain in the ATP binding pocket. Results of Q456N indicated that ATPase activity was reduced by half, while increasing both RTPase activity and helicase unwinding activity compared to WT suggesting that Q456 is important for both ATPase and RTPase activities (199). As single mutants, R457A and R458A in DENV2 retained ATPase activity but showed no detected RNA unwinding (143). However when R457A and R458A were mutated together as a double mutant, ATPase activity was significantly reduced suggesting that the ATPase active site requires at least one of the arginine residues for ATPase activity (199). The last two residues

mutated in DENV2 Motif VI were R460A and R463A. Results of these mutations indicated that ATPase, RTPase, and helicase unwinding activity decreased, except for the unwinding activity of R463A which increased as compared to WT (199). These results suggested that R460 and R463 in DENV2 are important for both ATPase and RTPase activity with varying effects on helicase unwinding activity. Overall, we can conclude that the arginine residues in Motif VI are critical for ATPase, RTPase, and helicase unwinding activity. Similar to the DENV2 results, HCV NS3 helicase Motif VI mutations also indicate that the arginine residues are critical for ATPase activity and RNA helicase activity (194). The non-arginine residues mutated in HCV were shown to significantly decrease ATPase, while not affecting helicase unwinding activity. If these residues were also mutated in DENV2, we would expect similar results for ATPase and helicase unwinding activity.

Motifs Responsible for Interdomain Communication, RNA binding, and Translocation

Motifs Ia, IV, IVa, and V associate with interdomain communication, RNA binding, and translocation. Between flaviviruses and HCV, the conserved sequences vary slightly. In flaviviruses, Motif Ia contains the conserved sequence of LAPTRVVAAE; whereas in HCV, the conserved sequence is LNPSVAATPG. For Motif IV in flaviviruses, the conserved sequence is VWFVPSI; while in HCV, the conserved sequence is LIFCHSK. The conserved sequence of Motif IVa in flaviviruses is IQL(N/S)RKTF; while in HCV, the conserved sequence is VAYYRGLD. The flavivirus NS3 helicase Motif V conserved sequence is FVVTTDISEMGAN; while in HCV, the conserved sequence of Motif V is VAVATDALMTGFT. Each motif associated with ssRNA only contains a couple of residues that interact with ssRNA. These residue-ssRNA interactions occur in either one of two ways: 1) residue-ribose 2'-hydroxyl group interactions or 2) residue-phosphate backbone interactions (Figure 1.4). In DENV2 NS3 helicase, residue P223 from Motif Ia (Figure 1.4A), and residue P363 from Motif IV (Figure 1.4B) interacts with the ribose 2'-hydroxyl group of ssRNA; and residue R225 from Motif Ia (Figure 1.4A), residue I365

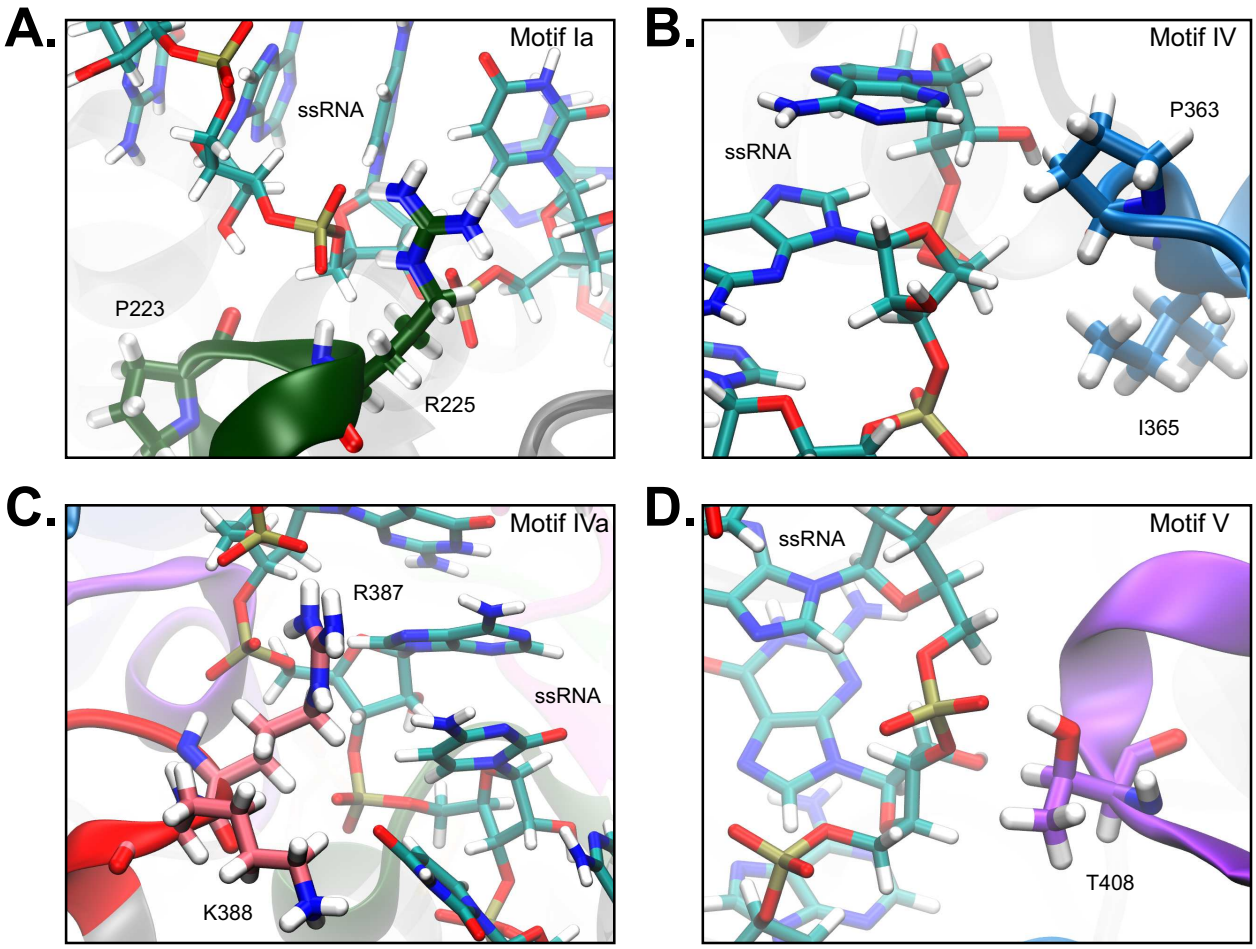

Figure 1.4. Flavivirus NS3 helicase interactions with ssRNA within the RNA binding cleft. Subdomain 3 forms the RNA binding cleft with subdomains 1 and 2 (PDB code 2JLV). Residues within Motif Ia (in dark green), Motif IV (in blue), Motif IVa (in red), and Motif V (in purple) interact with ssRNA lining the RNA binding cleft across subdomains 1 and 2. A. Motif Ia residues, P223 and R225, interact with the ribose 2'hydroxyl group and the phosphate backbone of ssRNA, respectively. B. Motif IV residues, P363 and I365, interact similarly to Motif Ia residues. P363 interacts with the ribose 2'hydroxyl, whereas I365 interacts with the phosphate backbone of ssRNA intermediate. C. Motif IVa residues, R387 and K388, interact with the RNA phosphate backbone. D. Motif V residue, T408, interacts with the RNA phosphate backbone as well.

from Motif IV (Figure 1.4B), residues R387 and K388 from Motif IVa (Figure 1.4C), and residue T408 from Motif V (Figure 1.4D) interacts with the phosphate backbone of ssRNA. We know that these residues are involved in RNA binding and translocation due to DENV2 and HCV mutational studies that will be discussed further during the remainder of this subsection.

Between all four RNA interacting motifs, only five mutations have been experimentally tested against NS3 helicase functions (Table 1.2). Motif Ia residue S231 (from HCV NS3 helicase) was mutated to alanine (201). This HCV residue is equivalent to T224 in DENV2, which is located between two residues that interact with ssRNA, P223 and R225 (Figure 1.4A). When biochemically tested, the S231A mutation exhibited increased ATPase and ssRNA binding activity, but helicase unwinding activity was unaltered as compared to wild-type. These results suggested that residue S231 did not affect the ability of the surrounding residues to interact with ssRNA during unwinding activity (201). In DENV2 NS3 helicase, Motif IV residue I365, one of the residues that interacts directly with ssRNA (Figure 1.4B), was mutated to alanine to determine if this interaction was critical for NS3 helicase functions. The I365A mutant resulted in no helicase unwinding activity, while ATPase activity remained constant suggesting that residue I365 was essential for unwinding ssRNA, but not for ATPase activity (199). Motif IVa residue R393 from HCV NS3 helicase was also mutated to alanine for similar reasons as the mutation I365A in Motif IV. HCV residue R393 (equivalent to R387 in DENV2, Figure 1.4C) also interacts directly with ssRNA; thus the R393A mutation was designed to determine if the R393-ssRNA interaction is critical for NS3 helicase function (202). Results from this R393 mutation exhibited decreased helicase unwinding activity, but ATPase activity remained the same suggesting that in HCV, R393 interactions with ssRNA are critical for helicase unwinding activity, but not for ATPase activity. HCV NS3 helicase Motif V residue, T411 was also mutated to alanine due to the same reasons again. Motif V T411 in HCV is equivalent to T408 in DENV2, one of the residues that interacts with the phosphate backbone of ssRNA (Figure 1.4D). Previous studies

Table 1.2. *Flaviviridae* NS3 helicase mutations found within Motifs Ia, IV, IVa, and V. The mutations are characterized by *Flaviviridae* virus, either DENV2 or HCV. Previous mutational studies tested for various NS3 helicase functions including NTPase activity, helicase unwinding activity, RTPase activity, and nucleic acid binding. Results from these mutational studies are reported as follows: the percentage as compared to WT (%), as active as WT (+++), increased activity (++++ or ++++), decreased activity (++ or +), no activity (-), and not determined (nd).

Motif	Virus (Residue Range)	Mutation (Reference)	NTPase Activity	Helicase Activity	RTPase activity	Nucleic acid binding
Ia	HCV (aa228-237)	S231A (201)	+++++	+++	nd	++++
IV	DENV2 (aa359-365)	I365A (199)	++++	-	++	nd
IVa	HCV (aa389-396)	R393A (202)	+++	++	nd	++
V	DENV2 (aa404-416)	G414A (199)	++	++	++	nd
	HCV (aa407-419)	T411A (201)	+++++	-	nd	nd

observed increased ATPase activity, decreased ssRNA binding activity, and no helicase unwinding activity for HCV mutation, T411A (201). These results suggested that residue T411 is critical for NS3 helicase functions similar to the other ssRNA interacting residues. The last mutation, G414A in DENV2 Motif V, is different than the rest of the mutations because it is located near the ATP binding pocket. Previous biochemical results indicated decreased ATPase, RTPase, and helicase unwinding activities suggesting that G414A may be critical for the communication between the two binding pockets (199). The G414A mutation in DENV2 Motif V is the first mutation that begins to address the how the active sites are linked together.

Thus far, both sets of mutational studies have provided evidence that helicase unwinding activity requires ATP hydrolysis and that specific residues in the RNA binding cleft directly interact with ssRNA. However, the NS3 helicase field still lacks the understanding of how the ATPase and helicase unwinding activities are linked together. Previous computational studies implemented molecular dynamic simulations of DENV4 NS3 helicase to begin investigating how the ATPase activity is linked to helicase unwinding activity (203). Davidson *et al.* simulated various substrate states of NS3 helicase to determine how the structure has changed over the course of the ATP hydrolysis cycle (203). Analyses from these simulations provided molecular level insight into what regions of the helicase were undergoing conformational changes due to the presence of bound substrates during ATP hydrolysis. One of the findings that came from these simulations was the correlated movements of Motif V to the ATP binding pocket and the RNA binding cleft (203). These results suggested that Motif V may act as a central communication hub within an allosteric pathway between the two active sites. The research presented in this dissertation will focus on investigating the role of NS3 helicase Motif V in flaviviruses, so that we have a better understanding of the linkage between the ATPase active site and the helicase unwinding active site. Some of the questions that will be addressed include: 1) what residues in Motif V are critical for NS3 helicase functions, 2) what influence do

these residues have on NS3 helicase structure, and 3) how are these residues playing a role in viral genome replication and infection in cell culture, and also dissemination in mosquitoes? To probe these questions, three approaches will be utilized: virology, enzymology, and molecular dynamic simulations. Each approach will provide insight into a different aspect of the flavivirus NS3 helicase structure/function relationship. The goal of this dissertation is to not only provide insight into how the ATPase and helicase unwinding active sites are connected but also to provide the fundamental research required for targeted drug and anti-viral therapeutic development. Before diving into the findings of this research, the concepts of the three disciplines will be discussed within Chapter 2 allowing all readers to have a basic understanding of the results presented throughout the dissertation.

CHAPTER 2 – TECHNIQUES FOR STUDYING VIRUSES AT THE ORGANISM, VIRUS/CELLULAR, AND PROTEIN LENGTH SCALES

Targeted drug and antiviral therapeutic development requires understanding the mechanism of how flaviviruses replicate within cells. One of the key components of the replication complex is the flavivirus NS3 helicase, which is responsible for unwinding the genomic replicative form in an ATP-dependent manner during viral genome replication. However, the allosteric mechanism of how ATP hydrolysis powers helicase translocation and unwinding and its influence on overall viral genome replication is not well understood. Previous studies have suggested that NS3 helicase Motif V is central to the allosteric pathway between the ATP binding pocket and the RNA binding cleft (199, 203). Some of the interesting questions regarding this specific motif include: 1) how are viral infection in mosquitoes/cells and viral genome replication kinetics in cells controlled and modulated by NS3 Motif V; 2) which Motif V residues influence helicase unwinding, ATPase and RNA binding activities; and 3) how do molecular-level interactions in Motif V modulate its function? These questions necessitate multiscale insight into how Motif V plays a role in the allosteric pathway during flaviviral genome replication, and thus requires the bridging of different techniques that span the following length scales: organism, virus/cellular, and protein. Within these length scales, there are many techniques commonly used to investigate viral infected organisms, viral infected cells, and the structure-function relationship of viral proteins. A select number of techniques were chosen to address the above questions and are discussed here within this chapter to provide a fundamental understanding of the basic principles behind those techniques.

Overview of Techniques for Studying Viruses in Organisms and Cells

Studying viruses at the organism and virus/cellular length scales requires the expertise of virologists who typically asked very broad (macroscopic level) scientific questions regarding

aspects such as viral infection, viral replication, evading host cell degradation, viral spread and transmission, and disease caused by viruses. These macroscopic level questions include: 1) what is the genome organization of viruses; 2) how do viruses replicate inside the vector or host; 3) how infectious are viruses in humans and in animals; 4) what are the vectors that transmit viruses; 5) how are viruses transmitted between vector and host; and 6) what are the diseases that result from viral infections? This dissertation investigates a number of these questions with regards to how flavivirus NS3 helicase Motif V mutations affect viral infection and replication in mosquitoes and cells. At the organism length scale, a West Nile virus (subtype Kunjin) infectious clone is utilized to probe the effects of Motif V mutations on viral infection, dissemination, and transmission in mosquitoes. A Kunjin infectious clone consists of all eleven viral proteins, structural and nonstructural, for the virus to effectively infect cells, propagate, and spread to new cells within a mosquito organism. At the virus/cellular length scale, the Kunjin infectious clone mentioned above and a Kunjin sub-genomic viral replicon is utilized to examine the effects of viral replication kinetics and viral genome replication kinetics in cells. Typically, sub-genomic viral replicons contain all the required replication machinery for viral replication, but lack the structural proteins required for assembly and cell exit (204). For flaviviruses, like Kunjin, the sub-genomic replicon contains all the nonstructural proteins and a fragment of the capsid protein for replication, but lacks the membrane and envelope proteins for transmission.

Infection, dissemination, transmission, viral replication kinetics, and viral genome replication kinetics experiments all require either quantitative or qualitative post-analysis techniques for determining the viral contents present in any one given sample. Viral contents include viral proteins, viral genomes, or viral particles. The quantitative techniques for determining the viral proteins in a sample include western blots and enzyme-linked immunosorbent assays (ELISA). The amount of viral genome from an infectious clone is determined through either quantitative PCR (qPCR) for DNA genome based viruses or reverse transcribed quantitative PCR (RT-

qPCR) for RNA genome based viruses. The amount of viral genome from a sub-genomic viral replicon is determined through a luciferase-based assay. Orthogonal to qPRC and RT-qPCR, the amount of virus in a sample (viral titer) is determined qualitatively through either a plaque assay or a focus forming assay (Figure 2.1A) (205). The work performed at the organism and virus/cellular length scales presented in this dissertation utilized the following post-processing techniques: plaque assay, focus forming assay, and luciferase assay. The concepts of plaque assays, focus forming assays, luciferase assays are discussed in the following subsections.

Concepts Behind Plaque Assays and Focus Forming Assays

Plaque assays and focus forming assays are common techniques used for determining the viral titer post sample collection in an experiment investigating viral infection, dissemination, transmission in mosquitoes and viral replication kinetic experiments in cells. Both of these assays are also utilized for determining the viral titer of a new viral sample in the lab. Knowing the viral titer is essential for the design and execution of any of the experiments mentioned above. The viral titer provides a way to control how many viral particles per number of cells are present during any one given experiment, whether it be in mosquitoes or in cell culture. Regardless of the situation, plaque assays and focus forming assays start in the same way with preparing 10-fold dilutions of a virus sample with an unknown viral titer. The 10-fold dilutions are applied to monolayer cells (i.e. Vero cells) and incubated for a short period of time to allow for viral attachment to cells. After virus attachment, agar is applied to restrict the spread of new viruses to only neighboring cells during a second, longer incubation period. As the viruses infect neighboring cells, the cells produce viral antigens and eventually die due to increased cytotoxicity within the cells leaving behind a clearing amongst the monolayer of cells. As the second incubation ends, the cells are processed either by plaque assay or focus forming assay to determine the viral titer. In a plaque assay, crystal violet is used to stain the healthy cells so any clearings left behind by the death of any viral infected cells is highlighted by crystal violet

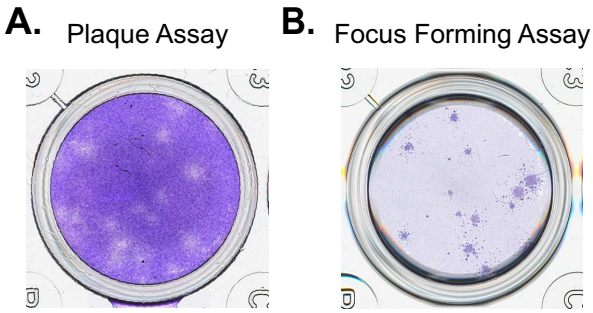

Figure 2.1. Visual of plaques and foci from viral titer assays. A) Plaques, clearing of virus infected cells, from a 3-day incubation plaque assay. B) Foci, zone of virus infected cells, from a 3-day incubation focus forming assay.

(Figure 2.1A). The viral titer is determined by counting the number of plaques present. In focus forming assays, a primary antibody against viral antigen is utilized to detect intact-live virus infected cells. A secondary antibody tagged with horseradish peroxidase (HRP) binds to the primary antibody. Then, 3,3',5,5'-Tetramethylbenzidine (TMB) reacts with HRP causing the virus infected cells to turn purple also known as foci (Figure 2.1B). The viral titer is determined by counting the number of foci.

Focus forming assays are typically more sensitive than plaque assays because viral antigen is detected, not cellular death. Plaques are sometimes extremely difficult to identify because the zone of clearing are too small or not well defined. The incubation period for forming plaques could be extended, but aging media for too long can result in an increasingly acid environment causing uninfected cells to die as well. Thus, using a more sensitive assay, like the focus forming assay, is more accurate in determining the viral titer. Plaque assays and focus forming assay are used widely throughout virology in addition to determining the viral titer of a new viral stock. Of the experiments presented in this dissertation, the infection, dissemination, and transmission experiments in mosquitoes and the viral replication kinetic experiments in cell culture utilize plaque assays and focus forming assays to determine the viral titer of samples at various time points within both organism and virus/cellular length scales.

Concepts Behind Luciferase Assays

Luciferase assays are another widely used technique for determining the genome replication levels within transfected cells. This assay utilizes a sub-genomic viral replicon system designed to introduce a reporter gene, like luciferase, in the place of the structural proteins to allow for expression of a bioluminescence enzyme after viral replication has occurred in the transfected cells. The modified sub-genomic replicon is then placed in a DNA plasmid that is transcriptionally controlled by a cytomegalovirus (CMV) promoter, which enables the replicon to

be launched in cells from DNA instead of RNA (204). By using a DNA-launched system, the very challenging procedure of purifying capped sub-genomic RNA is avoided. Ultimately, this modified sub-genomic replicon based system allows scientists to track how well a virus can replicate within cells through the measurement of the bioluminescence signal of luciferase. As viral replication occurs within cells, the sub-genomic RNA is translated into luciferase and viral proteins. Luciferase enzyme will accumulate in transfected cells. In an end-point assay, luminescence measurements can be obtained with the addition of the luciferase substrate, D-luciferin, after breaking open the cells releasing the luciferase into the media. The observed luminescence signal of luciferase is indictive of the amount of viral genome replication within the transfected cells. The viral genome replication experiment is closely related to enzymatic activity experiments discussed in the next section.

Overview of Techniques for Studying Viral Protein Function and Structure

Studying viruses at the protein length scale requires purifying viral proteins in an isolated environment to study their structure-function relationship. For studying at the protein length scales, scientists ask microscopic and atomistic level scientific questions, all revolving around how the structure of a protein relates to its functions. These molecular level questions include: 1) what is the structure of the protein of interest; 2) how many domains and subdomains are found within the protein; 3) what structural regions of the protein are critical for enzymatic activity; 4) within those structural regions, what residues are essential for function; and 5) how do mutations to those residues affect protein function? This dissertation probes several of these questions regarding what flavivirus NS3 helicase Motif V residues are critical for enzymatic function and how do they influence NS3 helicase function and overall pathogenesis of flaviviruses (previously described). At the protein length scale, a dengue 4 virus NS3 helicase is isolated to examine the structural dynamics and enzymatic function of NS3 helicase.

Proteins are complex macromolecules, and thus research at the protein length scale probes both the function and structure of a protein. The techniques for investigating the function and structure of a protein include enzymatic activity assays, protein x-ray crystallography, protein NMR, cryogenic-electron microscopy (cryo-EM), and molecular dynamics (MD) simulations. Several enzymatic activities assays are utilized in this dissertation to probe helicase unwinding activity, ATP hydrolysis activity and RNA binding activity of NS3 helicase. The other techniques (crystallography, NMR, cryo-EM, and MD simulations) are all used to probe the molecular level insight into the structure of a protein. Crystallography, NMR, and cryo-EM are specifically used for determining the structure of a protein. However, these techniques are constrained to only providing structural information due to the static nature of the resulting protein structure. Whereas, MD simulations utilize the resulting structure from the other structural techniques to investigate the dynamics of a protein. MD simulations provide mechanistic insight into how a protein fluctuates in physiological conditions and thus is comparable to enzymatic activity assays. The work performed at the protein length scale within this dissertation utilizes several enzymatic activity assays as well as MD simulations to investigate the relationship between NS3 helicase function and its structure. The concepts behind the enzymatic activity experiments and MD simulations are discussed in the following subsections.

Concepts Behind the Enzymatic Activity of Proteins

For studying viral proteins in enzymatic activity assays, the viral proteins of interest must be isolated from the viruses themselves or purified from bacterial or mammalian cells. Typically, viral proteins are purified from bacteria or mammalian cells because isolating the target viral protein from an infectious sample requires molecular tags that could potentially kill the virus. If the viral infection never establishes, then the target protein cannot be extracted for protein purification. Thus viral proteins are purified through a DNA launched plasmid that is codon optimized for expression in either bacterial cells or mammalian cells. Specifically, the purification

of recombinant (isolated) flavivirus NS3 helicase protein presented in this dissertation is purified via an *E. coli* codon optimized expression DNA plasmid. The DNA expression plasmid contains the isolated NS3 helicase gene tagged with six histidine residues that is under the control of an upstream T7 polymerase promoter region. Once the *E. coli* are in the exponential growth phase, the addition of isopropyl β-D-1-thiogalactopyranoside (IPTG) induces the expression of NS3 helicase. This expression happens because IPTG causes the dissociation of the lac repressor from the lac operon, allowing for the T7 RNA polymerase to initiate transcription and translation of NS3 helicase. After NS3 helicase expression, the bacterial cells are lysed open and the protein is purified via a series of affinity and size exclusion columns. After protein purification, the recombinant NS3 helicase is subjected to the following enzymatic activity assays: helicase unwinding activity, ATP hydrolysis activity, and RNA binding affinity activity.

The helicase unwinding activity assay probes the ability of flavivirus NS3 helicase to translocate and unwind the replicative form during viral replication in a molecular-beacon based assay (206, 207). In the molecular-beacon based unwinding activity assay, three nucleic acid strands (oligos) are annealed together to generate a double-stranded RNA complex (Figure 2.2). The larger RNA oligo is a complementary template strand that binds both the RNA oligo tagged with an Alexa-488 fluorophore and a DNA oligo tagged with a quencher for Alexa-488. When the smaller oligos are bound to the template strand, the fluorescence is quenched, but when they are unbound, the oligos form a hairpin structure that cannot rebind to the template strand. This double-stranded RNA complex is preincubated with Mg^{2+} and purified NS3 helicase, all of which are held at a constant initial concentration in each reaction. Multiple reactions are performed at increasing concentrations of ATP since helicase unwinding activity is ATP-dependent. During each reaction containing ATP, the flavivirus NS3 helicase unwinds the double-stranded RNA complex, releasing the tagged oligos from the template strand. Once the tagged oligos are unbound from the template stand, an increase in fluorescence is observed over time because

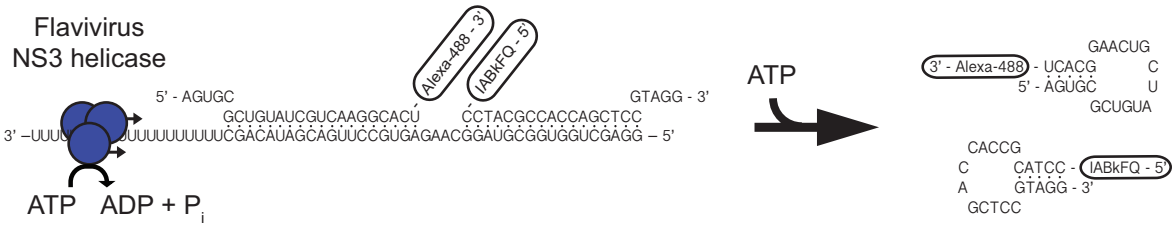

Figure 2.2. Mechanism of Flavivirus NS3 helicase unwinding activity assay. The double-stranded RNA complex is unwound in an ATP-dependent manner. The Alexa-488 tagged RNA oligo is quenched by the Iowa black fluorescence quencher when in complex with the template strand. As helicase unwinding occurs, the two smaller oligos are released from the template strand forming hairpin structures seen on the right. These hairpin structures cannot rebind to the template strand allowing for fluorescence to increase as the helicase continues to unwind double-stranded RNA complex.

the Alexa-488 fluorophore is not quenched. The progress curves are subjected to nonlinear regression fits to calculate the initial observed rate of reaction (k_{obs}) for each curve. Then, k_{obs} values are plotted against ATP concentration and fit to the Michaelis-Menten equation (Equation 2.1),

$$\nu = \frac{(V_{max}[S])}{(K_M + [S])}, \quad (2.1)$$

where $\mathrm{V_{max}} = \mathrm{k_{cat}[E]_t}$, ν is the velocity, k_{cat} is the apparent first-order rate constant in s^{-1}, $[E]_t$ is the concentration of the enzyme, $[S]$ is the concentration of the ATP substrate, K_M is the concentration of the substrate at one-half k_{cat}. The Michaelis-Menten constant (K_M), turnover rate (k_{cat}), and the specificity constant (k_{cat}/K_M) are determined from fitting to Equation 2.1. By fitting to Equation 2.1, we are assuming that the conversion between enzyme-substrate complex to enzyme plus product is fast and irreversible. We are also assuming that the enzyme-substrate complex is in thermodynamic equilibrium with free enzyme and substrate. Because of these assumptions, we are able to fit to the Michaelis-Menten equation. The kinetic values determined from Equation 2.1 represent how fast a helicase enzyme functions in relation to other helicases within a cell. This is valuable information because knowing the kinetics of a native enzyme enables us to compare mutations to that enzyme providing how the structure relates to function. This concept extends to the other biochemical assays as well.

The unwinding activity of NS3 helicase is ATP hydrolysis dependent. NS3 helicase ATP hydrolysis activity is measured through a colorimetric ATPase activity assay based off of the RNA helicase assay (207). The contents of the reactions remained the same; however instead of measuring the fluorescence of Alexa-488, the absorbance at 650 nm is measured in an end-point assay. The reactions are stopped sequentially by the addition of BIOMOL Green that binds inorganic phosphate, a byproduct of ATP hydrolysis. When BIOMOL Green binds inorganic phosphate, a color change occurs. As more inorganic phosphate accumulates in the

solution due to increasing rates of ATP hydrolysis, the color change intensifies. Initial rates of reaction are determined from the progress curves generated by the end-point reactions. Data are then fit to the substrate inhibition equation (Equation 2.2),

$$v = \frac{(V_{max}[S])}{\left(K_M + [S]\left(1 + \frac{[S]}{K_i}\right)\right)}, \qquad (2.2)$$

where K_i is the inhibition constant. From the fit, the k_{cat}, K_M, k_{cat}/K_M and the K_i are determined for the ATPase assay. These kinetic values provide insight into how quickly hydrolysis occurs within helicases and are comparable to other purified helicases.

RNA binding affinity is another activity of NS3 helicase that is measurable through an activity assay. In RNA binding affinity assays, a single-stranded RNA oligo tagged with a fluorophore, like Alexa-488, is utilized for binding helicases. Typically, RNA binding affinity assays measure the fluorescence polarization of fluorophores. Before binding occurs, the RNA tagged with fluorophore is tumbling freely and quickly in solution. After binding occurs, the fluorophore is tumbling more slowly in solution because the helicase has a slower rate of tumbling compared to a smaller molecule. Due to this differentiation, the fluorescence polarization signal increases as more of the fluorophore begins to bind to NS3 helicase. A number of reactions are performed with increasing concentrations of NS3 helicase. As the concentration of helicase increases the fluorescence polarization increases, and these values are plotted against each and fit to a nonlinear regression resulting in the binding affinity or K_d of NS3 helicase to single-stranded RNA.

All three of the enzymatic activity assays discussed in this subsection all have limitations associated with them. Due to the fact that the enzymes are purified and suspended in a buffered solution to keep them stable, the enzymes may function differently in this artificial system than in their natural state within a cell. In cells, the enzymes interact with many different biomolecules,

so the functions observed in the enzymatic activity assays are not reality. Regardless, when residues are mutated from wild-type, the activities of the mutant NS3 helicase are comparable with the wild-type helicase. From these mutational studies, hypotheses are formed about how these select residues influence NS3 helicase functions, but the structural dynamics of the helicase is still not well understood.

Concepts Behind Molecular Dynamics Simulations of Proteins

Investigating the structural dynamics of flavivirus NS3 helicase necessitates the use of MD simulations. MD simulations propagate the atomic positions of the modeled protein structure over time by numerically solving Newton's equations of motion. The potential energy of non-bonded interactions within the structure is defined by the molecular mechanics Hamiltonian,

$$H(r^N) = \sum_{i,bonds} \frac{k_i}{2}(r_i - r_i^\circ)^2 + \sum_{j,angles} \frac{k_{j,\theta}}{2}(\theta_j - \theta_j^\circ)^2 + \sum_{l,torsions} \frac{k_{l,\emptyset}}{2}(1 + \cos(n_l \emptyset_l - \delta_l)) +$$

$$\sum_{i<j} 4\varepsilon_{ij}\left[\left(\frac{\sigma_{ij}}{r_{ij}}\right)^{12} - \left(\frac{\sigma_{ij}}{r_{ij}}\right)^{6}\right] + \sum_{i<j} \frac{q_i q_j}{4\pi\varepsilon_0 r_{ij}}, \qquad (2.3)$$

where k_i, r_i°, $k_{j,\theta}$, θ_j°, $k_{l,\emptyset}$, n_l, δ_l, ε_{ij}, σ_{ij}, and q_i represent the force field parameters. The first term in Equation 2.3 is a sum over harmonic potentials each with force constant k_i that defines the interaction between covalently bonded pairs of atoms at a minimum energy value of r_i°. The second term is the sum of valence angles described by the harmonic potential with force constant $k_{j,\theta}$ and equilibrium value θ_j°. A valence angle is the angle between three atoms A, B, C where A and C are bonded to B. The third term is the torsion potential, describing the energy that rotates around a central bond. The fourth and fifth terms are non-bonded terms describing the van der Waals interactions through a Lennard-Jones potential and the electrostatic interactions through a Coulomb potential, respectively. These non-bonded terms are calculated between all pairs of atoms that are separated by at least three bonds within the same molecule or in different molecules completely. Force fields are optimized to accurately predict the potential energy of specific molecules (208). There are different force fields for each of the

following macromolecules: proteins (ff14SB, CHARMM36, GROMOS-87), nucleic acid (DNA.OL15 for DNA; RNA.OL3 for RNA), lipids (lipid17), carbohydrates (GLYCAM), and small molecules (GAFF). These force fields are available through a variety of software packages including AMBER(209), CHARMM(210, 211), GROMACS(212), and OPLS(213, 214), and NAMD(215).

MD simulations presented in this dissertation are focused on flavivirus NS3 helicase solvated in salt water to mimic physiological conditions. These simulations utilize the following force fields within the AMBER software package: ff14SB for proteins, RNA.OL3 for RNA, and GAFF for small molecules (209, 216). The simulations undergo a minimization, heating, and equilibration process before production runs are performed. During minimization, there are two steps performed; the first step applies harmonic restraints on all solute atoms allowing for only the protein to move into an optimal starting structure. The second step removes the harmonic restraints allowing for all atoms to move into a stable starting structure. Following minimization, the system is heated to physiological temperatures (310.0 K) with a harmonic restraint on all solute atoms. After heating, the harmonic restraints are removed slowly over a series of 5 equilibration steps. Once the harmonic restraints are removed, the protein system is in the production run phase, but the system may not be fully equilibrated. Therefore, after collecting approximately 500 ns of data, a root mean square deviation calculation is performed to analyze if the simulation is still in equilibration. The equilibration portion is removed from the interpreted data presented in this dissertation. On average, the flavivirus NS3 helicase simulations were simulated for a total of 1 μs using a NVIDIA GPU taking approximately 3-4 weeks in real time per run. The resulting raw data from these simulations contain the coordinates of all the atoms in a given system written out to a file at specific intervals over the course of the simulation. The raw data represents the microscopic ensemble of the system. Analyses of the raw data convert the microscopic ensemble to a macroscopic observable. The macroscopic

observables provide insight into the structural dynamics of the target protein. Several analyses were designed to probe the structural dynamics of flavivirus NS3 helicase during helicase unwind activity and ATP hydrolysis activity. These analyses include the probability of finding a lytic water in the ATP binding pocket and the projected covariance magnitude of Motif V residues on the helical gate within NS3 helicase. Analyses performed on the MD simulations in conjunction with the results from the enzymatic activity assays provide insight into the structure-function relationship of NS3 helicase. The concepts behind the analyses performed on the MD simulations presented in this dissertation are discussed within this subsection.

The ATP hydrolysis activity occurs within the ATP binding pocket of flavivirus NS3 helicase. In the previous subsection, the ATP hydrolysis activity assay probed the ability for NS3 helicase variants to hydrolyze ATP via an absorbance observable. To obtain mechanistic insight into how the structure of NS3 helicase mutants influence the ATP hydrolysis active site, the MD simulations were analyzed for the probability of finding a lytic water within the ATP binding pocket. A lytic water is defined by three collective variables. These collective variables are (1) the nucleophilic attack distance of less than 5 Å between the ATP γ-phosphorous atom and the water oxygen atom, (2) the nucleophilic attack angle of greater than 160 degrees between the terminal phosphoanhydride bond of ATP and the water oxygen atom, and (3) the dipole moment angle of greater than 90 degrees between the water molecule's dipole moment vector and the terminal phosphoanhydride bond of ATP. The first two metrics describe the geometric positioning of water within the hydrolysis active site, and the third metric describes the chemically relevant orientation of water to its nucleophilic attack on the terminal ATP phosphate group. The lytic waters described by these collective variables are identified throughout the entire simulation, and thus the probability of finding a lytic water is determined. The probability of a lytic water is then compared to the results obtained from the ATP hydrolysis activity assay described in the previous subsection. Together, the results from the

lytic water analysis and the ATP hydrolysis activity assay provide molecular insight into the function-structure relationship of NS3 helicase. Similar comparisons are made for the helicase unwinding activity of NS3 helicase.

Recall that NS3 helicase unwinding activity is ATP hydrolysis dependent suggesting the presence of an allosteric pathway between the ATP binding pocket and the RNA binding cleft within NS3. In the previous subsection, the helicase unwinding activity assay examines the overall ability of NS3 helicase variants to unwinding a double-stranded RNA complex via a fluorescence observable. However, this assay is limited to investigating the function of NS3 helicase without providing details into how the structural dynamics influence the allosteric pathway leading to helicase unwinding activity. Analysis of MD simulations provides a way to probe the allosteric effect of a NS3 helicase Motif V mutant via determining how the mutation has perturbed the energy transduction pathway between the ATP binding pocket and the RNA binding cleft. The analysis designed to investigate the coupling between the two substates pockets is known as the projected covariance magnitude (Equation 2.4),

$$Projected\ Covariance\ Magnitude = \| C_{ij} \cdot \hat{P} \|, \qquad (2.4)$$

where C_{ij} is the covariance matrix tensor, and $\hat{P}$ is the unit vector along the translocation direction; and the covariance matrix tensor is described by Equation 2.5,

$$C_{ij} = \langle (x_i - \langle x_i \rangle)(x_j - \langle x_j \rangle) \rangle, \qquad (2.5)$$

where x_i is position of particle i; $\langle x_i \rangle$ is the average position of particle i; x_j is position of particle j; and $\langle x_j \rangle$ is the average position of particle j. The covariance matrix tensor is dotted with the unit vector, and then the magnitude is determined by taking the Frobenius norm of those results. In other words, the projected covariance magnitude represents the fluctuation between source residues and sink residues projected onto a vector in a different plane. In this dissertation, the analysis is utilized to probe how the residues within NS3 helicase Motif V influence the entrance to the

RNA binding cleft at the helical gate. Recall that the helical gate is responsible for separating the double-stranded RNA intermediate into two single-stranded RNA molecules and thus is the first step in the unwinding of the replicative form during viral replication (168). For this analysis, three residues were chosen, one source residue (G414), and two sink residues (S364, K366). G414 is located within NS3 helicase Motif V, and coordinates with the lytic water within the ATP binding pocket (203). S364 and K366 span the helical gate entrance between subdomain 2 and subdomain 3, and both residues were determined to have a large magnitude covariance with G414. The covariance tensors between G414-S364 and G414-K366 are dotted into the helical gate open/closing vector to obtain how the fluctuation perturbs the opening/closing of the helical gate. Reduced magnitudes between source and sink residues represent a negative effect on helical gate dynamics, while increased magnitudes represent a positive effect. Once the results of the projected covariance magnitude are determined, they are compared against the results from the helicase unwinding activity assay.

Both the probability of finding a lytic water and the projected covariance magnitude provide molecular information about simulations and are able to be compared with biochemical activity data. However, the comparison between simulation and experiments are sometimes challenging to achieve because in experiments the state of the protein of interest is not controllable. In experiments, the unbinding and binding events of substrates are macroscopically observed; the events happen very quickly, if they ever happen. The molecular level insight into how the substrate interacts with protein cannot be observed in a biochemical assay. Whereas in simulation, the protein of interest is pre-bound with the desired substrates before the simulation even begins. The unbinding event of substrates may never be observed in a simulation because of the extremely short timescales. Due to this differentiation between simulation and experiment, the results are not easily comparable between the two techniques. Regardless of this challenge, simulation analyses provide

molecular level insight into how residues within enzymes play a role in maintaining enzyme structure. These analyses are compared with experiments to elucidate how the structure of an enzyme relates to its function. This comparison is important because if we only relied on biochemistry experiments, we would not learn about the dynamic information pertaining to the structure of an enzyme and how it relates to the function. We need both fields to understand the structure-function relationship fully. Using assays in combination with virology and computational chemistry, we can get an entire picture of how structure relates to function which in turn relates to viral infection.

CHAPTER 3 – MOTIF V REGULATES ENERGY TRANSDUCTION BETWEEN THE FLAVIVIRUS NS3 ATPASE AND RNA-BINDING CLEFT[1] (217)

Overview

The unwinding of dsRNA intermediates is critical for the replication of flavivirus RNA genomes. This activity is provided by the C-terminal helicase domain of viral nonstructural protein 3 (NS3). As a member of the superfamily 2 (SF2) helicases, NS3 requires the binding and hydrolysis of ATP/NTP to translocate along and unwind double-stranded nucleic acids. However, the mechanism of energy transduction between the ATP- and RNA-binding pockets is not well understood. Previous molecular dynamics simulations conducted by our group have identified Motif V as a potential "communication hub" for this energy transduction pathway. To investigate the role of Motif V in this process, here we combined molecular dynamics, biochemistry, and virology approaches. We tested Motif V mutations in both the replicon and recombinant protein systems to investigate viral genome replication, RNA-binding affinity, ATP hydrolysis activity, and helicase-mediated unwinding activity. We found that the T407A and S411A substitutions in NS3 reduce viral replication and increase the helicase unwinding turnover rates by 1.7 and 3.5 respectively, suggesting that flaviviruses may use suboptimal NS3 helicase activity for optimal genome replication. Additionally, we used simulations of each mutant to probe structural changes within NS3 caused by each mutation. These simulations indicate that Motif V controls communication between the ATP-binding pocket and the helical gate. These results help define the linkage between ATP hydrolysis and helicase activities within NS3 and provide insight into the biophysical mechanisms for ATPase-driven NS3 helicase function.

Introduction

Arthropod-borne flaviviruses, such as yellow fever virus, Japanese encephalitis virus, Zika virus,

[1] This chapter is from reference (217). Kelly E. Du Pont contributed to everything.

West Nile virus (WNV), and dengue virus, are a major health concern in the tropical and subtropical regions of the world (15, 17). Infection from these viruses cause disease symptoms ranging from flu-like illness to encephalitis, hemorrhagic fever, coma, and potentially death (218). Over half of the world population is at risk for infection from one or more of these viruses (7, 8). Dengue virus, specifically, infects around 50 million people each year, and of those individuals, 20,000 contract dengue hemorrhagic fever leading to their mortality (219). Additionally, WNV over the past 20 years within the 48 continental United States has around 50,000 clinical infections with a 5% mortality rate (9, 220) (and see https://www.cdc.gov/westnile/statsmaps/index.html (accessed September 12, 2019)). Currently, there are no approved antiviral drugs for treating flaviviral infections and the vaccines in circulation, like the yellow fever vaccine, are not readily available worldwide for most flaviviruses (72, 74, 221). In order to develop new antiviral treatments (drugs and vaccines) for these viruses, a fundamental understanding of how these flaviviruses replicate is required.

Flaviviruses (*Flaviviridae* family) have a positive-sense single-stranded RNA (ssRNA) genome that is ~11 kb in length. The viral RNA genome is translated into a single polyprotein that is subsequently cleaved by host and viral proteases into three structural proteins (C, prM, and E) and eight nonstructural proteins (NS1, NS2A, NS2B, NS3, NS4A, 2K, NS4B, and NS5) (2, 160). The structural proteins contribute to the formation of mature viral particles, whereas the nonstructural proteins are responsible for replication of the viral genome and protecting the virus from attacks by the host cell innate immune system (160). Once the viral proteins are post-translationally processed, the positive-sense genomic ssRNA is used as a template to create a negative-sense anti-genomic RNA, forming a double-stranded RNA (dsRNA) intermediate complex (130, 222). The nascent negative-sense ssRNA serves as a template strand for producing new positive strand RNAs that can be packaged into viral particles, translated into new proteins, or interfere with the RNA decay pathway (223, 224). Therefore, the unwinding of

dsRNA intermediate to produce a free negative ssRNA for positive strand synthesis is a critical component for the replication of flavivirus RNA genomes (222). This function is achieved by the C-terminal helicase domain of NS3.

Helicases are ubiquitous enzymes that are classified into superfamilies based on their primary structure and highly conserved motifs (176, 225, 226). NS3 helicase (NS3h) is a member of superfamily 2 (SF2) helicases (170). The structure of NS3h consists of three subdomains; subdomain 1 and subdomain 2 are RecA-like structures that are highly conserved across SF2 helicases (227). The third subdomain is unique to the viral/DEAH-like subfamily of SF2 helicases and interacts with subdomain 1 and 2 to form the RNA binding cleft. NS3h is a multifunctional enzyme, possessing three enzymatic activities: RNA helicase, nucleoside triphosphatase (NTPase), and RNA 5'-triphosphatase (RTPase) (143–145, 175, 203, 228). Previous studies have shown that the two latter activities share a catalytic active site where NTP binds between subdomain 1 and subdomain 2 (141, 142, 145, 199). The RNA helicase active site is distinct from that of the NTPase/RTPase active site, located at the helical gate between subdomain 2 and subdomain 3 of NS3 (168, 181, 229). The helical gate and β-wedge are responsible for splitting the dsRNA intermediate into two ssRNA strands: the positive-sense viral ssRNA and the negative-sense template ssRNA (168). Single-molecule and structural biology studies have suggested that the negative-sense ssRNA template enters the RNA binding cleft, where the helicase utilizes the energy produced from the hydrolysis of one ATP molecule to power translocation and unwinding of the dsRNA intermediate one base at a time (130, 141, 169, 184–187, 222). A fundamental unanswered question within the SF2 helicase field is how ATP hydrolysis causes structural changes within the helicase to result in translocation and unwinding of dsRNA intermediates.

Between the ATPase active site and the RNA binding cleft, there are eight structural Motifs (I,

Ia, II, III, IV, IVa, V, and VI) that are highly conserved in the viral/DEAH-like subfamily of SF2 helicases (Figure 3.1) (170). These structural Motifs play a critical role in substrate binding and are responsible for enzymatic activities within the helicase. One of these Motifs, Motif V, was reported by Davidson *et al.*(203) as a potential link between the ATP-binding pocket and the RNA-binding cleft due to strong correlations between residues within Motif V and both binding pockets found within the helicase. Additionally, Mastrangelo *et al.*(229) reported that Motif V may be one of the main components of the driving force pulling the helicase along the ssRNA due to conformational changes initiated by the binding of ATP, which propagated through Motif V opening the helical gate. At least two residues within Motif V have direct interactions with either ATP hydrolysis active site or the bound ssRNA molecule. G414 coordinates with the lytic water found within the ATPase active site, and T408 interacts with the phosphate backbone of the bound ssRNA (203). In addition to these interactions, Motif V has strong coupling between the other highly conserved Motifs that interact with the ATP binding pocket and the RNA binding cleft suggesting that Motif V may be central to the communication between these two binding pockets (203, 230). Therefore, we investigated the role of Motif V as a critical link between the two binding pockets. We utilized a combination of all-atom molecular dynamics simulations, biochemical assays and virological assays to understand the role of Motif V in internal enzymatic communication leading to helicase function. Our results show residues within Motif V control not only the enzymatic activities of the helicase but also the ability for the flaviviruses to replicate *in vitro*. This is due to importance of the secondary structure of Motif V, as indicated through molecular dynamics simulation.

Results

Motif V Mutants Affect Viral Genome Replication

As previously discussed in Davidson *et al.*, Motif V may play a role in the communication between the ATP binding pocket and the RNA binding cleft/helical gate (203). As one of the

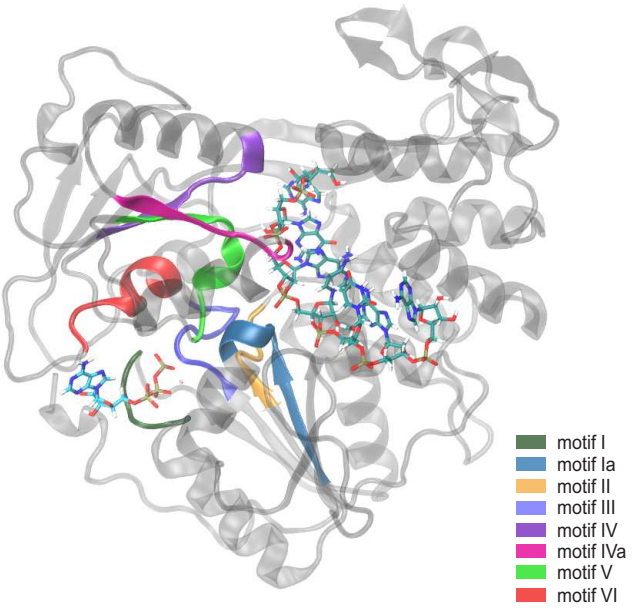

Figure 3.1. Eight structural motifs of Flavivirus NS3 helicases are highly conserved. The structural motifs (Motifs I, Ia, II, III, IV, IVa, V, and VI) are located between the ATP-binding pocket and RNA-binding cleft within the NS3 helicase structure (PDB code 2JLV). Each motif is highlighted as follows: Motif I in *dark green*; Motif Ia in *blue*; Motif II in *orange*; Motif III in *royal blue*; Motif IV in *purple*; Motif IVa in *magenta*; Motif V in *lime green*; and Motif VI in *red*.

highly conserved Motifs in SF2 helicases, Motif V consists of 13 residues spanning position 404 through position 416 (Figure 3.2A). Eight of these residues are 100% conserved across all flaviviruses, both mosquito and tick-borne (Figure 3.2B). The other five residues are highly conserved in flaviviruses that infect insects and mammals, and are more variable in tick-borne restricted flaviviruses (Table A.1). Interestingly, the conserved residues across all the flaviviruses interact with either the ssRNA or ATP substrates. These highly conserved residues include T408, D409, I410, E412, M413, G414, A415, N416. Of the mostly conserved residues, T407 and S411 mainly interact with each other through a hydrogen bond that is hypothesized to stabilize the α-helical secondary structure of Motif V (Figure 3.2C). The other mostly conserved residues, F404, V405 and V406, interact primarily with other hydrophobic residues in the surrounding area. Generally, all of Motif V interacts with either a bound substrate or other highly conserved Motifs that interact with bound substrate. Therefore, we investigated the importance of each residue in Motif V on viral replication.

We individually mutated every residue within NS3h Motif V in a luciferase-expressing WNV replicon system and determined replication efficiency for each mutant. Each Motif V mutation was designed to interrupt specific WT residue-residue interactions or residue-substrate interactions. As a negative control, D664 in the NS5 polymerase catalytic active site was mutated to valine (D664V) in order to disrupt viral genome replication (150, 231–233). Additionally, the NS3 mutants A286L (Motif II) and R387M (Motif IVa) were used as controls for ablating ATPase activity and RNA binding affinity, respectively (194, 198–200, 202, 234). The small hydrophobic sidechain of A286 interacts with other hydrophobic residues stabilizing Motif II interactions with bound ATP. By introducing a bulky hydrophobic residue with A286L, the Motif II interactions with ATP will be perturbed resulting in a disruption in ATP hydrolysis activity. The guanidium head group of R387 interacts with the phosphates of the RNA backbone. By removing the guanidium head group with R387M, important protein-RNA

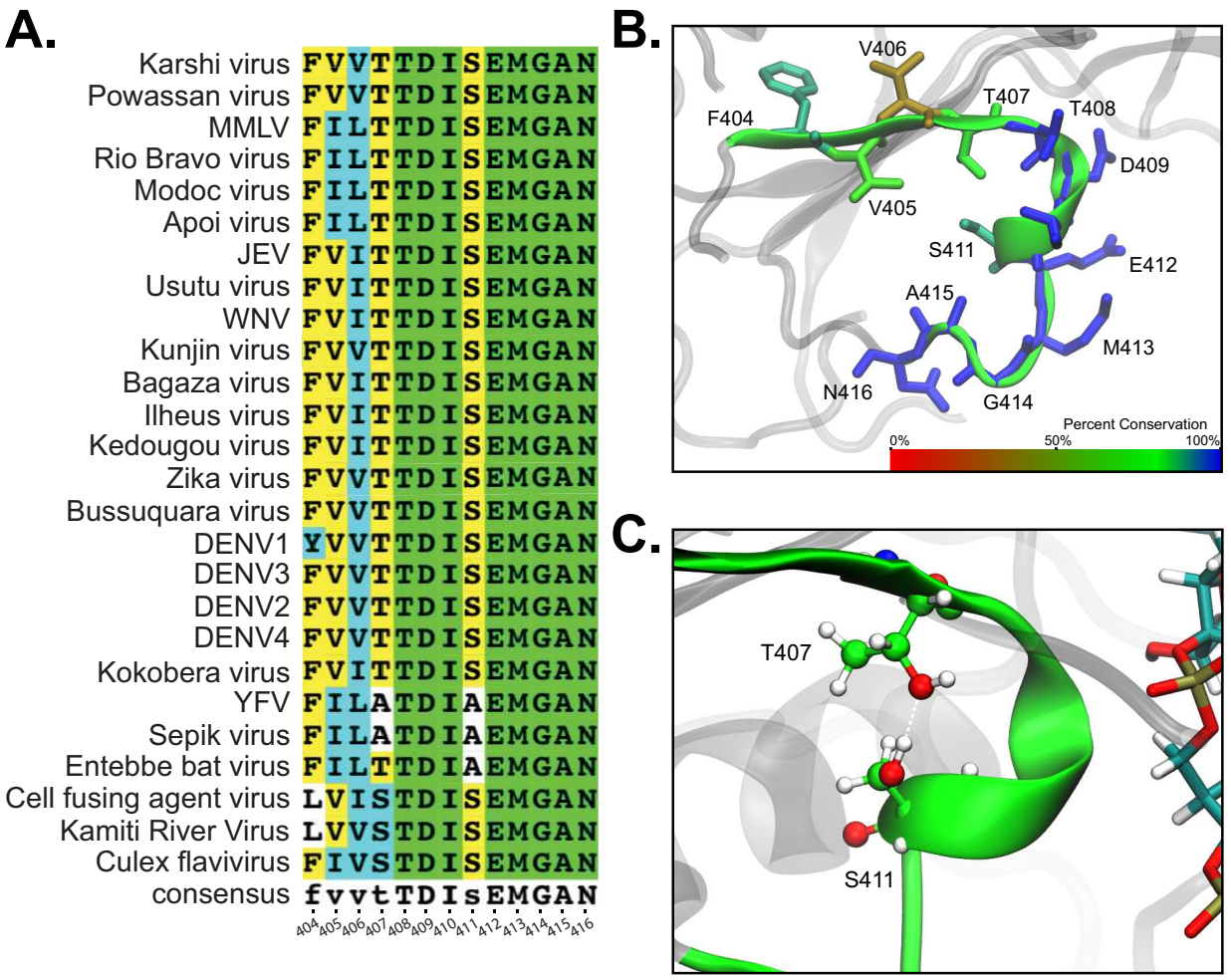

Figure 3.2. The majority of Motif V residues are highly conserved across all flavivirus NS3 helicases. A) the sequence of Motif V from all flaviviruses, multiple species and insect-restricted. B) the percentage conservation for each residue within Motif V is projected onto the secondary structure (PDB code 2JLV). The color bar ranges linearly from *red* (0.0% conserved) to *blue* (100.0% conserved). C) T407 and S411 interact through a hydrogen bond.

interactions will be interrupted. NS5 D664V and NS3 A286L and R387M ablated viral genome replication, as expected (Figure 3.3A). All of the Motif V mutants, except for V405M, V406M, T407A, T408S, S411A and A415G, ablated viral genome replication as well. V405M and T407A reduced replication to approximately 2.5%, whereas the I406M and A415G mutants reduce viral genome replication to less than 20%. T408S and S411A were approximately 48% and 39% active, respectively compared to WT NS3h. The results from the viral genome replication were projected onto the structure of Motif V (Figure 3.3B). We noted that residues with ablated viral replication consisted mostly of the highly conserved residues, suggesting that these highly conserved residues that interact with either the RNA or the ATP play an important role in viral replication. Interestingly, T408 and A415, both highly conserved residues, still maintain a reduced level of viral replication, suggesting that there may not be a direct correlation between residue conservation and effect on replication.

As mentioned before, residues T407 and S411 interact with each other through a hydrogen bond (Figure 3.2C). However, the T407A mutant nearly ablates genome replication while the S411A mutation only reduces genome replication by approximately 60%. Both mutations should disrupt the hydrogen bond, but T407A and S411A have significantly different replication levels suggesting that these two mutations have other interactions that potentially affect one or more of the NS3h functions during viral replication. These NS3h functions include the ability for the helicase to bind RNA, the ability to hydrolyze ATP, and the ability to unwind the dsRNA intermediate. Therefore, in order to determine whether or not these mutations have an effect on the individual helicase functions, we tested both T407A and S411A biochemically.

NS3 helicase Residues T407 and S411 Affect ATPase and Helicase Functions but not RNA Binding Affinity

We designed/adapted three biochemical assays to observe how the T407 and S411 mutations

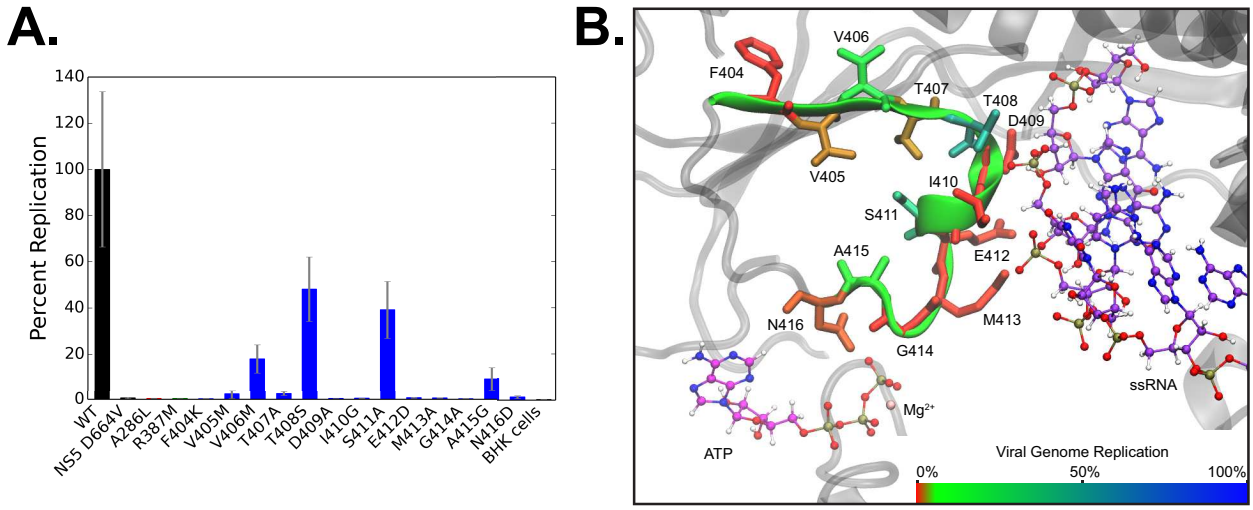

Figure 3.3. Mutations in Motif V negatively affect viral genome replication. A) mutations to remove specific interactions within the central location of Motif V between ATPase active site and the RNA-binding cleft were tested in viral genome replication. B) results from the viral genome replication were projected onto the structure of NS3 helicase Motif V (PBD code 2JLV) with the hydrogen bond highlighted between residues T407 and S411. The color bar ranges linearly from *red* (0% replication) to *blue* (100% replication). These data suggest that the hydrogen bond between Thr407 and Ser411 is important for viral genome replication. *Error bars,* S.E.

would affect the individual helicase functions. Recombinant WT, T407A, S411A, A286L (ATPase control) and R387M (RNA binding control) NS3h were purified and tested in an RNA binding affinity assay, an ATPase activity assay and a helicase unwinding activity assay. We used DENV4 NS3 proteins for this work due to established expression and purification protocols being in place (207) and the high degree of conservation between WNV and DENV in Motif V. To start, the RNA binding affinity of WT, T407A, S411A, A286L, and R387M were tested via a fluorescence polarization assay (235). Fluorescence polarization for a single-stranded RNA oligo labeled with an Alexa-488 fluorophore (5 nM) was measured as the NS3 helicase increased in concentration (Figure 3.4A). The binding affinity or K_d for WT NS3h was 1.9 ± 0.8 μM, while the K_d for R387M was 76.4 ± 31.0 μM (Table 3.1A). The R387M K_d was significantly different compared to WT, suggesting that R387M does not bind the ssRNA as well as WT. Additionally, a similar trend was observed for WT and A286L. On the other hand, T407A (2.0 ± 1.1 μM) and S411A (1.4 ± 0.2 μM) were not significantly different as compared to WT. This data suggests that neither the T407A and S411A mutations affected ssRNA binding to NS3.

We next investigated how these mutations affected NS3 ATPase activity. We utilized a colorimetric assay to observe ATP hydrolysis via inorganic phosphate production and release for WT, T407A, S411A, A286L and R387M (207). All reactions contained 50 nM NS3h, 5 nM dsRNA and increasing concentrations of ATP. Progress curves were obtained for each NS3h various ATP concentrations (Figure 3.4B). We noticed at the high concentrations of ATP a substrate inhibition over time. Therefore, we used the substrate inhibition equation to calculate the enzyme kinetics for the ATPase activity assay. The catalytic efficiency (k_{cat}/K_M) for A286L ($0.0033 \pm 0.0022 \times 10^{-3}$ $\mu M^{-1}s^{-1}$) was significantly reduced as compared to WT ($0.0672 \pm 0.019 \times 10^{-3}$ $\mu M^{-1}s^{-1}$). The twenty-fold decrease in catalytic efficiency was due to a significant increase in the Michaelis-Menten constant (K_M) for A286L (285.1 ± 150.5 μM) as compared to WT (17.3 ±

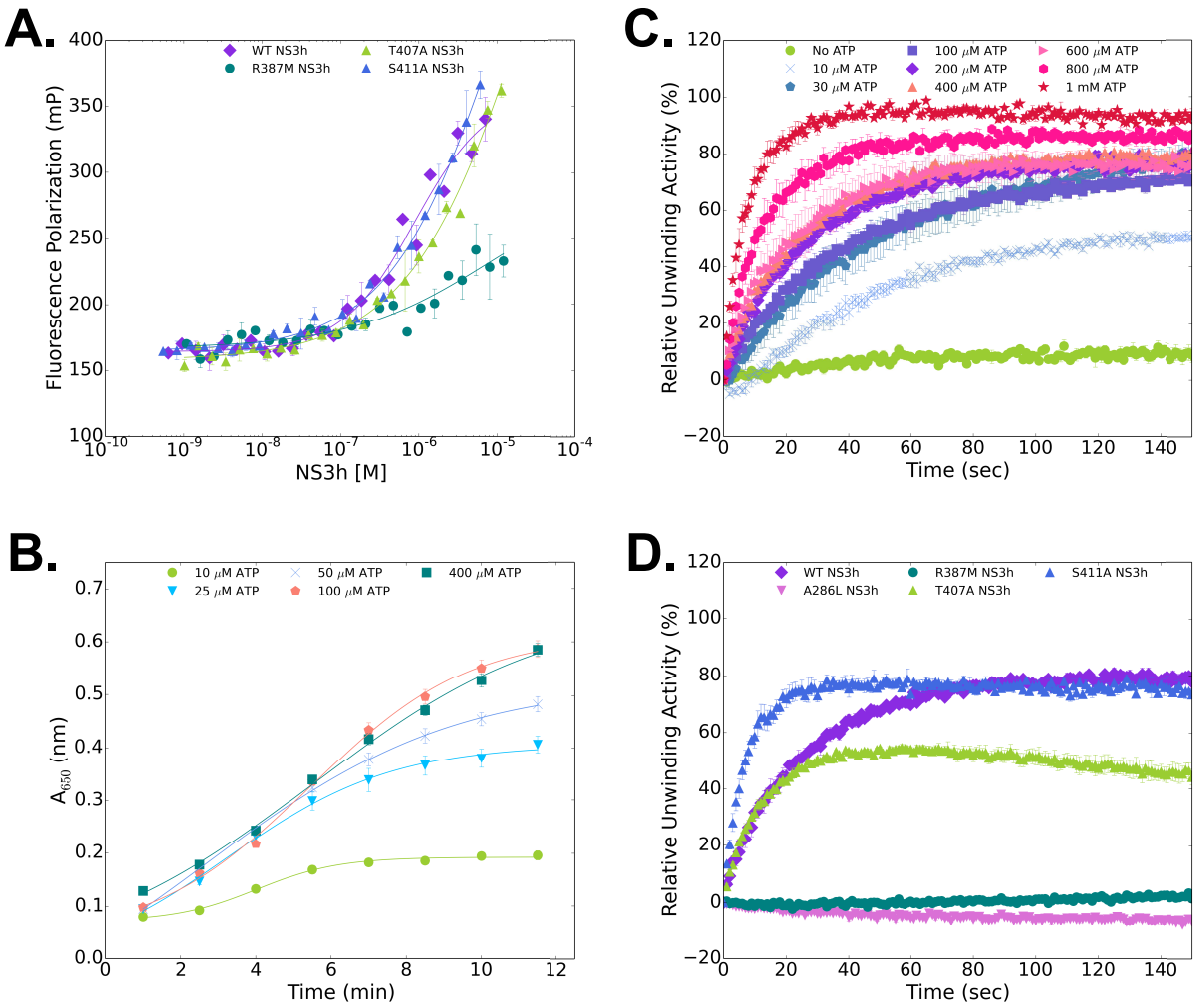

Figure 3.4. Experimental design of biochemical assays. A) RNA-binding affinity of NS3h was measured using fluorescence polarization of a single-stranded RNA (52). WT and NS3h variants are shown. B) ATPase activity was measured using BIOMOL Green absorbance at 650 nm over time. WT NS3h ATPase activity at five concentrations of ATP is shown here. C) RNA helicase-unwinding activity was measured by the increase of fluorescence over time. The WT NS3h data presented here are representative of the ATP-dependent unwinding activity obtained for each NS3h variant. D) WT, A286L, R387M, T407A, and S411A NS3h-unwinding activities were compared at 400 μM ATP. *Error bars,* S.E.

Table 3.1. Enzyme kinetics of WT, A286L, R387M, T407A and S411A NS3 helicase. A) K_d was determined from the RNA-binding affinity assay data. B) k_{cat}, K_m, and k_{cat}/K_m were determined for the ATPase activity assay through fitting the data to the substrate inhibition equation. C) k_{cat}, K_m, and k_{cat}/K_m were determined for the helicase-unwinding activity assay for each NS3h variant through fitting the Michaelis–Menten equation to the K_{obs} *versus* ATP concentration.

A. RNA Binding Affinity

NS3h variant	K_d (μM)	Fold Difference
WT	1.9 ± 0.8	
A286L	6.7 ± 0.4	3.5
R387M	76.4 ± 31.0	39.7
T407A	2.0 ± 1.1	1.0
S411A	1.4 ± 0.2	0.7

B. ATP Hydrolysis Activity

NS3h variant	k_{cat}(s^{-1})	K_M (μM)	k_{cat}/K_M ($\mu M^{-1}s^{-1}$)
WT	1.2 ± 0.1 x10^{-3}	17.3 ± 4.6	0.0672 ± 0.019 x10^{-3}
A286L	0.9 ± 0.4 x10^{-3}	285.1 ± 150.5	0.0033 ± 0.0022 x10^{-3}
R387M	1.6 ± 0.3 x10^{-3}	49.5 ± 21.2	0.0314 ± 0.015 x10^{-3}
T407A	1.2 ± 0.2 x10^{-3}	33.7 ± 12.1	0.0364 ± 0.0142 x10^{-3}
S411A	1.8 ± 0.5 x10^{-3}	71.5 ± 34.8	0.0257 ± 0.0143 x10^{-3}

C. Helicase Unwinding Activity

NS3h variant	k_{cat} (s^{-1})	K_M (μM)	k_{cat}/K_M ($\mu M^{-1}s^{-1}$)
WT	47.6 ± 4.4 x10^{-3}	24.5 ± 11.3	1.9 ± 0.8 x10^{-3}
A286L	0.0	0.0	0.0
R387M	0.0	0.0	0.0
T407A	80.8 ± 6.0 x10^{-3}	14.4 ± 6.2	5.6 ± 2.2 x10^{-3}
S411A	166.6 ± 15.5 x10^{-3}	58.0 ± 21.6	2.9 ± 0.9 x10^{-3}

4.6 μM) whereas the turnover rate (k_{cat}) was consistent between the two systems (Table 3.1B). This data demonstrates that A286 is critical for ATP hydrolysis. Additionally, the k_{cat}/K_M for R387M (0.0314 ± 0.015 x10^{-3} $\mu M^{-1}s^{-1}$) was reduced by a factor of two as compared to WT. Similar to A286L, the slight decrease in the catalytic efficiency of R387M was due to an increase in K_M (49.5 ± 21.2 μM), whereas the k_{cat} was not significantly different from WT. Interestingly, the increase in ATPase K_M coupled with the decrease in RNA binding K_d for R387M as compared to WT suggests that RNA binding promotes ATP binding, consistent with a previous report that ATP hydrolysis is stimulated by RNA (145). When WT NS3 helicase is compared to T407A and S411A, we observe similar turnover rates yet increased Michaelis-Menten constants. These results suggest that T407A and S411A hydrolyze ATP at a similar rate to WT but more substrate is needed for the same catalytic efficiency. Overall, however, ATP hydrolysis was not increased or decreased by the T407A or S411A mutations.

Since both RNA binding and ATP hydrolysis were minimally affected by T407A and S411A, we then examined how these mutations affected overall helicase unwinding activity. We utilized a molecular-beacon based helicase activity assay to identify the effects of translocation and unwinding of double-stranded RNA (dsRNA) for WT, A286L, R387M, T407A and S411A (207, 236). Progress curves were obtained for each reaction containing NS3h variants (50 nM), dsRNA (5 nM) and increasing concentrations of ATP from the absence of ATP to 1 mM ATP (Figure 3.4C). Each reaction was pre-incubated before the addition of ATP. For initial comparison, progress curves of WT, A286L, R387M, T407A and S411A NS3h at 400 μM ATP were normalized to the maximum relative fluorescence unit of WT resulting in a relative unwinding activity compared to WT (Figure 3.4D). The A286L (ATPase defective) and R387M (RNA binding defective) mutations ablate helicase unwinding activity, as expected. The progress curves for T407A and S411A indicate that the mutations deviate from WT activity. To quantify the enzyme kinetics for each NS3h variant, we utilized a

nonlinear regression fit on the progress curves that were not normalized. From the nonlinear regression we determined an initial rate of reaction (k_{obs}) for each NS3h variant at all ATP concentrations. A plot consisting of k_{obs} verse ATP concentration was fit to the Michaelis-Menten equation to determine the k_{cat}, K_M, and k_{cat}/K_M (Table 3.1C). WT NS3 helicase unwound dsRNA with a k_{cat} of 47.6 ± 4.4 x10^{-3} s^{-1} and K_M of 24.5 ± 11.3 μM (Table 3.1C). The dsRNA was unwound at a k_{cat} of 80.8 ± 6.0 x10^{-3} s^{-1} and a K_M of 14.4 ± 6.2 μM for the T407A mutant, and at a k_{cat} of 166.6 ± 15.5 x10^{-3} s^{-1} and a K_M of 58.0 ± 21.6 μM for S411A. These kinetics for T407A and S411A were significantly different compared to WT, which suggests that both mutations are catalytically more efficient than WT NS3h.

The Interaction Between T407 and S411 Controls NS3 Helicase Function

T407A and S411A exhibit increased helicase activity, so we wanted to investigate if this was due to the absence or presence of a hydrogen bond between the two residues. Therefore, we constructed three additional mutations (T407C, S411C and a double mutant T407C/S411C) in both the replicon and recombinant protein systems to test viral genome replication, RNA binding affinity, ATPase activity, and helicase unwinding activity. Replacing residues T407 and S411 with cysteine residues would largely retain the hydrogen bonding potential for each residue but would remove the methyl group from T407. T407C/S411C can be used to create a disulfide bond (~ 2 Å) under oxidized conditions, locking 407 and 411 into a closer and more rigid interaction than a hydrogen bond (2.5-3 Å). First, we investigated the effects of T407C, S411C and T407C/S411C on viral genome replication in our replicon system. The viral genome replication of T407C was significantly reduced (13.0 ± 8.0 %), while the double-mutant indicated a reduction to genome replication at 52.7 ± 30.0 % as compared to WT NS3 helicase (Figure 3.5). On the other hand, S411C exhibited similar genome replication activity as WT. These results suggest that the hydroxyl group of T407 is responsible for part of the effect in genome replication since the cysteine mutation recovers replication by ~2-3 fold compared to T407A.

Additionally, these results indicate that the T407 methyl group may be the important component of the threonine sidechain due to the absence of viral replication in both T407A and T407C, which both lack the methyl group. The S411C mutant shows a complete recovery of replication efficiency, so the effect seen in S411A is due to the removal of the hydroxyl group. This data suggests overall that the hydrogen bond between T407 and S411 plays some role in replication but the methyl in T407 plays a different and potentially more important role in replication. Therefore, we investigated the individual NS3 helicase functions for these mutations in the recombinant protein system to further understand the role of the methyl and hydroxyl groups found in T407 and S411.

The T407C, S411C, and T407C/S411C mutants were expressed in BL21 DE3 pLysS competent cells to promote a reducing environment. WT and T407C/S411C mutant were also expressed in T7 Shuffle competent cells to promote an oxidizing environment for disulfide bond formation. All of the purified NS3 helicase variants were then tested in the three biochemical assays: RNA binding affinity, ATPase activity and helicase unwinding activity. These cysteine mutations were tested under reducing conditions (TCEP) with the exception of the oxidized WT and T407C/S411C expressed in T7 Shuffle which were tested in both reducing (TCEP) and non-reducing conditions. In all three assays, the BL21 expressed WT compared to T7 Shuffle expressed WT have differing K_d, k_{cat} and K_M values suggesting that the expression cell lines provide a different environment and therefore the T7 Shuffle expressed NS3 helicases cannot be directly compared to the BL21 expressed helicases (Table 3.2). In the RNA binding affinity assay, the BL21 expressed S411C and T407C/S411C were not significantly different in their binding affinities compared to WT, whereas T407C indicated a weaker RNA binding affinity of 8.0 ± 2.5 μM, which was a 4.2 fold difference compared to WT (Table 3.2A). Additionally, the reduced T7 expressed T407C/S411C showed a 1.3 fold increase in K_d as compared to the reduced T7 Shuffle expressed WT. Similarly, the WT and T407C/S411C expressed in T7

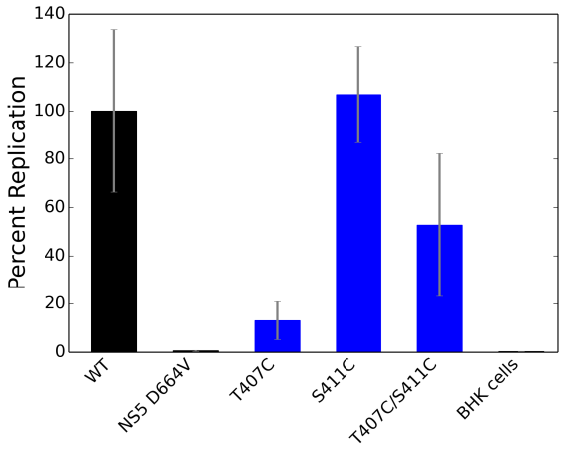

Figure 3.5. Examining the role of T407 and S411 interaction in NS3h function. Additional mutations to force covalent bonds between the T407 and S411 residues were tested in viral genome replication. *Error bars,* S.E.

Table 3.2. Enzyme kinetics of T407C, S411C, and T407C/S411C NS3 helicase. A) K_d was determined from the RNA-binding affinity assay data. B) k_{cat}, K_m, and k_{cat}/K_m were determined for the ATPase activity assay through fitting the data to the substrate inhibition equation. K_m is related to the ATP concentration. C) k_{cat}, K_m, and k_{cat}/K_m were determined for the helicase-unwinding activity assay for each NS3h variant through fitting the Michaelis–Menten equation to the K_{obs} versus ATP concentration.

A.

RNA Binding Affinity

NS3h variant	K_d (μM)	Fold Difference
WT	1.9 ± 0.8	
T407C	8.0 ± 2.5	4.2
S411C	0.6 ± 0.3	0.3
T407C/S411C	1.4 ± 0.8	0.7
WT reduced†	3.4 ± 1.4	
WT oxidized‡	4.5 ± 1.5	
T407C/S411C reduced†	4.4 ± 1.1	1.3
T407C/S411C oxidized‡	2.6 ± 1.4	0.6

B.

ATP Hydrolysis Activity

NS3h variant	k_{cat} (s^{-1})	K_M (μM)	k_{cat}/K_M ($\mu M^{-1}s^{-1}$)
WT	$1.2 \pm 0.1 \times 10^{-3}$	17.3 ± 4.6	$0.0671 \pm 0.0189 \times 10^{-3}$
T407C	$1.4 \pm 0.2 \times 10^{-3}$	24.4 ± 7.4	$0.0565 \pm 0.0184 \times 10^{-3}$
S411C	$1.2 \pm 0.1 \times 10^{-3}$	23.4 ± 4.8	$0.0498 \pm 0.0109 \times 10^{-3}$
T407C/S411C	$0.9 \pm 0.1 \times 10^{-3}$	19.3 ± 6.9	$0.0443 \pm 0.0168 \times 10^{-3}$
WT reduced†	$1.8 \pm 0.2 \times 10^{-3}$	43.0 ± 8.5	$0.0428 \pm 0.0094 \times 10^{-3}$
WT oxidized‡	$2.9 \pm 0.8 \times 10^{-3}$	116.5 ± 49.7	$0.0249 \pm 0.0128 \times 10^{-3}$
T407C/S411C reduced†	$1.8 \pm 0.1 \times 10^{-3}$	35.1 ± 6.5	$0.0512 \pm 0.0104 \times 10^{-3}$
T407C/S411C oxidized‡	$1.7 \pm 0.2 \times 10^{-3}$	49.9 ± 12.1	$0.0341 \pm 0.0093 \times 10^{-3}$

C.

Helicase Unwinding Activity

NS3h variant	k_{cat} (s^{-1})	K_M (μM)	k_{cat}/K_M ($\mu M^{-1}s^{-1}$)
WT	$47.6 \pm 4.4 \times 10^{-3}$	24.5 ± 11.3	$1.9 \pm 0.8 \times 10^{-3}$
T407C	$64.2 \pm 5.2 \times 10^{-3}$	4.1 ± 3.0	$15.7 \pm 10.8 \times 10^{-3}$
S411C	$219.4 \pm 16.2 \times 10^{-3}$	166.3 ± 33.7	$2.8 \pm 1.2 \times 10^{-3}$
T407C/S411C	$81.8 \pm 46.7 \times 10^{-3}$	81.7 ± 113.1	$1.0 \pm 0.9 \times 10^{-3}$
WT reduced†	$39.4 \pm 2.7 \times 10^{-3}$	21.9 ± 7.7	$1.8 \pm 0.6 \times 10^{-3}$
WT oxidized‡	$32.5 \pm 1.7 \times 10^{-3}$	10.8 ± 3.4	$3.0 \pm 0.9 \times 10^{-3}$
T407C/S411C reduced†	$21.1 \pm 1.7 \times 10^{-3}$	14.7 ± 6.6	$1.4 \pm 0.6 \times 10^{-3}$
T407C/S411C oxidized‡	$21.2 \pm 2.0 \times 10^{-3}$	4.2 ± 4.4	$5.1 \pm 5.2 \times 10^{-3}$

Shuffle cells under non-reducing conditions were also not significantly different with a 0.6 fold difference. All of this data suggest that T407C slightly decreases RNA binding affinity potentially due to the lack of the methyl group, which may play a role in RNA binding to the helicase.

The NS3 helicase mutants expressed in BL21 and T7 Shuffle competent cells were tested for their ability to hydrolyze ATP. T7 Shuffle expressed NS3 helicases were tested in both oxidizing and reducing conditions. T407C, S411C, and T407C/S411C expressed in BL21 cells all showed insignificant differences in both k_{cat} and K_M as compared to WT. The k_{cat} for oxidized WT and T407C/S411C were not significantly different with a k_{cat} of 2.9 ± 0.8 x10^{-3} s^{-1} and a k_{cat} of 1.7 ± 0.2 x10^{-3} s^{-1}, respectively, whereas the K_M for WT (116.5 ± 49.7 μM) and T407C/S411C (49.9 ± 12.1 μM) under oxidized conditions were significantly different (Table 3.2B), suggesting that the disulfide bond present in the oxidized form of T407C/S411C increases ATP hydrolysis activity. On the other hand, WT and T407C/S411C expressed in T7 Shuffle cells under reduced conditions exhibit an insignificant difference for either k_{cat} and K_M. Overall, these data suggest that hydrolysis of ATP is similar between WT and the cysteine mutations meaning that the cysteine residues do not influence ATP hydrolysis directly.

Finally, the various cysteine NS3 helicase mutants as well as WT expressed in both BL21 and T7 Shuffle cells were tested in the helicase unwinding activity assay. When comparing T407C, S411C and T407C/S411C expressed in BL21 cells to WT, we observe a higher k_{cat} with a lower K_M for each mutant except for T407C, which exhibits a higher K_M value (Table 3.2C). This data suggest that both S411C and T407C/S411C unwind dsRNA faster than WT even though they do not bind ssRNA as well. T407C also unwinds dsRNA faster than WT, but the affinity for ssRNA is stronger suggesting that T407C is a more catalytically efficient helicase overall compared to WT. The catalytic efficiency of WT and T407C/S411C expressed in T7 cells

indicates no significant difference in the ability to unwind dsRNA substrates suggesting that the double-mutant exhibits similar overall unwinding activity compared to WT.

In silico mutations of T407 and S411 validate experimental assays

We further investigated how each mutant, alanine and cysteine, affected either the binding energy of the substrates or the overall secondary structure of NS3 helicase in the ssRNA+ATP substrate state using all-atom molecular dynamics simulations. Each mutant (A286L, R387M, T407A, T407C, S411A, S411C, T407C/S411C) was simulated in triplicate for 1 μs using the ff14SB force field within the AMBER18 software package. Once the simulations were completed, the root-mean squared deviation (RMSD) was calculated in reference to the initial starting structure to determine the equilibration time that would be excluded for all other analyses. The three analyses performed on the simulations were a nonbonding interaction energy analysis, a probability of finding a lytic water in the ATP binding pocket, and a projected covariance magnitude analysis. These analyses were specifically designed to be compared results between simulation and the three biochemical assays.

First, we utilized the nonbonding interaction energy analysis to provide insight into how the mutations affect RNA binding affinity from simulation. The nonbonding interaction energy was calculated between the bound ssRNA and the entire protein for each NS3 helicase variant. The more negative the linear interaction energy, the more strongly bound the ssRNA substrate is in the helicase RNA binding cleft. All of the mutations exhibit strong ssRNA binding as compared to WT with the exception of A286L, R387M and T407C mutants (Table 3.3A). The A286L and R387M mutations increase in their nonbonding interaction energies as compared to WT by 5.3% and 13.8%, respectively. These data suggest that A286L and R387M bind ssRNA weakly compared to WT. Additionally, T407C exhibits a nonbonding interaction energy of -708.6 ± 36.7

Table 3.3. T407 and S411 mutations do not affect nonbonding interaction energies of bound ssRNA to NS3 helicase. A) the nonbonding interaction energies were calculated between all residues in the protein and all nucleotides of the single-stranded RNA substrate bound into the RNA-binding cleft of NS3 helicase. The post-analysis AMBER18 Tools package, cpptraj, was utilized to calculate the linear interaction energy (kcal/mol) for each mutation run in triplicate with an interaction cutoff of 12 Å, and short-range, electrostatic energies were calculated with a dielectric of 1. The resulting linear interaction energies were the average over the three simulations. B) the projected covariance magnitude represents the fluctuations of G414 and residues S364 and K366 projected onto the helical gate access site axis. Each mutant is reported here as well as the -fold difference compared with WT NS3h.

A.

RNA Binding Energy

NS3h variant	Linear Interaction Energy (kcal/mol)
WT	-747.4 ± 3.9
A286L	-707.7 ± 0.0
R387M	-644.5 ± 0.0
T407A	-744.8 ± 23.0
T407C	-708.6 ± 36.7
S411A	-743.3 ± 11.9
S411C	-736.7 ± 11.7
T407C/S411C reduced	-730.6 ± 27.2
T407C/S411C oxidized	-744.6 ± 18.4

B.

Projected Covariance between G414 and the Helical Gate

NS3h variant	Response Magnitude (Å^2)	Fold Difference
WT	0.032 ± 0.008	1.0
A286L	0.023 ± 0.0	0.7
R387M	0.060 ± 0.0	1.9
T407A	0.224 ± 0.088	7.0
T407C	0.045 ± 0.010	1.4
S411A	0.049 ± 0.007	1.5
S411C	0.057 ± 0.023	1.8
T407C/S411C reduced	0.019 ± 0.001	0.6
T407C/S411C oxidized	0.062 ± 0.021	1.9

kcal/mol. The more positive nonbonding interaction energy suggests that T407C binds ssRNA more weakly than WT. The lower nonbonding interaction energy correlates well with the reduced RNA binding affinity for T407C (Table 3.2A), validating our computational approach. In additional, we observed an increase in sidechain mobility in the T407C mutant simulation compared to WT (Figure A.1), suggesting that the threonine at position 407 may control fluctuations within Motif V allowing for the helicase to bind ssRNA strongly.

Next, we investigated how the mutations affect the ATP binding pocket through determining the probability of finding a lytic water in the ATP hydrolysis active site. In order to do this, we utilized three collective variables to select for lytic waters: (1) the nucleophilic attack distance between the water oxygen atom and the ATP-γ-phosphate atom, (2) the nucleophilic attack angle between the water oxygen atom and the terminal phosphoanhydride bond of ATP, and (3) the angle between the water dipole moment and the terminal phosphoanhydride bond of ATP. Once the lytic waters were determined, the simulations were analyzed to determine the probability of finding a lytic water throughout the entire equilibrated portion of the simulations. The WT simulations indicate that $63 \pm 5\%$ of the time, a lytic water was found within the ATP binding pocket. All of the mutations are not significantly different compared to the WT, except for A286L ($44.9 \pm 0.11\%$), R387M ($52.5 \pm 0.12\%$), and T407A ($34.7 \pm 16.8\%$). These probabilities suggest that A286L, R387M, and T407A mutations have negatively affected the ATP hydrolysis active site due to the low probability of finding a lytic water in the ATP binding pocket during the simulations. However, when we compare the probability of finding a lytic water to the turnover rate determined from the ATPase assay, we observe no significant difference between the mutations and the WT NS3 helicase (Figure 3.6A). On the other hand, comparing the probability of finding the lytic water to the turnover rate determined from the helicase assay, we observe S411A and S411C are set apart from the rest of the mutations, suggesting that these two

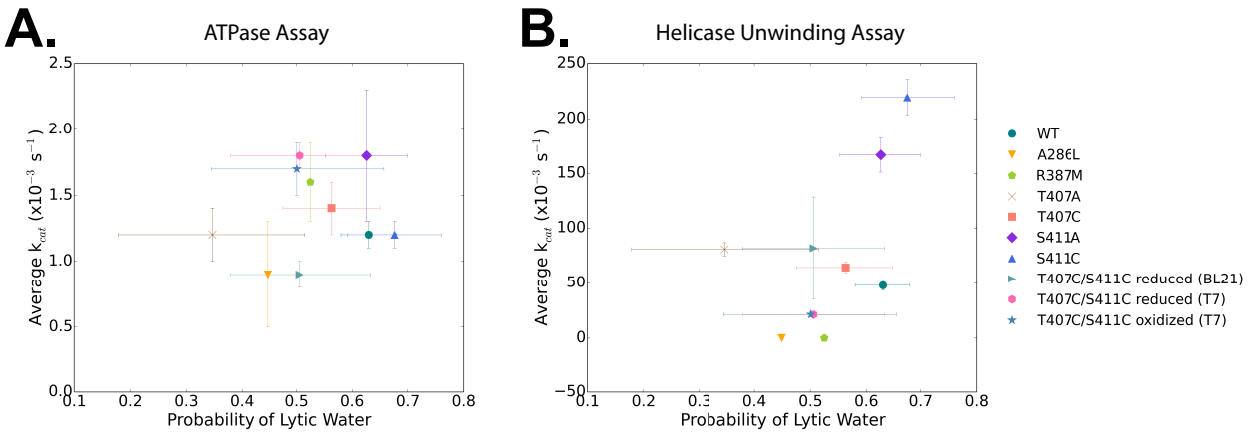

Figure 3.6. Simulations of mutants do not indicate altered probability of finding a lytic water in the ATPase active site. A) the average k_{cat} (s^{-1}) from the ATP hydrolysis activity assay is plotted against finding a lytic water in the ATP binding pocket. B) the average k_{cat} (s^{-1}) from the helicase-unwinding activity assay is plotted against the probability of finding a lytic water in the ATP-binding pocket. *Error bars,* S.E.

mutations are catalytically more efficient than WT and the other mutations because they are more likely to have a lytic water in the ATPase active site (Figure 3.6B).

Lastly, we implemented a projected covariance analysis to examine how the mutants affect the dynamics of the helical gate through changes in fluctuations between the ATPase active site and the helical gate. As previously mentioned, during replication, the helical gate and β-wedge are responsible for unwinding the dsRNA intermediate into two ssRNA molecules (168). One of the two strands enters into the RNA binding cleft through the helical gate access site. The ssRNA strand in the access site interacts with surrounding residues S364, I365, K366, D603, P604, and M605 found within two α-helices (α-helix 2 in subdomain 2 (α2') and α-helix 6 in subdomain 3 (α6")) that flank either side of the incoming ssRNA (229). Previous studies have suggested that the dynamics of the helical gate are controlled by the presence of bound ATP (229). Therefore, we wanted to determine how the mutations within Motif V affect the connection between the ATP binding pocket and the helical gate. We quantified this connection as the positional covariance of ATP pocket residues (sources) and helical gate residues (sinks). Specifically, we investigated the covariance of G414 (Motif V, source) and S364 and K366 (α2´, sink residues) along the helical gate opening/closing coordinate. This quantified as the average of the projections of the covariance tensors between source and sinks along helical gate opening/closing direction (Table 3.3B).

The WT simulations indicated a projected covariance of 0.032 ± 0.008 Å^2 suggesting that there was a correlation between the fluctuations seen between the ATP binding pocket and the helical gate. Both T407C (0.045 ± 0.010 Å^2) and S411C (0.057 ± 0.023 Å^2) were not significantly different compared to WT, even though their fold differences indicated an increase in projected covariance along the helical access. All of the rest of the mutations were significantly different

compared to WT (Table 3.3B). Both A286L (0.023 ± 0.0 Å^2) and reduced T407C/S411C (0.019 ± 0.001 Å^2) showed a decrease in fold difference (0.7 and 0.6 respectively) compared to WT, suggesting that these mutations negatively affect the dynamics of the helical gate (Table 3.3B). R387M, T407A, S411A and oxidized T407C/S411C indicate an increase in fold difference (1.9, 7.0, 1.5 and 1.9 respectively) compared to WT (Table 3.3B), suggesting that the fluctuations through Motif V positively affect the motion of the helical gate promoting translocation and unwinding of the dsRNA intermediate. Interestingly, when we compared the projected covariance magnitude fold differences to the turnover rate fold differences of the helicase unwinding activity assay, all of the data support each other except for A286L, R387M and oxidized T407C/S411C. Both A286L and R387M were unable to unwind dsRNA in the helicase unwinding assay, but in simulation these mutants indicated a decrease and an increase in the projected covariance along the helical gate axis, respectively. The difference observed between simulation and experiment may be due to the pre-bound state of the simulation, whereas in experiment the helicase still needs to bind the RNA. Additionally, the turnover rate of the oxidized double mutant indicated a decreased rate compared to WT, while the projected covariance magnitude indicated an increased fluctuation projected onto the helical axis compared to WT. This discrepancy might be due to the inability to control the state of the disulfide bond in experiment.

Discussion

In this study, a combination of computational, biochemical and virological experiments were utilized to investigate the role of Motif V in NS3 helicase functions. WT simulations pointed to Motif V as a key player in the communication between the ATP binding pocket and the RNA binding cleft. To determine how Motif V may play a role in the communication, mutations were introduced in both replicon and recombinant protein systems. The mutations were tested in a viral genome

replication assay and results suggested that the residues within Motif V affect how the virus replicates. From the viral replication assay, residues T407 and S411 sparked our interest due to the differing replication activity with prior knowledge of their interaction through a hydrogen bond that may stabilize Motif V structure. We tested both alanine and cysteine mutations in an RNA binding affinity assay, an ATP hydrolysis activity assay and a helicase unwinding activity assay as well as simulated theses mutations in all-atom molecular dynamics. Results in this paper suggest that the methyl group in the sidechain of T407 may play a role in decreasing helicase unwinding activity through stabilizing interactions with residues T408, K366, and R387. These residues all interact with the bound RNA allowing for viral replication. We can directly compare between the helicase unwinding assay and viral replication assay because the helicase rates we observed biochemically appears to be in line with how fast dsRNA unwinding would likely need to occur *in vivo* during genome replication. Overall, our data suggests that Motif V is critical for the communication between the ATP binding pocket and the RNA binding cleft in NS3 helicase.

Initial analyses of WT simulations supported results reported in Davidson *et al.* that Motif V may play a critical role in the communication between the ATP binding pocket and the RNA binding cleft (203). This led us to mutating all of Motif V residues (404 to 416) in the replicon system. Interestingly, only two Motif V mutations have been studied previously within the *Flaviviridae* virus family: T411A in HCV and G414A in dengue 2 virus (199, 201). Both of these mutations were tested biochemically but were not tested for their effect on viral genome replication. Therefore, our replicon data represents the first replication-based examination of the effect of Motif V mutations on viral genome replication. We observed that the majority of the mutations ablated viral replication activity with the exception of residues V405, V406, T407, T408, S411 and A415. Interestingly, most of the highly conserved residues ablated viral replication, but not all did, suggesting that the highly conserved residues can have some variability with the type of amino acid at those positions. Of the residues that did not ablate activity, T407 and S411 were of most

interest due to the variable nature of these residues across all flaviviruses and the hydrogen bond that may stabilize the secondary structure of Motif V during replication. Therefore, we focused on these two positions for the remainder of the discussion.

T407 and S411 were mutated to alanine residues in the recombinant NS3 helicase and were expressed, purified and tested in RNA binding affinity, ATPase activity, and helicase unwinding activity assays along with two controls A286L and R387M. These three assays provide specific insight into how the helicase binds ssRNA and the rates of (1) ATP hydrolysis and (2) dsRNA unwinding. The rates determined from the latter two assays cannot be directly compared because the time scales are different due to the fact that the ATPase assay is an end-point assay while the helicase unwinding activity assay is a continuous assay. The results from the RNA binding affinity assay indicated that T407A and S411A bind ssRNA as strongly as WT while in the absence of ATP. We noted that ATP inhibited RNA binding in the fluorescence polarization assay, and thus ATP was left out of the reactions. The results from the ATP hydrolysis activity assay indicated that T407A and S411A hydrolyze ATP as well as WT. On the other hand, T407A and S411A seem to unwind dsRNA more quickly than WT in the molecular beacon helicase assay, suggesting that T407 and S411 are involved in the linkage between the ATP binding pocket and the RNA binding cleft. If the individual activities of RNA binding and ATP hydrolysis are unaffected by these mutations but the over ability for the helicase to unwind dsRNA is affected, then these two mutations must play a role in the communication between the substrate binding pockets. The observation that T407 and S411 increased helicase turnover rate was surprising and suggested that one or both of these residues may naturally act to weaken the effect of ATP hydrolysis on helicase activity giving rise to the intriguing possibility that the helicase has evolved to slow down its ATPase-dependent helicase activity. Position 407 is found predominately as a threonine and 411 found as serine (Figure 3.2A and Table A.1), but in a small group of flaviviruses position 407 can be alanine or serine and 411 can be alanine. This may indicate that the helicase function in

other flaviviruses (yellow fever virus, Sepik virus, Entebbe Bat virus, Cell Fusing Agent, Kamiti River virus, and Culex flavivirus) could be faster than most other flaviviruses.

We further investigated which aspects of the threonine and serine residues may play a critical role in the regulation of helicase unwinding activity by introducing cysteines at positions 407 and 411 individually or as a double-mutant, T407C/S411C. T407C, S411C and T407C/S411C were mutated in both the replicon and recombinant protein systems. We observed an increase in replication activity for the T407C mutation, a full recovery for the S411C mutation, and an increase in replication activity for the double-mutant. T407C was the only mutation that weakened the ability of the helicase to bind ssRNA. The ATP hydrolysis activity is unchanged for all of the cysteine mutations, and the helicase unwinding activity indicate T407C and S411C increase unwinding activity while the double mutant under oxidizing and reducing conditions remain as active as WT. The combination of these data suggest that the methyl group in the sidechain of T407 may be important for slowing down helicase function. We observed a catalytically more efficient T407A in unwinding dsRNA, but a significant reduction in viral replication activity. When we mutate T407 to a cysteine (similar to a threonine but lacking in the methyl group), we recover some replication activity. When we mutated S411 to cysteine, we completely recover viral replication suggesting that while the hydrogen bond between T407 and S411 is important, T407 has a separate function related to its methyl group. The methyl group in the T407 sidechain normally interacts with the phenylalanine ring of F361 via hydrophobic interactions, potentially stabilizing the residues T408, K366, and R387, which all interact with the RNA phosphate backbone (Figure A.1A). By removing the methyl from T407 with the T407C mutation, the sidechain of position 407 is able to rotate and interact not only with F361 but also L385, potentially causing RNA interacting residues to become more variable with their interactions with bound ssRNA. As a result, these three residues that interact with the RNA may become more catalytically efficient in unwinding the dsRNA substrate. Results reported in Appleby *et al.* examining residues equivalent to R387 and T408 (R393 and

T411) suggest that both residues play a direct role in the translocation along the ssRNA through conformational changes that are observed between nucleotide-bound and nucleotide-free states of HCV NS3 (184). When comparing our results to HCV NS3, mutations at position 407 may disrupt the interactions that R387 and T408 have with the phosphodiester backbone of ssRNA such that Motif V does not undergo the same structural rearrangements to allow for T408 to shift to the next nucleotide in the bound ssRNA molecule as previously described (184). In the T407C mutation, the viral replication recovers some activity suggesting that the hydroxyl group in T407 is also potentially important for proper viral replication due to the ability to form a hydrogen bond like interaction with S411. Overall, when the helicase becomes catalytically more efficient in the absence of the T407 methyl, viral genome replication decreases. It is unclear why this is the case, but one hypothesis is that reduced replication may be due to a rate mismatch between T407A, T407C, and S411A NS3 and the RNA-dependent RNA polymerase of NS5. If this is the case, it may suggest that the NS3 helicase and NS5 polymerase have co-evolved to match their catalytic rates so that RNA is fed at an optimal rate between the two enzymes.

All of the NS3 helicase mutations were simulated using the ff14SB force field within the AMBER18 software package to better define how the mutations affected NS3 helicase function. Three analyses were performed on the simulations in order to determine how the structure of the helicase has changed due to the presence of the mutations. The first analysis we utilized was the nonbonding interaction energy analysis. The interaction energies determined from this analysis were compared to the RNA binding affinity (K_d) obtained from experiment. We observed that in both computation and experiment, the mutations (T407A, T407C, S411A, S411C, and T407C/S411C) did not significantly change the ability for the helicase to bind ssRNA. The only mutation that weakened the binding of ssRNA in the helicase was R387M, which was expected because this mutation was a control for RNA binding. As we moved forward with our analysis of the simulations, we investigated how the mutations affected the probability of finding a lytic water

in the ATPase active site (Figure 3.6). When we compared the probability of finding a lytic water in the ATP binding pocket to the turnover rate determined from the ATPase assay, we observed that none of the mutations significantly changed the probability of finding a lytic water. When comparing the probability of a lytic water to the turnover rate of the helicase activity, we observed that S411A and S411C were set apart from the rest of the mutations suggesting that these two mutations play a role in controlling the rate of unwinding activity through the hydrogen bond with T407. Interestingly, when T407 is mutated to a cysteine, we observe an increase in mobility at position 407 (Figure A.1). The cysteine residue lacks the methyl group and contains a thiol group instead of a hydroxyl group found in the threonine sidechain. The lack of the methyl group seems to allow for the thiol group to fluctuate frequently throughout the simulation (Figure A.1B and A.1C), suggesting a potential hydrophobic interaction between T407 and nearby hydrophobic residues (such as L385) that may influence the position of T407 within Motif V. This supports our previous results for T407 in that the methyl groups orientation is critical for helicase function. Additionally, the projected covariance magnitude analysis indicated that T407A increased by 7.0 compared to WT suggesting that the methyl and hydroxyl group of threonine are important for stabilizing the interactions of position 407 with its surrounding residues. Without either of those functional groups at position 407, Motif V may allow more structural changes to occur that positively affect the helical gate. This is evident when we take into account the projected covariance of T407C. T407C indicated a slight increase compared to WT, which is similar to what is observed in the k_{cat} of T407C from the helicase unwinding assay. The thiol group of the cysteine potentially interacts with S411 stabilizing Motif V enough to control the structural changes within the helicase to allow for optimal translocation and unwinding of dsRNA.

This work provides detailed computational, biochemical, and virological insight into how the helicase utilizes the energy produced from ATP hydrolysis to power translocation and unwinding of the viral double-stranded RNA intermediates. We have learned that the methyl group in T407 is

potentially critical for regulating the helicase to maintain an optimal rate of translocation and unwinding during replication. If the T407 is mutated to an alanine or a cysteine, the viruses we examined are not able to replicate the viral genome efficiently *in vitro*. This T407 residue within Motif V interacts with S411, which seems to properly orient T407 potentially stabilizing the structure of Motif V. When we remove that interaction between T407 and S411 with a mutation to S411, the helicase is able to unwind dsRNA intermediates with more catalytic efficiency suggesting that T407 is responsible for regulating translocation and unwinding dsRNA intermediates. As previously mentioned, the role of Motif V in SF2 helicases is not well understood. This work has provided computationally driven experimental insight into how Motif V plays a role in the communication between the ATP binding pocket and the RNA binding cleft in the viral-DEAH subfamily of SF2 helicases (170). Additional work will be required to determine if the results we observe here for flaviviruses hold in other subfamilies of SF2 helicases. Ultimately, the data from this paper suggests that flaviviruses may utilize suboptimal NS3 helicase activity for optimal genome replication, and that Motif V may play an inhibitory role for helicase activity during viral infection *in vitro* and *in vivo*. The role of Motif V in controlling helicase function will need to be further defined, which may eventually lead to the development of novel vaccine candidates or antiviral drug targets.

Experimental procedures

Plasmids and Mutagenesis

The DNA expression plasmid used in the protein purification protocol for dengue 4 NS3 (Accession Number: AQV12689) was adapted from Luo and co-workers (219). The QuikChange mutagenesis (Agilent Technologies) method was used to mutate specific residues (A286L, R387M, T407A, T407C, S411A, S411C, and T407C/S411C) within the WT dengue NS3h plasmid optimized for expression in *E. coli*. Plasmids for each mutation were submitted to GENEWIZ for sequencing to verify each sequence.

Protein Expression and Purification

WT dengue NS3h gene with an N-terminal thioredoxin, 6X-histidine tag, thrombin cleavage site was synthesized and cloned into a T7 expression plasmid. The wild-type (WT) NS3h construct was transformed into BL21 DE3 pLysS or T7 Shuffle *E. coli* competent cells. 5 mL Luria broth (LB) cultures containing ampicillin (50 μg/mL) and chloramphenicol (34 μg/mL) were grown overnight at 37 °C, and the next day the entire 5 ml culture was added to a 750 mL LB culture containing 50 μg/mL of ampicillin. 750 mL cultures were incubated until an OD_{600} of 0.6 was reached, the cultures were induced with a final concentration of 400 μM IPTG for 18 hours, and bacteria collected by centrifugation. Bacteria were resuspended with 20 mL low imidazole buffer (LIB) (50 mM Tris-Base pH 8.00, 400 mM NaCl, 10 mM imidazole, 5% glycerol, and 12 mM $CaCl_2$ and stored at -80 °C until use. Pre and post-induction samples were collected and used to verify protein expression by SDS-PAGE gel analysis.

For the protein purification, LIB (20 mL) was added to the frozen bacterial pellets. Once thawed, bacterial cells were disrupted 3 times on a 110S Microfluidizer (Microfluidics), the lysate clarified by centrifugation using a JA-25.50 rotor for 20 minutes at 17,000 rpm at 4 °C, and supernatant filtered using a 0.45 μM syringe filter. Protein purification was achieved using a multi-step approach. The thioredoxin-dengue NS3h complex was first purified from the filtered lysate with nickel affinity chromatography using a HisTrap HP (GE) column on an AKTA Pure FPLC system (GE). The protein complex was eluted off the Ni-column with a linear gradient of high imidazole buffer (HIB) (50 mM Tris-Base pH 8.00, 400 mM NaCl, 10 mM imidazole, and 5% glycerol). Fractions containing the NS3h complex were collected, dialyzed against 350 ml of LIB containing $CaCl_2$ for two hours using a Slide-A-Lyzer Dialysis Cassette (3-12 mL (Life Tech)). 75 μL of soluble thrombin (GE Life Sciences) was added to

the dialyzed protein for an overnight incubation at 4°C. A second Ni-column was subsequently used to remove thioredoxin from NS3h, which was collected in the flow-through fraction. The flow through fraction was concentrated using a Vivaspin Turbo 15 ultrafiltration spin column (Satorius), then applied to a HiLoad 16/600 Superdex 200 pg (GE Life Sciences) gel filtration column to further purify and buffer exchange the isolated NS3h in gel filtration buffer (50 mM Hepes at pH 8.00, 400 mM NaCl and 20% glycerol). Purified NS3h was concentrated in Vivaspin spin columns before storage at -80°C in single use aliquots. All buffers were made with RNAse free H_2O. The concentration of NS3h variants were confirmed on by SDS-PAGE (Figure A.2). The recombinant WT NS3h was also confirmed by mass spectrometry (data not shown).

RNA Helicase Unwinding Activity Assay

For the ATP dependent helicase assay(207, 236), all reactions were performed in 96-well black microplates (Thermo Scientific) in a final volume of 120 μL and they contained 50 nM NS3h, 0.05 mM TCEP, 0.01% Tween20, 5 μg/μL BSA, 1.25 mM $MgCl_2$, 25 mM MOPS (pH 6.5), 5 nM RNA complex, and varying concentrations of ATP (Jena Bioscience) ranging from 1 μM to 1 mM. The RNA complex consists of an RNA tagged Alexa-488 oligo (5'-AGUGCGCU-GUAUCGUCAAGG-CACU-3'-AlexF488N) and a DNA tagged Iowa Black Fluorescent Quencher (5'-IABkFQ-CCTACGCCACCAGCTCCGTAGG-3') bound to an RNA template (5'-GGAGCUGGUGGCGUAGGCAAGAGUGCCUUGACGAUACAGCUUUUUUUUUUUUUUUUU UU-3'). The RNA complex was annealed through a slow cooling process by boiling H_2O to 95°C and allowing to cool to room temperature over an hour. The control with no $MgCl_2$ contained 20 mM EDTA. Reactions were scanned individually at 37°C using a Victor X5 multilabel plate reader (Perkin Elmer) instrument for 300 seconds. Rates were determined

from where the progress curves were exponential and linear with time. Data were then fit to the Michaelis-Menten equation (Equation 3.1) using Python2.7

$$\nu = \frac{(V_{max}[S])}{(K_M + [S])}, \quad \text{(Eq. 3.1)}$$

where $\mathrm{V_{max}} = \mathrm{k_{cat}[E]_t}$, ν is the velocity, k_{cat} is the apparent first-order rate constant in s^{-1}, $[E]_t$ is the concentration of the enzyme, *[S]* is the concentration of the ATP substrate, K_M is the concentration of the substrate at one-half k_{cat}. The Michaelis-Menten constant (K_M), turnover rate (k_{cat}), and the specificity constant (k_{cat}/K_M) were determined from fitting to Equation 3.1.

RNA ATPase Activity Assay

A colorimetric ATPase activity assay was derived from the RNA helicase assay (207). The contents of the reactions remained the same. Using a 96-well clear plate, reactions were injected with BIOMOL Green (Enzo), incubated at 37°C for 15 seconds before measuring the absorbance at 650 nm on a Victor X5 multilabel plate reader. To obtain an entire curve for an individual ATP concentration, reactions were measured every 90 seconds for 12.5 minutes. Rates were determined from progress curves. Data were then fit to the substrate inhibition equation (Equation 3.2) using the R software environment (237)

$$\nu = \frac{(V_{max}[S])}{\left(K_M + [S]\left(1 + \frac{[S]}{K_i}\right)\right)} \quad \text{(Eq. 3.2)}$$

where K_i is the inhibition constant. From the fit, the k_{cat}, K_M, k_{cat}/K_M and the K_i were determined for the ATPase assay. K_i data are reported in Table A.2.

RNA Binding Affinity Assay

A fluorescence polarization (FP) assay was also adapted from the RNA helicase assay to determine RNA binding K_d as previously described (235). The FP assay reactions contained increasing concentrations of NS3h, 0.05 mM TCEP, 0.01% Tween20, 5 μg/μL BSA, 1.25 mM $MgCl_2$, 25 mM MOPS (pH 6.5) and 5 nM ppAGUAA tagged Alexa-488 RNA oligo. All

reactions were incubated at 37 °C for 10 minutes in a 384-well black plate within the plate reader before measuring the fluorescence polarization of the Alexa-488 fluorophore. Data was analyzed using nonlinear regression analysis in Prism8 using a maximum value of 400.0 based on protein binding previous reported (235).

Cell Culture and Virus Replicon Plasmids

Baby hamster kidney (BHK) cells were maintained in Hyclone Dulbecco's modified Eagle medium (DMEM) supplemented with 10% fetal bovine serum (FBS), 50 mM HEPES (pH 7.5), 5% penicillin/streptomycin and 5% L-Glutamine. Cells were grown in humidified incubators at 37 °C with 5% CO_2. West Nile virus replicon utilized in the viral genome replication assay was designed as a plasmid-launched virus replicon expressing the firefly luciferase as previously described (204, 238). Additional site-directed mutagenesis was performed on the wild-type WNV replicon using the QuikChange mutagenesis (Agilent Technologies) method to produce the following mutations: NS5 D664V and NS3h A286L, R387M, F404K, V405M, V406M, T407A, T407C, T408S, D409A, I410G, S411A, S411C, E412D, M413A, G414A, A415G, N416D and T407C/S411C double-mutant. The presence of the mutations were confirmed through GENEWIZ sequencing.

Viral Genome Replication Assay

BHK cells were plated into 24-well plates at 50,000 cells/well and allowed to adhere to the plates overnight. The next day, WT and mutant WNV replicon plasmids were transfected into the BHK cells at 250 ng per well using lipofectamine2000 (Life Technologies). 48 hours post-transfection, the cells were lysed with 1X lysis buffer from the Luciferase Assay Kit (Promega) and 20 μL of the lysates were transferred into a white 96-well plate. Using the plate reader, 100 μL of the luciferase assay reagent from the Luciferase Assay Kit was injected into each

sample before measuring the luminescence of the firefly luciferase signal. Data were obtained with an N≥3. The mean and standard error of the mean were plotted using Matplotlib (239).

All-atom Molecular Dynamics Simulations

An exemplar structure of the simulated DENV4 NS3h ssRNA+ATP substrate state (2JLV) was used for all simulations (168, 203). The ssRNA+ATP state was run for 9 systems of NS3h: WT, A286L, R387M, T407A, T407C, S411A, S411C and the double mutant T407C/S411C in oxidized and reduced conditions in triplicate for 1 μs each. All of the mutations were generated from the WT NS3 helicase.

All of the NS3h systems were simulated in explicit solvent MD using AMBER18 software package: ff14SB (protein) and RNA.OL3 (RNA) (209). Parameterization files for the ATP molecule (240) were obtained from the AMBER parameter database. Each system was solvated with a cubic box of TIP3P water with an average dimension of 85 Å. Sodium and chloride ions were added at a concentration of 100 mM to neutralize the system. The simulations were performed with periodic boundary conditions in an isothermal-isobaric (NPT) ensemble with a stochastic barostat of 1 bar and a Langevin thermostat of 310.0 K. The nonbonding interactions cutoff was 12 Å; particle mesh Ewald was used for treating long range electrostatics; and hydrogens were constrained with the SHAKE algorithm. An integration timestep of 2 fs was used. Positions and energies were written every 2 ps.

All systems were initially minimized with a 10,000 step minimization with harmonic restraints (force constant of 75 kcal $mol^{-1}Å^{-2}$) placed on all solute atoms and a 10,000 step minimization with no restraints. Following the minimization, each system was heated from 50.0 K to 310.0 K

in 10 K increments with a harmonic restraint of 75 kcal $mol^{-1}Å^{-2}$ on all solute atoms. Lastly, a series of five equilibration steps were implemented to slowly remove the harmonic restraint.

Data Analysis of MD simulations

All analyses of MD simulations were performed using Python 2.7 and the MDAnalysis package (241, 242). These analyses include the linear interaction energy analysis, the lytic water analysis and the projected covariance magnitude analysis. Further details of each analysis, except for the linear interaction energy, were described below. Plots were created using Matplotlib(239), and VMD(243) was utilized to visualize simulations and generate structural images. All scripts for the analyses are available on GitHub (https://github.com/mccullaghlab/T407_S411_Mutants_of_NS3h).

Waters within the NTPase active site were defined as "lytic" using three collective variables: (1) the nucleophilic attack distance between the water oxygen atom and the ATP γ-phosphorous atom, (2) the nucleophilic attack angle between the water oxygen atom and terminal phosphoanhydride bond of ATP, and (3) the dipole moment angle between the water molecule's dipole moment vector and the terminal phosphoanhydride bond of ATP. The first two metrics describe the geometric positioning of waters within the hydrolysis active site. Waters that have a nucleophilic attack distance less than 5Å and a nucleophilic attack angle greater than 160 degrees have the potential to be the lytic water due to their positioning relative to the terminal phosphate group. The third metric describes the chemically relevant orientation of a water in regard to its nucleophilic attack on this phosphate group. An ideally positioned water with a dipole moment angle of greater than 90 degrees is defined as "lytic". A water that meets all three of these collective variable conditions is positioned in a small volume of the NTPase active site, is hydrogen bonding with the active site's proton acceptor (Glu285) (data not shown), and the water's dipole moment vector is approximately facing the

terminal phosphoanhydride bond vector, as proposed in the SN2 mechanism for the hydrolysis reaction.

The projected covariance magnitude represents the fluctuation between G414 (source residue) and S364 and K366 (sink residues) projected onto the vector spanning the helical gate between subdomain 2 and subdomain 3 of NS3h. G414 was chosen as the source residue due to its coordination with the lytic water within the ATP binding pocket(203), and S364 and K366 were chosen as the sink residues due to their location in the helical gate and large magnitude covariance with G414. The covariance tensors between G414-S364 and G414-K366 were then dotted into the helical gate open/closing vector to obtain how the fluctuation perturbs the opening/closing of the helical gate.

CHAPTER 4 – A HYPERACTIVE KUNJIN VIRUS NS3 HELICASE MUTANT DEMONSTRATES INCREASED DISSEMINATION AND MORTALITY IN MOSQUITOES[2] (244)

Overview and Importance

The unwinding of double-stranded RNA intermediates is critical for replication and packaging of flavivirus RNA genomes. This unwinding activity is achieved by the ATP-dependent nonstructural protein 3 (NS3) helicase. In previous studies, we investigated the mechanism of energy transduction between the ATP and RNA binding pockets using molecular dynamics simulations and enzymatic characterization. Our data corroborated the hypothesis that Motif V is a communication hub for this energy transduction. More specifically, mutations T407A and S411A in Motif V exhibit a hyperactive helicase phenotype leading to the regulation of translocation and unwinding during replication. However, the effect of these mutations on viral infection in cell culture and *in vivo* is not well understood. Here, we investigated the role of Motif V in viral replication using T407A and S411A West Nile virus (Kunjin subtype) mutants in cell culture and *in vivo.* We were able to recover S411A Kunjin but unable to recover T407A Kunjin. Our results indicated that S411A Kunjin decreased viral infection, and increased cytopathogenicity in cell culture as compared to WT Kunjin. Similarly, decreased infection rates in surviving S411A-infected *Culex quinquefasciatus* mosquitoes were observed, but S411A Kunjin infection resulted in increased mortality compared to WT Kunjin. Additionally, S411A Kunjin increased viral dissemination and saliva positivity rates in surviving mosquitoes compared to WT Kunjin. These data suggest that S411A Kunjin increases pathogenesis in mosquitoes. Overall, these data indicate that NS3 Motif V may play a role in the pathogenesis, dissemination, and transmission efficiency of Kunjin virus.

[2] This chapter is from reference (244). Kelly E. Du Pont and Nicole R. Sexton contributed equally to this work. K.E.D. performed the biochemical and in vitro mutant virus characterization and conceptualized the mosquito experiments; N.R.S. designed the final mosquito experiments and analyzed the mosquito data.

Kunjin and West Nile viruses belong to the arthropod-borne flaviviruses, which can result in severe symptoms including encephalitis, meningitis, and death. Flaviviruses have expanded into new populations and emerged as novel pathogens repeatedly in recent years demonstrating they remain a global threat. Currently, there are no approved anti-viral therapeutics against either Kunjin or West Nile viruses. Thus, there is a pressing need for understanding the pathogenesis of these viruses in humans. In this study, we investigate the role of the Kunjin virus helicase on infection in cell culture and *in vivo*. This work provides new insight into how flaviviruses control pathogenesis and mosquito transmission through the nonstructural protein 3 helicase.

Introduction

Kunjin virus, a West Nile virus (WNV) subtype, causes encephalitis epidemics in horses that are localized to Australia (245–248). Whereas, WNV has a much larger global impact present in almost every major continent except for South America and Antarctica (9, 248) and regularly results in encephalitis in humans as well as horses (249). Within the United States alone, approximately 3 million people are thought to have been infected with West Nile virus between 1999 and 2010 (45, 250, 251). Kunjin and WNV share a natural transmission cycle between *Culex* mosquito vectors and bird reservoir hosts (246). Humans and horses are considered dead-end hosts because they do not contribute to viral perpetuation. In humans, around 80% of WNV infected individuals are asymptomatic and the majority of symptomatic individuals experience a mild febrile illness. However, approximately 1:150 infections result in severe symptoms including meningitis and/or encephalitis, and ~9% of these cases are fatal (249, 252). Currently, there are vaccines against WNV for horses, but not for humans; no vaccines are available for Kunjin virus (9). Thus, there is a need for the development of vaccines and/or antiviral therapies for Kunjin and WNV infections. Developing a fundamental understanding of

how Kunjin and WNV replicate within hosts, including the mosquito vector, is essential to the development of interventional strategies.

Kunjin and WNV belong to the *flavivirus* genus within the *Flaviviridae* family. *Flaviviridae* is a group of single-stranded positive-sense RNA viruses with genomes of approximately 11 kb in length (160, 183, 253). Kunjin virus is a subtype of WNV with a nucleotide and amino acid sequence identity of 82% and 93%, respectively (254–256). However, Kunjin virus results in low morbidity compared with WNV infections in humans, making it an excellent tool to study WNV replication with well-established molecular tools while minimizing risk (257). Additionally, Kunjin virus is less cytopathic than WNV, allowing for differences in virus-induced cell viability to be more easily visualized. Proteins and processes involved in viral replication are conserved across the flavivirus genus including for Kunjin, WNV, dengue, yellow fever, Japanese encephalitis, and Zika viruses (160, 258). Initially, the viral RNA genome is translated into a single polyprotein which is cleaved by host and viral proteases into three structural proteins (C, prM, and E) and eight nonstructural proteins (NS1, NS2A, NS2B, NS3, NS4A, 2K, NS4B, and NS5) (2, 160, 258). The viral NS replication proteins then generate a negative-sense anti-genomic RNA that is in complex with the positive-sense genomic RNA, forming the double-stranded RNA (dsRNA) intermediate complex (130, 222). The negative-sense anti-genomic RNA serves as a template for positive-strand synthesis (222); therefore, unwinding of the dsRNA intermediate is required for replication. Unwinding is achieved by the C-terminal helicase domain of NS3 (168, 181, 229).

NS3 helicase domain is a multi-functional viral protein that houses three enzymatic activities: RNA helicase, nucleoside triphosphatase (NTPase), and RNA 5’triphosphatase (RTPase) (145, 175, 228, 259). NS3 helicase is a member of the superfamily 2 (SF2) helicases (170). The helicase domain consists of three subdomains (1, 2, and 3). Subdomains 1 and 2 are RecA-like

structures that are highly conserved across all SF2 helicases, while subdomain 3 is unique to the viral/DEAH-like group of SF2 helicases (227). Additionally, there are eight structural motifs (Motifs I, Ia, II, III, IV, IVa, V, and VI) that are highly conserved across all viral/DEAH-like subfamilies with the SF2 helicases (170). These structural motifs are responsible for both substrate binding and enzymatic function within the helicase. The helicase domain is responsible for translocation and unwinding of the double-stranded RNA intermediate in an ATP-dependent manner during viral replication (182). Previous studies further identified Motif V as potentially critical for translocation and unwinding of the double-stranded RNA intermediate (203, 217). Motif V was described as a potential link between the ATP binding pocket and the RNA binding cleft through strong correlation between residues within Motif V and both binding pockets (203). The strongly correlated movements between ATP binding pocket and RNA binding cleft residues in our simulations suggest a physical linkage between the two sites that may be important for ATP driven helicase function. Additionally, mutants T407A and S411A in Motif V increased unwinding activity and decreased viral genome replication as compared to wild-type (WT), suggesting that the hydrogen bond between these two residues in WT inhibits helicase unwinding activity *in vitro* and *in vivo* (217). These data suggested that Motif V may serve as a molecular throttle on NS3 helicase function, but what effect these residues play on the larger viral replication cycle was not clear.

To better understand the effects NS3 Motif V mutations have on flavivirus replication, we sought to investigate the role of Motif V T407 and S411 residues on helicase function in cell culture and *in vivo* by introducing alanine mutations in full-length infectious Kunjin virus: T407A Kunjin and S411A Kunjin. Only the S411A Kunjin was recovered and it resulted in reduced viral yields compared with wild-type (WT) Kunjin. Additionally, S411A Kunjin showed increased cytopathic effect in comparison to WT Kunjin in cell culture. Similarly, when WT or S411A Kunjin viruses were intrathoracically injected into *Culex quinquefasciatus* mosquitoes, S411A Kunjin resulted in

increased mortality compared with WT Kunjin. Upon further investigation of mosquito infection, S411A Kunjin viruses were found to disseminate and transmit more effectively than WT Kunjin viruses, even though the overall infection rate was lower than WT Kunjin. Overall, our data suggest that flaviviruses may use NS3 Motif V to help control cytotoxicity induced by NS3 during infection and limit virus-induced mortality in mosquito vectors.

Results

S411A Kunjin virus increases cytopathic effect in cell culture

Previously, Motif V residues, T407 and S411, were mutated to alanine to disrupt a hydrogen bond that potentially stabilizes the Motif V secondary structure of NS3 helicase during viral replication (Figure 4.1). These mutations were shown to decrease viral genome replication in a replicon-based system, while increasing helicase unwinding activity biochemically (217). In the present study, we introduced these mutations into the full-length infectious Kunjin virus to investigate the effects of these mutations on infectivity compared to WT Kunjin both in cell culture and in mosquito infections. We utilized a novel mutagenesis and a bacteria-free viral launch system to generate the T407A Kunjin and S411A Kunjin viruses in Vero cells. The first generation of S411A Kunjin was recovered from infected cells, and the presence of the alanine mutation was verified with sequencing (Figure 4.2). The sequencing results provided insight into the stability of the alanine mutation in that the mutation did not revert back to the WT Kunjin sequence. On the other hand, we were unable to recover the T407A Kunjin despite repeated attempts, which was consistent with our previously reported decrease in T407A viral genome replication in replicon assays (217). Second generation stocks of WT Kunjin and S411A Kunjin were generated and the viruses were titered for further experiments. We noted the plaque morphology for both WT Kunjin and S411A Kunjin (Figure 4.3). WT Kunjin showed large, faint plaque sizes with a diameter of 3.3 ± 0.7 mm (Figure 4.3A), while S411A Kunjin showed small, but distinctly clear plaque sizes with a diameter of 1.5 ± 0.3 mm (Figure 4.3B). S411A Kunjin

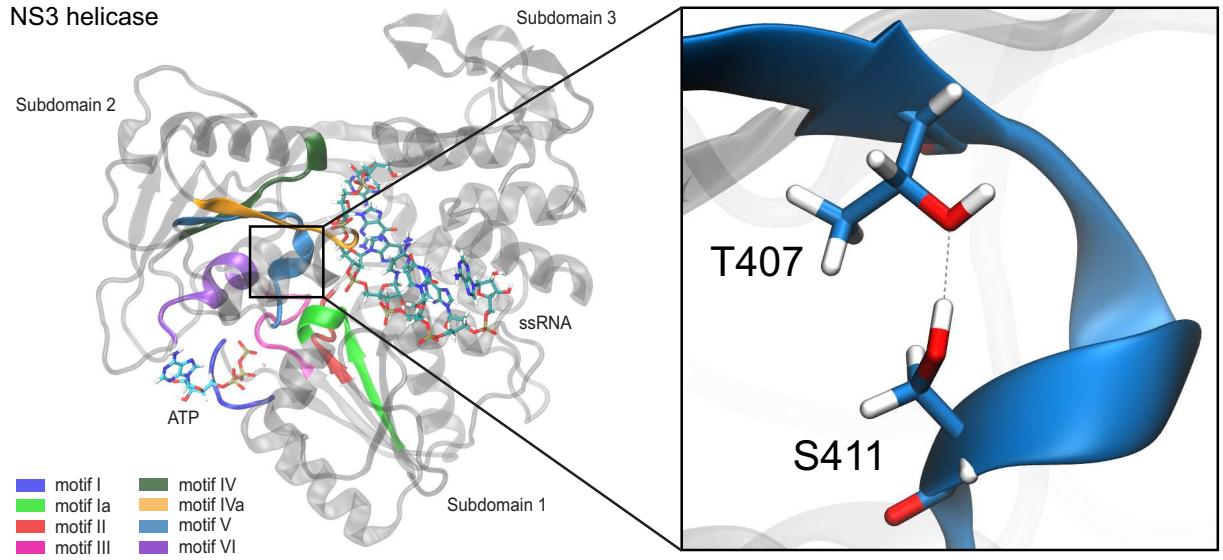

Figure 4.1. S411 and T407 interaction within Motif V in NS3 helicase structure (PDB code 2JLV). NS3 helicase consists of three subdomains: subdomain 1, subdomain 2, and subdomain 3. All highly conserved structural motifs (I, Ia, II, III, IV, IVa, V, and VI) are located within subdomains 1 and 2. Within Motif V, residues T407 and S411 interact with each other through a hydrogen bond as shown in the inset.

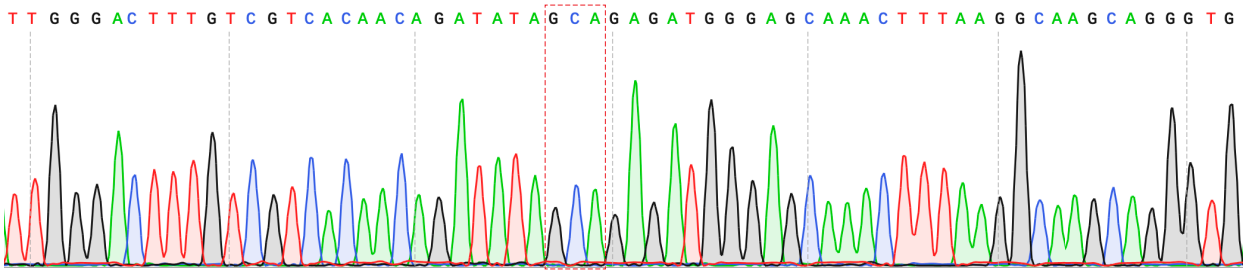

Figure 4.2. Verification of alanine mutation in S411A Kunjin virus via Sanger sequencing. Results from Sanger sequencing verifies alanine mutation for position 411 through the presence of the alanine codon (highlighted in red box). The original serine codon within the red box was TCT. Two nucleotides were changed to introduce the alanine mutation. Refer to GenBank accession number (AY274504.1) for wild-type Kunjin FLSDX.

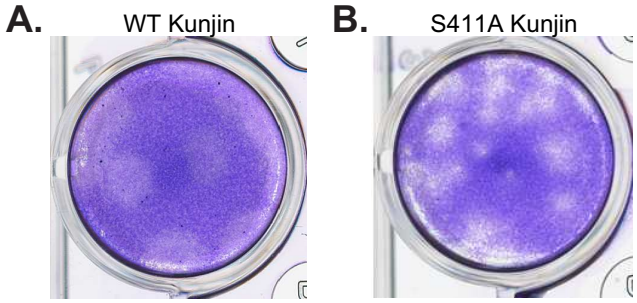

Figure 4.3. Plaque morphology suggests an increased cytopathic effect for S411A Kunjin. Viral titers for second generation WT and S411A Kunjin viruses were obtained via 4 day incubation plaque assays with Vero cells and the plaque morphology is shown for A) WT Kunjin and B) S411A Kunjin. The average diameter ($\varnothing_{avg}$) are reported for both WT Kunjin and S411A Kunjin. The measured diameters were statistically analyzed via t-test (p-value: 0.000003).

plaque sizes were significantly different than WT Kunjin plaque sizes suggesting a potential decrease in viral cell-to-cell spread and an increase in cytopathic effect for S411A Kunjin infected cells compared to WT Kunjin. Since these results suggest that S411A Kunjin may be more toxic to cells than WT Kunjin during infection, we further investigated the effect of the S411A Kunjin on cell viability.

S411A Kunjin reduces NADH and intracellular ATP levels leading to increased cellular death

We utilized resazurin and CellTiter-Glo assays to quantify virus-induced cell killing in HEK293T and Vero cells infected with either WT Kunjin or S411A Kunjin at a multiplicity of infection (MOI) of five PFU/cell. Both of these assays estimate cell viability through the measurement of metabolically active cells using fluorescence and luminescence, respectively. In the resazurin assay, resazurin, a nonfluorescent dye, converts to resorufin, a highly fluorescent dye, in response to the reducing environment of heathy, growing cells (260–262). We measured the relative fluorescence units (RFU) of resazurin in uninfected, WT Kunjin, or S411A Kunjin infected Vero and HEK293T cells every 24 hours for six days (Figure 4.4A and B). We also measured media as a negative control to determine the baseline media fluorescence. The cell viability measurements of uninfected Vero and HEK293T cells increased gradually over the duration of the experiment suggesting that the cells are healthy and growing for the entirety of the experiment. The cell viability measurements during the first 72 hours for WT Kunjin infection in Vero and HEK293T cells were similar to that of uninfected cells. However, the fluorescent signals of the cell viability measurements were lower for infected cells than for uninfected cells. After 72 hours post infection (p.i.), cell viability measurements for WT Kunjin infections continued to increase in fluorescence reaching $7.5 \pm 0.3 \times 10^5$ RFU at 120 hours p.i. for Vero cells and $7.8 \pm 0.2 \times 10^5$ RFU at 96 hours p.i. for HEK293T cells. After which point, cell viability measurements decreased in fluorescence by 144 hours p.i. suggesting that WT Kunjin induced cell toxicity is overtaking cellular replication. In the case of S411A Kunjin infected Vero and

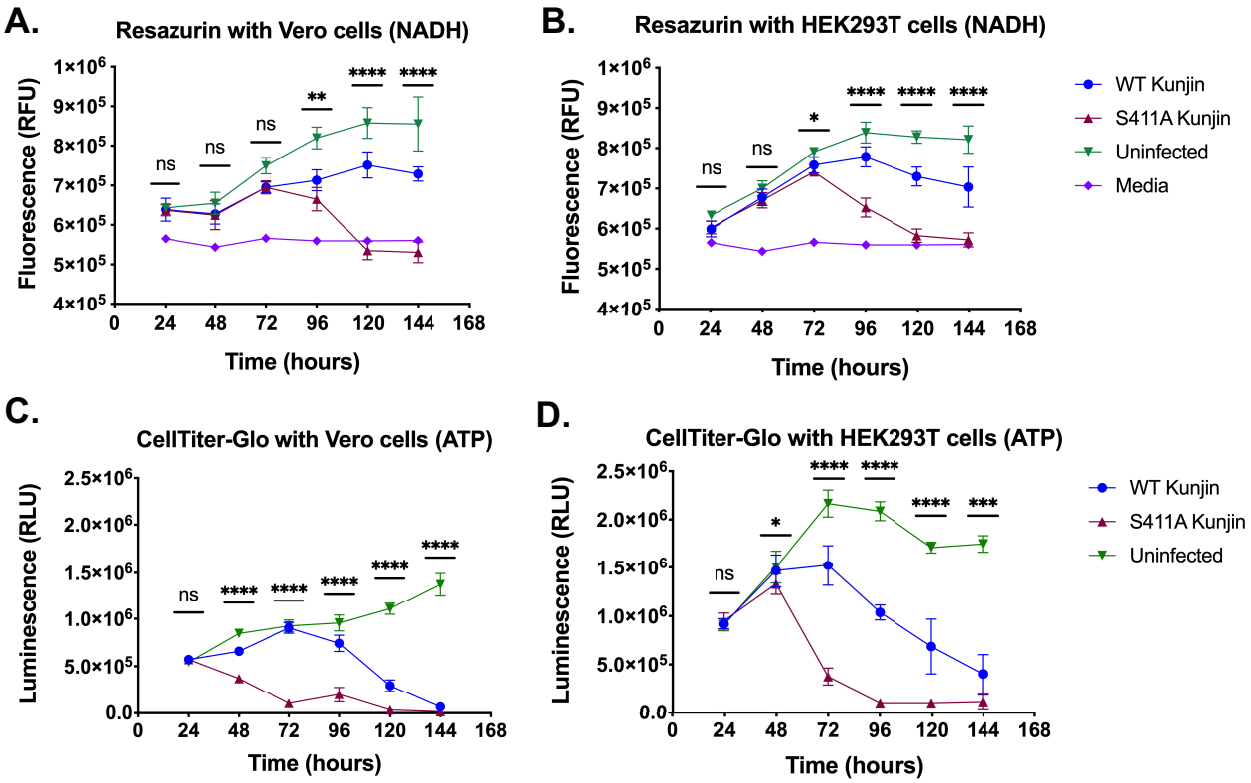

Figure 4.4. S411A Kunjin decreases cell viability. WT Kunjin and S411A Kunjin infected A) Vero cells and B) HEK293T cells were measured for cellular metabolism through resazurin. Similarly, WT Kunjin and S411A Kunjin infected C) Vero cells and D) HEK293T were measured for intracellular ATP levels through CellTiter-Glo. All infections were performed at a MOI of five PFU/cell in triplicate. Cell viability curves were statistically analyzed by unpaired t test and the significance for WT Kunjin verse S411A Kunjin was reported ($P \leq 0.0001$ = ****, $P \leq 0.001$ = ***, $P \leq 0.01$ = **, $P \leq 0.05$ = *).

HEK293T cells during the first 72 hours, cell viability measurements demonstrated similar levels of fluorescence to that of uninfected cells. Although the cell viability measured for S411A Kunjin was decreased compared to uninfected cells. As the S411A Kunjin infection continued, cell viability measurements significantly reduced in fluorescence between 96 and 144 hours p.i. ending with 5.3 ± 0.3 $x10^5$ RFU for Vero cells and 5.7 ± 0.2 $x10^5$ RFU for HEK293T cells. Together, these data suggest that cells are relatively healthy in Kunjin infected cells for at least the first 72 hours in Vero and HEK293T cells; after which point population cell viability in S411A Kunjin infected cells is negatively affected immediately in both cell lines, whereas a 24 hour and 48 hour delay are observed for decreased cell viability measurements with WT Kunjin infection for HEK293T and Vero cells, respectively.

Another way to infer metabolically active cells or cell viability is through detection of intracellular ATP levels. We utilized the CellTiter-Glo assay which uses the luciferase reaction, an ATP-dependent reaction, to convert luciferin to oxyluciferin and several byproducts including light (260). The byproduct, light, was measured in relative luminescence units (RLU) for uninfected, WT Kunjin or S411A Kunjin infected Vero and HEK293T cells every 24 hours for six days (Figure 4.4C and D). Over the course of the experiment, uninfected Vero cells progressively increased in luminescence from 5.5 ± 0.3 $x10^5$ to 1.4 ± 0.1 $x10^6$ RLU (Figure 4.4C) suggesting that the uninfected cells were healthy and metabolically active for the six-day experiment. However, cell viability measurements of uninfected HEK293T cells increased linearly for the first 72 hours; after which point, the cell viability measurements decreased and then leveled off at 1.7 ± 0.07 $x10^6$ RLU (Figure 4.4D), suggesting that uninfected HEK293T cells become less metabolically active after 96 hours compared to the Vero cells. As for infection with WT Kunjin, the cell viability measurements steadily increased for the first 72 hours for Vero cells and for the first 48 hours for HEK293T cells similar to the observed cell viability measurements of uninfected Vero and HEK293T cells. At 96 hours p.i. in Vero cells and 72 hours p.i. in HEK293T

cells, cell viability measurements of WT Kunjin infected cells decreased compared to uninfected cells. The population cell viability of WT Kunjin infected cells continued to decrease reaching 6.5 ± 3.0 $x10^4$ RLU in Vero cells and 4.0 ± 2.0 $x10^5$ RLU in HEK293T cells at 144 hours. These data suggested that infection with WT Kunjin negatively affected cell viability after 72 hours p.i. compared to uninfected cell viability. On the other hand, cell viability measurements with S411A Kunjin infection decreased after 24 hours p.i. in Vero cells and after 48 hours p.i. for HEK293T cells. For the remainder of the experiment, the population cell viability continued to decrease in S411A Kunjin infected Vero and HEK293T cells suggesting that both Vero and HEK293T cells are extremely sensitive to S411A Kunjin and thus cell viability is significantly reduced in the presence of the mutated virus. Together, these results suggest that infection with S411A Kunjin in either Vero or HEK293T cells negatively affected cell viability more quickly than infection with WT Kunjin.

S411A Kunjin results in decreased and delayed viral replication kinetics

The results presented in the previous section indicated that S411A Kunjin induced increased cellular death during infection. This prompted the question: how does increased cellular death resulting from infection with S411A Kunjin affect replication kinetics of the virus? Therefore, we performed a multi-step replication kinetics experiment with WT or S411A Kunjin infected HEK293T cells at a MOI of 0.01 PFU/cell over a five day period. Every 12 hours the media containing viruses were collected and viral titers were determined via focus forming assays (Figure 4.5). At 12 hours post infection, the WT and S411A Kunjin viral titers were not significantly different. At 24 hours p.i., S411A Kunjin remained in the lag phase while WT Kunjin had entered the exponential replication phase, demonstrating delayed replication with the S411A Kunjin infection. Over the last four days of infection, S411A Kunjin maintained and expanded the initial delay in exponential replication and reached an ~1 log lower peak viral titer compared to WT Kunjin. Overall, these data suggest that S411A Kunjin does not replicate as

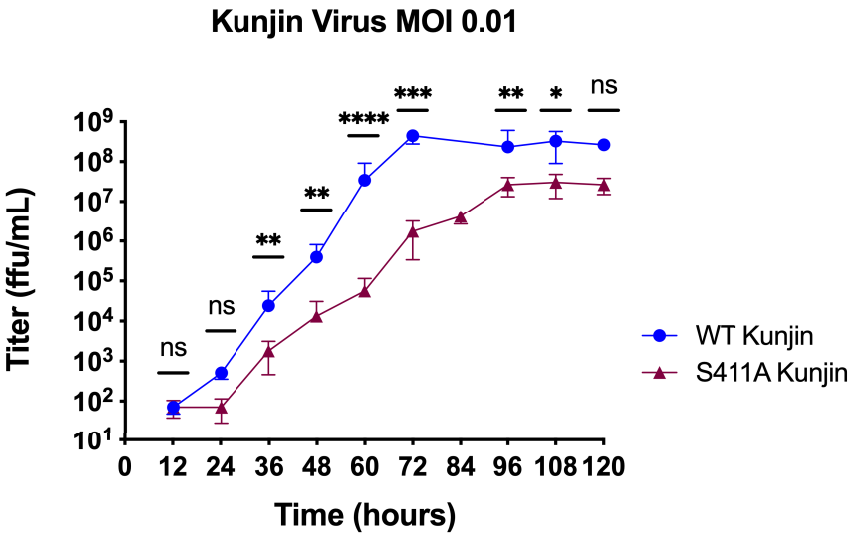

Figure 4.5. S411A Kunjin decreases and delays viral replication kinetics. Replication kinetics experiments were performed in triplicate for WT and S411A Kunjin viruses. HEK293T cells were infected at a MOI of 0.01 PFU/cell. Viral samples (media) were collected every 12 hours for 5 days and processed to obtain viral titers using Vero cells in focus forming assays. Viral replication curves were compared by F test and the significance for WT Kunjin verse S411A Kunjin was reported ($P \leq 0.0001$ = ****, $P \leq 0.001$ = ***, $P \leq 0.01$ = **, $P \leq 0.05$ = * , $P > 0.05$ = ns).

efficiently as WT Kunjin. These results are consistent with data reported by Du Pont *et al.*, suggesting that the increased helicase unwinding activity seen with the recombinant S411A NS3 helicase negatively affects viral replication in fully infectious S411A Kunjin virus (217). Considering the observations that S411A Kunjin resulted in decreased viral replication and increased cellular death, we next investigated the effects of the S411A mutation on Kunjin infection *in vivo*.

S411A Kunjin results in increased mortality in mosquitoes compared to WT Kunjin when IT injected but not when bloodfed.

For the *in vivo* studies, we did not have access to a colony of *Cx. annulirostris* mosquitoes, the primary vector for Kunjin virus, but we had an established colony of *Cx. quinquefasciatus* that are infectable by Kunjin virus. *Cx. quinquefasciatus* mosquitoes were bloodfed with defibrinated calf's blood diluted by half with titer equilibrated WT Kunjin, S411A Kunjin, or media alone as a negative control. Similarly, female *Cx. quinquefasciatus* mosquitoes were subjected to intrathoracic injection (IT) of 345 plaque forming units (PFU) per mosquito of WT Kunjin, S411A Kunjin, or conditioned media. Mosquito mortality was recorded daily for 15 or 9 days, respectively. Overall, virus exposed mosquito mortality was low in both the bloodfed and IT injected cohorts (Figure 4.6), consistent with previous observations of Kunjin virus in *Cx. quinquefasciatus* mosquitoes (263). When bloodfed, no difference was observed in mortality rates for mosquitoes exposed to WT Kunjin vs. S411A Kunjin. However, the small rate of mortality for virus exposed mosquitoes (~10%) was significantly different from mosquitoes exposed to media alone (Figure 4.6A). In contrast with bloodfed data but consistent with cell culture and replication kinetics data, when virus was introduced through IT injection, to bypass the midgut barrier, only S411A Kunjin resulted in increased mortality (Figure 4.6B). Together these data suggest that S411A Kunjin is more lethal to mosquitoes than WT Kunjin once the virus has been able to establish an infection and/or transverse through the mosquito midgut

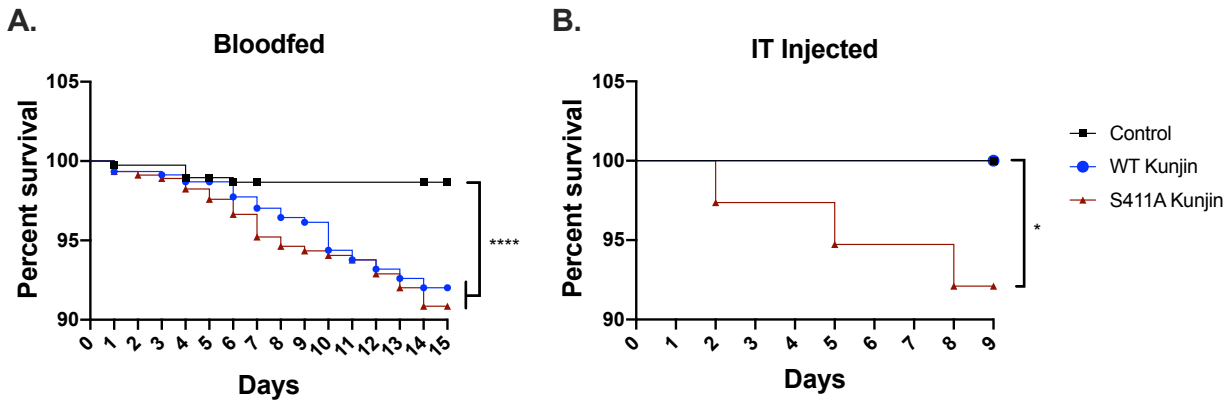

Figure 4.6. S411A Kunjin viruses are more lethal to *Cx. quinquefaciatus* mosquitoes than WT Kunjin. Female *Cx. quinquefaciatus* mosquitoes were exposed to WT (blue circles) or S411A (red triangles) Kunjin virus through either A) infectious bloodmeals, or B) by IT injection. Control mosquitoes were exposed to bloodmeals containing media or injected with media alone. Mortality was recorded daily for 15 or 9 days respectively. Survival curves compared by Logrank test for trend (P<0.0001 = ****, P<0.05 = *) A) n = 425 mosquitoes/condition, B) n = 40 mosquitoes/condition. In B) WT and S411A Kunjin traces overlap.

barrier. This result led us to further investigate the specifics of infection of *Cx. quinquefasciatus* by WT and S411A Kunjin viruses.

S411A Kunjin has a lower infection rate but disseminates more efficiently than WT Kunjin

Similar to the mortality experiments, *Cx. quinquefasciatus* mosquitoes were infected with either WT Kunjin or S411A Kunjin by bloodmeal. Mosquito legs/wings, saliva, and bodies were collected after 7 days and determined to be positive or negative for infection by plaque assay. While ~58% of mosquitoes infected with WT Kunjin were positive for the virus at day 7, only ~8% of mosquitoes infected with S411A Kunjin were positive (Figure 4.7A). Dissemination was inefficient for WT Kunjin with only 6% of mosquitoes having positive titers in the legs and wings, demonstrating a strong barrier to escape from the midgut. Similarly, less than 2% of infected mosquitoes resulted in positive saliva samples (Figure 4.7A). Despite low infection rates for mosquitoes infected with S411A Kunjin, positive legs/wings and saliva were identified across multiple replicate experiments, with nearly 50% of infected mosquitoes having disseminated virus and 50% of those with disseminated virus having positive saliva. These data led to the question: does S411A Kunjin allow for higher relative rates of dissemination?

To answer this question a second, much larger cohort of *Cx. quinquefasciatus* mosquitoes were infected by bloodmeal with WT Kunjin or S411A Kunjin. Enough mosquitoes were dissected to generate and estimated 30 infected mosquitoes per condition: 60 exposed to WT Kunjin and 390 exposed to S411A Kunjin. Since mosquitoes continue to die up to 14 days post bloodfeed, mosquitoes were collected at 14 days post blood meal instead of 7 days in an attempt to assure sufficient numbers of S411A Kunjin infected mosquitoes. Again, WT Kunjin was observed to infect a larger percent of exposed mosquitoes compared with S411A Kunjin (~30% vs. ~15%) (Figure 4.7B,C), whereas, S411A Kunjin demonstrated higher rates of dissemination compared with WT Kunjin (Figure 4.7B,D). No legs/wings or saliva samples from WT Kunjin infected

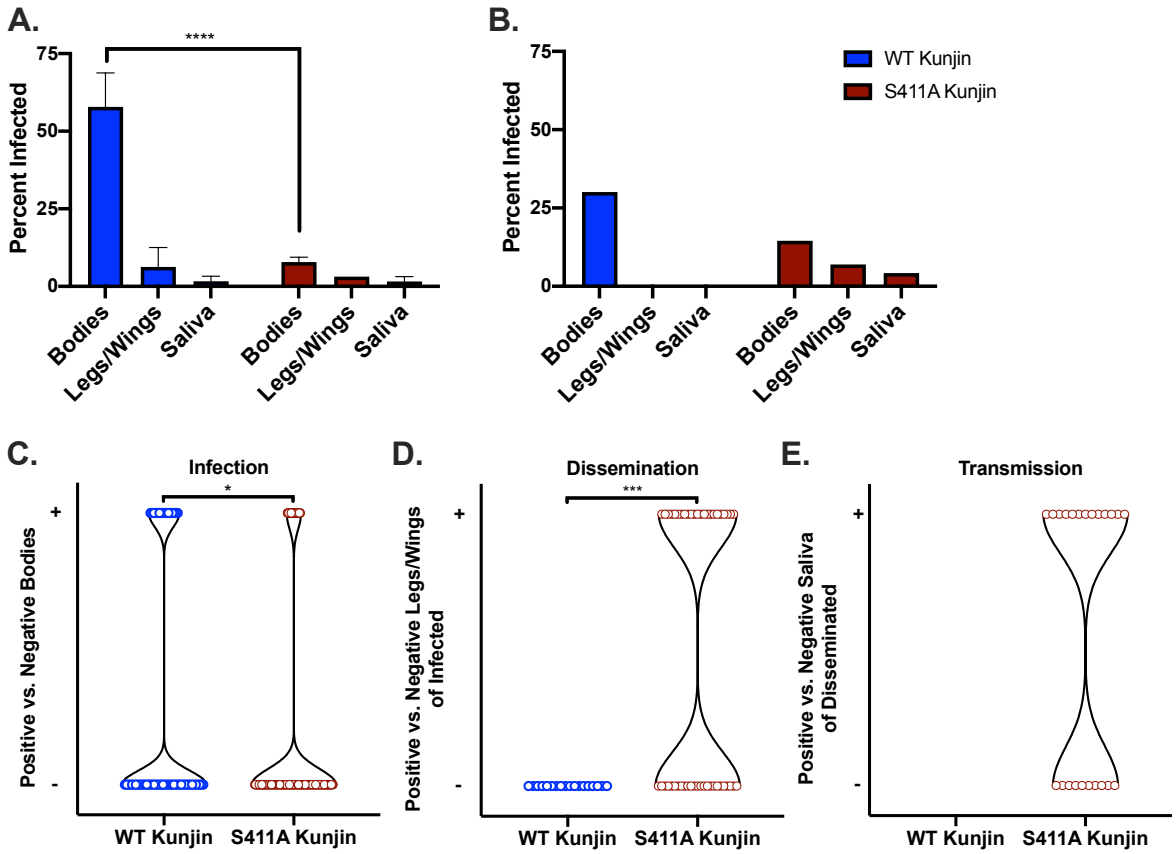

Figure 4.7. S411A Kunjin is less capable than WT Kunjin of infecting mosquitoes but disseminates and transmits more efficiently once established. Engorged female *Cx. quinquefascitus* mosquitoes exposed to infectious bloodmeals containing either WT or S411A Kunjin virus were housed for A) 7 or B to E) 14 days post bloodfeed. Mosquitoes were dissected and legs/wings, saliva and bodies were collected and tested for the presence or absence of Kunjin virus by plaque assay on Vero cells of undiluted samples. Data are shown as A and B) percent of total exposed infected, C) total negative and positive bodies, D) positive legs/wings from total infected, or E) total positive saliva from total disseminated. A) n = 64 mosquitoes/condition, B) WT Kunjin n = 60 mosquitoes, S411A Kunjin n = 390 mosquitoes. A) Error bars represent SEM. A, C-E) Infection, dissemination, and transmission compared using Fisher exact test (P<0.0001 = ****, P<0.001 = ***, P<0.05 = *).

mosquitoes were found to be positive at 14 days post blood meal (Figure 4.7B,D,E). In contrast and supporting these data from smaller cohorts collected at 7 days post blood meal, 48% of S411A Kunjin infected mosquitoes had infected legs/wings and 61% of mosquitoes with S411A Kunjin infected legs/wings resulted in positive saliva samples. These data demonstrate that the S411A Kunjin was less capable of infecting *Cx. quinquefasciatus* via blood meal compared with WT Kunjin. However, these data also suggest that when S411A Kunjin was able to establish infection in *Cx. quinquefasciatus* mosquitoes it is able to escape the midgut barrier more efficiently than WT Kunjin, resulting in dissemination, infection of the salivary glands, and delivery to the saliva. Finally, when considered in combination with the survival data, these data further support that when S411A Kunjin was able to establish infection in *Cx. quinquefasciatus* mosquitoes it is more lethal.

Discussion

Previous work by our group has supported the hypothesis that Motif V in flavivirus NS3 helicase is a communication hub for translocation and unwinding of the dsRNA intermediate during flavivirus replication (203, 217). More specifically, we found that NS3 Motif V residues T407 and S411 exhibit an increased helicase unwinding activity in biochemical assays when mutated to alanine residues, while we observed a reduction in replication of T407 and S411 mutant replicons. These previous results suggest that T407 and S411 are responsible for regulating NS3 helicase function during flavivirus replication. In this study we further investigated the role of T407 and S411 helicase residues in the full-length infectious Kunjin virus in cell culture and *in vivo* experiments. S411A Kunjin was successfully recovered and confirmed via sequencing (Figure 4.2). However, T407A Kunjin was not recovered which was consistent with the previous results indicating ablated viral genome replication activity (217). We utilized WT Kunjin and S411A Kunjin in several cell culture experiments including viral replication, resazurin and CellTiter-Glo assays. Additionally, we compared WT Kunjin and S411A Kunjin in several *in vivo*

experiments including infection, dissemination and transmission within *Cx. quinquefasciatus* mosquitoes. We observed that the S411A Kunjin reduced cell viability during infection leading to increased cytopathic effect observed in the plaque morphology and several metabolic assays in cell culture. Additionally, the results demonstrated a lower initial infection rate for S411A Kunjin than for WT Kunjin within mosquitoes. However, once infection was established, the more efficient dissemination of S411A Kunjin compared with that of WT Kunjin occurred, potentially causing the observed increased mortality rates in S411A Kunjin-infected mosquitoes compared to WT Kunjin-infected mosquitoes. Overall, our data suggest that the NS3 S411 in Motif V influences infection induced cellular death and subsequent mortality in mosquito vectors.

Plaque morphology of viruses is a classical indicator of the effects of a mutation on viral cytopathic effect in cells and spread between cells. We observed large and fuzzy plaques with WT Kunjin, while S411A Kunjin plaques were small and clearly defined (Figure 4.3), suggesting that S411A Kunjin is more toxic to cells, but is not able to spread as rapidly as WT Kunjin. Our previous work had indicated that the S411A mutation in a replicon-based system reduced viral genome replication (217), so the small plaque size was expected. However, the formation of clearer plaques was not. Therefore, we performed a more quantitative investigation of S411A Kunjin effect on cell viability using two assays (resazurin and CellTiter-Glo) that probed for different aspects of metabolically active cells, NADH content and ATP content. The results from both assays indicated that infection with S411A Kunjin results in a larger decrease in metabolic activity compared to WT Kunjin within both HEK293T and Vero cells (Figure 4.4). Previously, studies have shown that reduced intracellular ATP levels leads to proteasome inhibition that induces apoptosis leading to cellular death (264–269). Therefore, our metabolic activity data is consistent with our plaque morphology data in that infection with S411A Kunjin results reduced intracellular ATP levels and increased cytopathic effect through increased cell death. S411A Kunjin exhibited delayed and decreased viral replication kinetics compared to WT Kunjin (Figure

4.5) suggesting that even though the mutated Kunjin virus is more toxic to cells, it does not replicate as efficiently as WT Kunjin. These data are consistent with previous studies reporting a decrease in viral genome replication seen with S411A helicase replicon (217). The previously reported replicon data are a few orders of magnitude different than the viral replication kinetics due to the lack of spread from the replicon infected cell. The Kunjin virus replicon is an end-point experiment so once the replicon is transfected into the cells, it cannot exit the cells since it does not have the structural proteins that are required for viral assembly. Whereas viral replication kinetics is a continual experiment using infectious virus that can spread between cells. As subsequent infections occur, the reduced replication rates accumulate caused a higher reduction in replication as compared to in the replicon system.

An interesting but different hypothesis is that hyperactive NS3 helicase affects cellular mRNA. Studies on NS3 helicase function have focused primarily on its effect on genome replication and packaging (270), but our finding that a NS3 hyperactive helicase mutant increases cell death opens up the possibility that NS3 has roles in altering cellular physiology as well. Previously observed results indicated that recombinant NS3 S411A helicase mutant had a higher rate of helicase activity than the WT but did not have a significantly higher rate of ATPase activity (217), so it is unlikely that reduction of cell viability was due to decreased amounts of ATP from NS3 ATP degradation. However, it is possible that increased cytotoxicity is due to another effect of helicase activity on cellular physiology. The hyperactive NS3 helicase may be interacting with cellular RNAs leading to dysregulation of cellular homeostasis. NS3 could bind to cellular mRNAs and unwind their secondary structures, causing a disruption in RNA stability and recruitment of translational factors. This unwinding of cellular mRNAs would result in an imbalance within the cell inducing cellular apoptosis. We are currently exploring if NS3 effects cellular RNAs.

Observed reductions in cell viability led us to investigate the effect of S411A on infection in mosquitoes. Generally, the longevity of mosquitoes infected with flaviviruses are similar to that of uninfected mosquitoes (79, 271). During mosquito infection, flaviviruses must overcome four barriers: 1) midgut infection barrier, 2) midgut escape barrier, 3) salivary gland infection barrier, and 4) salivary gland escape barrier (272). For the first barrier, the virus must successfully infect and replicate in the midgut epithelial cells (83, 272). Infection is dependent on the arbovirus-specific interactions with the midgut epithelial receptors (86). If the virus cannot establish an infection in the midgut epithelial cells, then the mosquito cannot be infected by the virus. If the virus can establish infection in the midgut, then the next barrier is escaping the midgut by crossing the basal lamina which surrounds the midgut epithelium (272). After escaping the midgut, the virus can disseminate throughout the rest of the mosquito tissues. If the virus is able to penetrate into the salivary gland, the virus must replicate and be deposited into the apical cavities of acinar cells for the mosquito to transmit the virus to other hosts (272). Not all mosquitoes will be able to transmit virus due to unknown reasons. *Culex* mosquitoes in our study were bloodfed or submitted to intrathoracic injection (IT) with either WT or S411A Kunjin. Mosquito mortality was recorded for 15 days for bloodfed mosquitoes or 9 days for IT injected mosquitoes. Results indicated no significant difference in mortality between mosquitoes bloodfed with either WT or S411A Kunjin viruses. However, when combined with the low infection rates observed for S411A Kunjin (Figure 4.7) these results suggest that S411A Kunjin is more lethal than WT if infection is established after being taken up by a bloodmeal. Supporting this, mosquitoes that were intrathoracically injected with S411A Kunjin exhibited an increase in mortality compared to WT Kunjin. Interestingly, WT lethality was only observed in mosquitoes when administered by bloodfeed suggesting that Kunjin may result in death most commonly as a result of midgut infection. Together, our data suggests that S411A Kunjin viruses were inefficient at crossing the midgut infection barrier to establish infection (Figure 4.7). However, upon bypassing the midgut infection and midgut escape barriers through IT injection

S411A Kunjin was more lethal (Figure 4.6B). The basis for the observed increased mortality is not yet clear but could be due to increased cytopathic effect in infected cells similar to what was observed in cell culture.

To further investigate the distribution of WT Kunjin and S411A Kunjin infection within the *Cx. quinquefasciatus* mosquitoes, bodies, legs/wings, and saliva were collected after 7 or 14 days post-bloodfeed and analyzed for the presence of virus. 30 (day 14) to 50% (day 7) of mosquito bodies were positive for WT Kunjin infection, whereas less than 15% of bodies were positive for S411A Kunjin on either collection day. These data suggest that WT Kunjin was able to routinely establish infection within midgut epithelial cells, while S411A Kunjin did so less effectively. However, when legs/wings and saliva were analyzed, WT Kunjin was found at extremely low levels, while S411A Kunjin was found in over half of infected mosquitoes suggesting that once S411A Kunjin was able to cross the midgut escape barrier, it was able to replicate more efficiently in peripheral tissues than WT Kunjin. One interesting finding was that at 7 dpi some mosquitoes infected with WT Kunjin were observed to have virus present in legs and wings, and saliva but none were at 14 dpi. Since dissemination for WT Kunjin was rare, it is possible that mosquitoes that experience dissemination by WT Kunjin are more likely to die than those where the infection is maintained within the midgut. This phenomena is not typical in flavivirus infections of mosquitoes (273, 274).

Previous studies have suggested that arboviruses may require apoptosis to escape the midgut and infect the salivary glands of *Culex* mosquitoes (83, 275–278). Thus, taking into account the cell culture results suggesting S411A Kunjin induces increased cellular death, S411A Kunjin viruses may be able to exit the midgut more effectively than WT Kunjin due to increased induction of apoptosis. Even though S411A Kunjin has a lower initial infection rate, the mutant virus is more toxic to infected cells, and thus, the mutant virus may be able to induce apoptosis

and disseminate into the rest of the body leading to a higher potential transmission rate with increased salivary gland infection.

In conclusion, this study provides insight into how a hyperactive NS3 helicase mutant virus contributes to Kunjin virus replication and the effect on cellular responses during infection. S411A Kunjin negatively affects overall replication of the virus and increases the cytopathic effect in cells potentially resulting in increased mosquito mortality. Infection with S411A Kunjin results in less metabolic activity in cells and ultimately cellular death. When considering the increased mortality of mosquitoes IT injected with S411A Kunjin, it seems likely that cells within mosquitoes are undergoing similar cytopathic effect as was observed in cell culture. Cellular death in mosquitoes could allow S411A Kunjin to disseminate into the legs/wings and saliva more efficiently than WT Kunjin and result in increased mosquito death. Virus-induced mortality is not ideal for long-term maintenance of virus in mosquitoes, so flaviviruses appear to have evolved mechanisms to reduce their helicase activity to reduce virus-induced cell killing. Overall, these data indicate that NS3 helicase activity may have significant roles during viral infection in cell culture and *in vivo*, and that NS3 Motif V may play a central role in controlling virus-induced mortality in mosquito vectors to allow for efficient viral transmission.

Materials and methods

Cell Culture and Viruses

HEK293T and Vero (African Green Monkey kidney epithelial) cells were maintained in Hyclone Dulbecco's modified Eagle medium (DMEM) supplemented with 10% fetal bovine serum (FBS), 50 mM HEPES (pH 7.5), 5% penicillin/streptomycin and 5% L-Glutamine. All cells were grown in humidified incubators at 37 °C with 5% CO_2. The West Nile virus (Kunjin subtype) infectious clone was generously provided from Alexander Khromykh (University of Queensland) (279).

Virus Mutagenesis

To produce the T407A Kunjin and S411A Kunjin NS3 mutants viruses, a novel bacteria-free virus launch system was used based on *in vitro* NEBuilder assembly of PCR-amplified DNAs containing a eukaryotic Pol II promoter with PCR fragments containing viral genome sequences and direct transfection of assembled DNAs into Vero cells. Three PCR fragments were produced using the Q5 DNA polymerase system (New England Biolabs) according to the manufacturer's instructions (279). PCR fragment #1 contained the cytomegalovirus (CMV) immediate early promoter (612 bp) using pcDNA-3.1 as the PCR template. PCR fragment #2 (5867 bp) contained the 5' region of the Kunjin virus genome. PCR fragment #3 (5309 bp) contained the 3' end of the Kunjin virus genome in addition to a hepatitis delta virus ribozyme. The Kunjin virus infectious clone plasmid FLSDXHDVr was used as the PCR template for fragments #2 and #3 (280). Primer sequences used to produce PCR fragments with overlapping 5' and 3' ends for NEBuilder assembly were designed using the NEBuilder Assembly tool and are listed in Table 4.1.

The NS3 T407A and S411A mutations(217) were separately engineered into the Fragment #2 reverse primer and Fragment #3 forward primers. PCR products were gel extracted with the Qiagen Gel Extraction kit and quantified by UV spectrophotometry and agarose gel electrophoresis. To assemble the WT Kunjin, T407A Kunjin, or S411A Kunjin fragments, equal molar amounts of each fragment were mixed in a total DNA mass of 200 ng for each virus in ultrapure water in a final volume of 15 µL. An equal volume of New England Biolabs NEBuilder 2X Master Mix was added to the DNAs, and the reaction was incubated at 50°C for 4 hrs. The assembled DNAs were transfected directly into Vero cells by adding 1 µL of JetPrime transfection reagent (PolyPlus) to the assembly mixture, incubated at 22°C for 15 minutes, and the transfection mixture was added to 50% confluent Vero cells. DMEM media containing 10% fetal bovine serum and 50 mM HEPES (pH 7.5) was changed 24 hours after transfection, and

Table 4.1. NEBuilder Primers for T407A and S411A Kunjin Viruses. The mutant Kunjin viruses were generated from three fragments: #1, #2, and #3. Primers for fragments #2 and #3 contain the alanine mutation at either position 407 or 411 (highlighted in red). The product of Fragment #2 from the NEBuilder Assembly reaction will contain the specified mutation.

Fragment #	NEBuilder Primers	Primer Sequence (5'-overlap/spacer/ANNEAL-3')
#1: CMV	CMV Forward	atcggaatctGATTATTGACTAGTTATTAATAGTAATCAATTACG
	CMV Reverse	gcgaactactCGGTTCACTAAACGAGCTC
#2: 5' T407A Kunjin Virus	5' Kunjin Forward	tagtgaaccgAGTAGTTCGCCTGTGTGAG
	5' Kunjin (T407A) Reverse	atatatctgtGGCGACGACAAAGTCCCAATC
#3: 3' T407A Kunjin Virus	3' Kunjin (T407A) Forward	tgtcgtcgccACAGATATATCTGAGATGGG
	3' Kunjin Reverse	gtcaataatcTTCCGATAGAGAATCGAG
#2: 5' S411A Kunjin Virus	5' Kunjin Forward	tagtgaaccgAGTAGTTCGCCTGTGTGAG
	5' Kunjin (S411A) Reverse	ctcccatctcTGCTATATCTGTTGTGACGAC
#3: 3' S411A Kunjin Virus	3' Kunjin (S411A) Forward	agatatagcaGAGATGGGAGCAAACTTTAAG
	3' Kunjin Reverse	gtcaataatcTTCCGATAGAGAATCGAG

the cells were incubated for 6 additional days and monitored for cytopathic effect. Media was collected on day 6 as the P0 stock. Virus was amplified in a T75 flask seeded at 50% confluency for 7 additional days, and clarified media was collected as the P1 stock. Finally, the P1 stock was used to infect a T150 flask of 50% confluent Vero cells for 7 days, media was collected and clarified of cellular debris, and clarified media frozen at -80°C as the P2 stock. P2 stocks were quantified for infectivity via focus forming assay. T407A Kunjin was unrecoverable from infections. The presence of the S411A Kunjin was verified by extracting RNA from the P2 stock, reverse transcribing and PCR amplifying the NS3 region of Kunjin virus using Kunjin NS3 sequence forward (5'-ATGCACCAATATCCGACTTACA) and reverse (5'-TGGCCTCAGAATCTTCCTTTC) primers, and the sequence of the PCR 794 bp amplicon determine by Sanger sequencing.

Viral Infectivity

HEK293T cells were plated into 12-well plates at 20,000 cells/well and allowed to adhere to the plates overnight. The next day, the cells were infected at a MOI of 0.01 PFU/cell with either WT Kunjin or S411A Kunjin in triplicate under BSL2 conditions. Both intracellular and extracellular viral samples were collected every 12 hours for five days. The extracellular viral samples were processed through focus forming assays to determine the viral titer at each time point. The growth curves were plotting using matplotlib (239).

Resazurin Assay

HEK293T cells were plated into 96-well plates at 10,000 cells/well. Additionally, DMEM with 10% FBS was plated into one row for each plate as a negative control for resazurin. The following day, cells were either not infected or infected with either WT or S411A Kunjin at a MOI of five PFU/cell. The DMEM media was not infected. Every 24 hours over the course of six days, the cells as well as the negative control were treated with resazurin (0.15 mg/mL). The

treated plate was then incubated for 1 hour at 37°C with 5% CO_2 before measuring the fluorescence at an excitation wavelength of 560 nm and an emission wavelength of 590 nm on a Victor X5 multilabel plate reader (Perkin Elmer).

CellTiter-Glo Assay

Vero and HEK293T cells were plated into 96-well plates at 10,000 cells/well. The following day, cells in each plate were either not infected or infected with WT or S411A Kunjin at a MOI of five PFU/cell. Every 24 hours for the next six days, cells were treated with 1X of CellTiter-Glo and incubated at room temperature for 10 minutes before measuring luminescence with an exposure time of 0.5 seconds on a Victor X5 multilabel plate reader.

Mosquitoes

Cx. quinquefasciatus mosquito larvae(281), were propagated on a 1:1 mix of powdered Tetra food and powdered rodent chow. Adult mosquitoes were kept on a 16:8 light:dark cycle at 28°C with 70%-80% humidity. Water and sugar were provided ad libitum and citrated sheep blood was provided to maintain the colony. Mosquito infection experiments with Kunjin were performed exclusively on female mosquitoes and under BSL3 conditions.

Infection of mosquitoes with Kunjin virus and analysis

Cx. quinquefasciatus mosquitoes were either fed infectious bloodmeals or intrathoracically injected to introduce Kunjin virus. Bloodfed mosquitoes were fed an infectious bloodmeal of defibrillated calf blood diluted by half with 2.5 X 10^6 PFU/mL Kunjin virus, or media alone as a negative control. Bloodmeals also contained 2 mM ATP. For IT injection experiments, mosquitoes were injected with 138 nL WT or S411A Kunjin virus (~345 PFU/mosquito) using a Nanoject II (Drummond Scientific). Engorged female mosquitoes were maintained for up to 15 days under conditions described above but in the BSL3 insectary and mortality rate counted

daily. For infection, dissemination, and transmission experiments after 7 or 14 days of incubation, mosquitos were cold anesthetized and kept on ice while legs and wings were removed, mosquitoes were salivated for 30 minutes in a capillary tube filled with immersion oil, and bodies were collected. Legs/wings and bodies were homogenized at 24Hz for 1 minute in 500 mL mosquito diluent with a stainless steel bead, and saliva samples were stored in 250 mL mosquito diluent as previously described (282). All mosquito samples were clarified by centrifugation at 15,000 X g for 5 minutes at 4°C then determined to be positive or negative by infection with undiluted samples by tragacanth gum overlay plaque assay on Vero cell monolayers as previously described (283).

Visual Analysis of NS3

Dengue virus 4 NS3 helicase crystal structure (Protein Data Bank code 2JLV) was obtained for visual presentation. All structural images were generated using VMD (243). The interaction highlighted between residues 407 and 411 is the measured distance between the two residue sidechains.

CHAPTER 5 – CONCLUSION

Summary

Over half of the world's population is at risk of flaviviral infection due to the large presence of mosquito-borne flaviviruses worldwide such as dengue virus (DENV), Yellow Fever virus (YFV), West Nile virus (WNV), Japanese Encephalitis virus (JEV), Zika virus (ZIKV), and St Louis Encephalitis virus (SLEV). When infection occurs from these flaviviruses, a range of symptoms can arise in the form of a mild-illness of flu-like fevers to more severe diseases of encephalitis, hemorrhagic fevers, microcephaly, and Guillain-Barré syndrome all of which can potentially lead to death (3, 5, 6). Typically, the more severe diseases are caused by an antibody-dependent enhancement (ADE) of viral infection. ADE results from a secondary infection of a new flavivirus or a different subtype from the primary infection that interacts well with the antibodies developed for the primary infection. However the new flavivirus can enter cells that it would not normally be able causing a more severe flaviviral infection (64, 65). Of the flaviviruses discussed in this dissertation, JEV, YFV, and DENV all have vaccines developed for protecting against viral infection. Of the three vaccines, only the JEV vaccine and the YFV vaccine are effective at providing a life-long protection against viral infection. The DENV vaccine has been implicated with causing a more severe reaction due to ADE when distributed to individuals prior to them contracting a primary infection from one of the four serotypes of DENV (73, 74). Due to this complication, the DENV vaccine is not widely distributed especially in endemic countries. Ultimately, there is a pressing need for the development of vaccines for the remaining flaviviruses as well as a more effective DENV vaccine that can be distributed to individuals before a primary infection in addition to the advancement of anti-viral therapeutics for treating symptoms caused by flaviviral infections. A key component for the advancement of these interventional strategies is understanding how flaviviruses replicate at the molecular level within both mosquito vector and host. The work presented in this dissertation investigates the role of

nonstructural protein 3 (NS3) helicase Motif V on helicase unwinding function and its influence on mosquito pathogenesis.

NS3 is one of eight nonstructural proteins encoded in the positive-sense single-stranded RNA genome of flaviviruses and is involved in viral replication. Upon initial viral infection, the RNA genome is translated into a single polyprotein consisting of three structural proteins (envelope, pre-membrane, and capsid) and eight nonstructural proteins (NS1, NS2A, NS2B, NS3, NS4A, 2K, NS4B, and NS5). NS3 contains two domains: a N-terminal serine protease domain that cleaves the polyprotein at specific regions, and a C-terminal superfamily 2 (SF2) helicase domain that unwinds the replicative form during viral genome replication. The replicative form is a double-stranded RNA intermediate comprising of the negative-sense antigenomic RNA template strand in complex with the positive-sense genomic RNA strand. For replication of the genomic RNA strand, the replicative form is unwound in an ATP-dependent manner by NS3 helicase sending the negative-sense strand to the RNA-dependent RNA polymerase domain of NS5 for a round of replication. The eight highly conserved structural motifs (I, Ia, II, III, IV, IVa, V, VI) found within the SF2 helicase domain of NS3 contain residues responsible for ATP hydrolysis, RNA binding, and helicase unwinding activity. However, the linkage or allosteric pathway between ATP hydrolysis activity and helicase unwinding activity is not well understood. Furthermore, the influence of this linkage in NS3 helicase on overall viral replication kinetics in cell culture and the pathogenesis and transmission in mosquitoes is not well understood. Previous computational studies of NS3 helicase pointed to Motif V as a potential communication hub between ATPase activity and helicase unwinding activity. This dissertation utilizes a combination of virology, biochemistry, and computational simulations to elucidate the role of NS3 helicase Motif V in powering the translocation and unwinding function as well as its influence on viral replication kinetics in cell culture and viral pathogenesis in mosquitoes.

The work described in Chapter 3 investigated NS3 helicase Motif V residues T407 and S411 to determine how these residues play a role in helicase unwinding function. These residues were hypothesized to link the ATP binding pocket and the RNA binding cleft through hydrogen bond interactions. Alanine mutations at position 407 and 411 were examined initially in a sub-genomic replicon system to test viral genome replication. T407A and S411A mutants indicated nearly ablated and reduced to 60% viral genome replication activity, respectively. Due to these results, T407A and S411A mutants were examined in RNA binding affinity, ATP hydrolysis, and helicase unwinding activities via purified recombinant protein. The RNA binding affinity and ATPase activities of Motif V mutants T407A and S411A were unchanged, but helicase unwinding activity increased for both mutants compared to wild-type NS3 helicase. Additionally, Motif V mutants were simulated in all-atom molecular dynamics simulations to probe how these mutations affect the overall secondary structure or substrate binding states within NS3 helicase. These data from the simulations indicate that Motif V residues T407 and S411 connect the ATP-binding pocket with the helical gate of NS3 helicase. Thus, Motif V mutations T407A and S411A exhibit a hyperactive helicase phenotype leading to the regulation of translocation and unwinding during viral genome replication.

Chapter 4 examines how the hyperactive phenotype of NS3 helicase observed in Chapter 3 affects the pathogenesis and transmission of T407A and S411A West Nile virus (Kunjin subtype) in cell culture and in mosquitoes. Of the two Kunjin virus mutants, only S411A Kunjin virus was recovered. S411A Kunjin decreased viral replication kinetics, while increased cytopathogenicity as compared to WT Kunjin in cell culture. Similarly, in surviving S411A-infected *Culex quinquefasciatus* mosquitoes infection rates decreased compared to WT-infected mosquitoes. However, S411A Kunjin increased mosquito mortality compared to WT Kunjin. Additionally, S411A Kunjin increased viral dissemination and saliva positivity rates in surviving mosquitoes compared to WT Kunjin. These data suggest that S411A Kunjin increases

pathogenesis in mosquitoes compared with that of WT Kunjin. Overall, these computational simulation, biochemical assay, and virology data indicate that flavivirus NS3 helicase Motif V plays a role in the pathogenesis, dissemination, and transmission efficiency of Kunjin virus, not just regulation of translocation and unwinding during viral genome replication. The molecular level insights presented in this dissertation provide the fundamental research needed to targeted anti-viral therapeutic development against flavivirus infections.

Future Directions

The research presented in this dissertation covers a large range of techniques that address very specific hypotheses about residues T407 and S411 within Motif V of NS3 helicase. At the beginning of Chapter 3, each residue in Motif V was mutated to disrupt specific residue-residue or residue-substrate interactions and examined in the viral genome replication assay. From these results, mutations T407A and S411A were further investigated in the biochemical activity assays and in the simulations, but the remaining mutations tested in the viral genome replication assay were not discussed further. Some of the other Motif V mutations (F404K, D409A, I410G, E412D, M413A, G414A, and N416D) resulted in no viral genome replication activity similar to that of T407A. Since these mutations kill viral genome replication, they must also be critical for flavivirus replication in some way. However, the specifics on how these residues are essential for viral genome replication is not well understood. Further investigation using purified recombinant protein and molecular dynamics simulations is required for elucidating the role of these mutations in flaviviral genome replication. A couple of these residues are hypothesized to stabilize other motifs in the surrounding regions, like Motif Ia and Motif VI. Residues within Motif Ia and Motif VI have been previously shown to interact with ATP and single-stranded RNA. If the Motif V mutations destabilize these residue interactions with bound substrate in the other motifs, then we can calculate the linear interaction energy from the simulations to provide evidence for this hypothesis. Similar computational analyses can provide further evidence of the importance

of these Motif V residues. These data can be corroborated with biochemical activity data via RNA or ATP binding affinity results indicating decreased activity compared to WT, which can be confirmed through additional mutations of the corresponding residues that interact with the mutated Motif V residues.

The simulations and biochemical activity assay data may not provide enough molecular insight into how these Motif V residues affect viral genome replication because maybe the mutations cause disruptions with other viral proteins in cell culture. Therefore, co-immunoprecipitation assays with WT and Motif V mutants present in sub-genomic replicon systems can be used to determine if protein-protein interactions have been disrupted due to the mutations. Recall that for flaviviral replication, NS3 interacts with both NS5 and NS2B. Thus, these interactions would be expected in a co-immunoprecipitation assay. If the mutations disrupted these interactions, then the original residues play a role in stabilizing NS3 interactions between the other viral nonstructural proteins during viral replication.

Recall in Chapter 4, S411A Kunjin infected cells resulted in increased cytotoxicity, but decreased plaque sizes compared to WT Kunjin suggesting that S411A Kunjin is more toxic to cells while not spreading as effectively as WT Kunjin. These results were consistent with each other as well as previous viral genome replication activity results presented in Chapter 3. Interestingly, in Chapter 3, the S411A helicase mutant increased helicase unwinding activity while not changing ATPase activity. These results in conjunction with the increased cytotoxicity of S411A Kunjin-infected cells suggests that the reduced cell viability was not due to decreased amounts of ATP from NS3 helicase ATP degradation. Therefore, an alternative hypothesis was purposed in discussion of Chapter 4 stating that the hyperactive NS3 helicase may be interacting with cellular mRNAs leading to the dysregulation of cellular homeostasis and causing the observed increased cytotoxicity, but decreased viral transmission. Further research into this

hypothesis is required for determining if the hyperactive NS3 helicase is actually interacting cellular mRNAs. One approach for determining NS3 helicase protein interactions with cellular mRNAs is through colocalization experiments in cells. In the case of NS3 helicase interacting with cellular mRNA, the colocalization procedure would involve labeling the two molecular species with spectrally separated fluorescent probes that can be resolved with dual-color fluorescence fluctuation spectroscopy brightness analysis (284). If the NS3 helicase mutations affect the localization of mRNA to NS3, then the results suggest that Motif V residues influence how NS3 interacts with cellular RNA leading to the increased cytotoxicity and decreased viral transmission. The information gained from this type of experiment would provide evidence that NS3 helicase has evolved so that the helicase is not hyperactive allowing for the flavivirus to survive during viral infection in both the host and the mosquito vector.

REFERENCES

1. Lindenbach, B. D., Murray, C. L., Heinz-Jurgen, T., and Rice, C. M. (2013) Flaviviridae. in *Fields Virology*, 6th Ed. (Knipe, D. M., and Howley, P. M. eds), pp. 712–746, Lippincott Williams & Wilkins, Philadelphia
2. Chambers, T. J., Hahn, C. S., Galler, R., and Rice, C. M. (1990) Flavivirus genome organization, expression, and replication. *Annu. Rev. Microbiol.* **44**, 649–88
3. Suwanmanee, S., and Luplertlop, N. (2017) Dengue and Zika viruses: lessons learned from the similarities between these Aedes mosquito-vectored arboviruses. *J. Microbiol.* **55**, 81–89
4. World Health Organization (2019) *Hepatitis C Key Facts*
5. Howard, C. R. (2016) Aedes mosquitoes and Zika virus infection: an A to Z of emergence? *Emerg. Microbes Infect.* **5**, 1–2
6. Uno, N., and Ross, T. M. (2018) Dengue virus and the host innate immune response. *Emerg. Microbes Infect.* **7**, 1–11
7. World Health Organization (2020) *Vector-borne diseases Key facts*, Geneva, Switzerland
8. World Health Organization (2018) *Dengue and severe dengue Key facts*, Geneva, Switzerland
9. World Health Organization (2017) *West Nile Virus Key Facts*, Geneva, Switzerland
10. Reisen, W. (2013) Ecology of West Nile Virus in North America. *Viruses*. **5**, 2079–2105
11. Kauffman, E. B., and Kramer, L. D. (2017) Zika Virus Mosquito Vectors: Competence, Biology, and Vector Control. *J. Infect. Dis.* **216**, S976–S990
12. Guzman, M. G., and Harris, E. (2015) Dengue. *Lancet*. **385**, 453–465
13. Kularatne, S. A. M. (2015) Dengue fever. *BMJ*. **351**, h4661
14. Khetarpal, N., and Khanna, I. (2016) Dengue Fever: Causes, Complications, and Vaccine Strategies. *J. Immunol. Res.* **2016**, 1–14

15. Messina, J. P., Brady, O. J., Scott, T. W., Zou, C., Pigott, D. M., Duda, K. A., Bhatt, S., Katzelnick, L., Howes, R. E., Battle, K. E., Simmons, C. P., and Hay, S. I. (2014) Global spread of dengue virus types: mapping the 70 year history. *Trends Microbiol.* **22**, 138–46

16. Gan, V. C. (2014) Dengue: Moving from Current Standard of Care to State-of-the-Art Treatment. *Curr. Treat. options Infect. Dis.* **6**, 208–226

17. Bhatt, S., Gething, P. W., Brady, O. J., Messina, J. P., Farlow, A. W., Moyes, C. L., Drake, J. M., Brownstein, J. S., Hoen, A. G., Sankoh, O., Myers, M. F., George, D. B., Jaenisch, T., Wint, G. R. W., Simmons, C. P., Scott, T. W., Farrar, J. J., and Hay, S. I. (2013) The global distribution and burden of dengue. *Nature*. **496**, 504–7

18. Murray, N. E. A., Quam, M. B., and Wilder-Smith, A. (2013) Epidemiology of dengue: Past, present and future prospects. *Clin. Epidemiol.* **5**, 299–309

19. World Health Organization (2019) *Yellow fever virus Key Facts*, Geneva, Switzerland

20. Solomon, T., and Vaughn, D. W. (2002) Pathogenesis and clinical features of Japanese encephalitis and West Nile virus infections. *Curr. Top. Microbiol. Immunol.* **267**, 171–194

21. Misra, U. K., and Kalita, J. (2010) Overview: Japanese encephalitis. *Prog. Neurobiol.* **91**, 108–120

22. World Health Organization (2019) *Japanese encephalitis virus Key Facts*, Geneva, Switzerland

23. Endy, T. P., and Nisalak, A. (2002) Japanese Encephalitis Virus: Ecology and Epidemiology. *Curr. Top. Microbiol. Immunol.* **267**, 11–48

24. Solomon, T. (2006) Control of Japanese Encephalitis — Within Our Grasp? *N. Engl. J. Med.* **355**, 869–871

25. Mansfield, K. L., Hernández-Triana, L. M., Banyard, A. C., Fooks, A. R., and Johnson, N. (2017) Japanese encephalitis virus infection, diagnosis and control in domestic animals. *Vet. Microbiol.* **201**, 85–92

26. Jeffries, C. L., and Walker, T. (2015) The Potential Use of Wolbachia-Based Mosquito

Biocontrol Strategies for Japanese Encephalitis. *PLoS Negl. Trop. Dis.* **9**, e0003576

27. Adiga, R. (2016) Phylogenetic analysis of the NS5 gene of Zika virus. *J. Med. Virol.* **88**, 1821–1826

28. Cugola, F. R., Fernandes, I. R., Russo, F. B., Freitas, B. C., Dias, J. L. M., Guimarães, K. P., Benazzato, C., Almeida, N., Pignatari, G. C., Romero, S., Polonio, C. M., Cunha, I., Freitas, C. L., Brandão, W. N., Rossato, C., Andrade, D. G., Faria, D. D. P., Garcez, A. T., Buchpigel, C. A., Braconi, C. T., Mendes, E., Sall, A. A., Zanotto, P. M. de A., Peron, J. P. S., Muotri, A. R., and Beltrão-Braga, P. C. B. (2016) The Brazilian Zika virus strain causes birth defects in experimental models. *Nature*. **534**, 267–271

29. Shapshak, P., Somboonwit, C., Foley, B. T., Alrabaa, S. F., Wills, T., and Sinnott, J. T. (2015) Zika Virus. in *Global Virology I - Identifying and Investigating Viral Diseases* (Shapshak, P., Sinnott, J. T., Somboonwit, C., and Kuhn, J. H. eds), pp. 477–500, Springer New York, New York, NY, 10.1007/978-1-4939-2410-3_18

30. Massey, T. H., and Robertson, N. P. (2016) Zika virus and neurology: proving cause and effect. *J. Neurol.* **263**, 1255–1257

31. da Silva, S., Oliveira Silva Martins, D., and Jardim, A. C. G. (2018) A Review of the Ongoing Research on Zika Virus Treatment. *Viruses*. **10**, 1–18

32. Perreira, J. M., Chin, C. R., Feeley, E. M., and Brass, A. L. (2013) IFITMs Restrict the Replication of Multiple Pathogenic Viruses. *J. Mol. Biol.* **425**, 4937–4955

33. Petersen, L. R., Jamieson, D. J., Powers, A. M., and Honein, M. A. (2016) Zika Virus. *N. Engl. J. Med.* **374**, 1552–1563

34. Samarasekera, U., and Triunfol, M. (2016) Concern over Zika virus grips the world. *Lancet*. **387**, 521–524

35. Cao-Lormeau, V.-M., Blake, A., Mons, S., Lastère, S., Roche, C., Vanhomwegen, J., Dub, T., Baudouin, L., Teissier, A., Larre, P., Vial, A.-L., Decam, C., Choumet, V., Halstead, S. K., Willison, H. J., Musset, L., Manuguerra, J.-C., Despres, P., Fournier, E.,

Mallet, H.-P., Musso, D., Fontanet, A., Neil, J., and Ghawché, F. (2016) Guillain-Barré Syndrome outbreak associated with Zika virus infection in French Polynesia: a case-control study. *Lancet*. **387**, 1531–1539

36. Lima, G. P., Rozenbaum, D., Pimentel, C., Frota, A. C. C., Vivacqua, D., Machado, E. S., Sztajnbok, F., Abreu, T., Soares, R. A., and Hofer, C. B. (2019) Factors associated with the development of Congenital Zika Syndrome: a case-control study. *BMC Infect. Dis.* **19**, 277

37. Pomar, L., Malinger, G., Benoist, G., Carles, G., Ville, Y., Rousset, D., Hcini, N., Pomar, C., Jolivet, A., and Lambert, V. (2017) Association between Zika virus and fetopathy: a prospective cohort study in French Guiana. *Ultrasound Obstet. Gynecol.* **49**, 729–736

38. World Health Organization (2018) *Zika virus Key Facts*, Geneva, Switzerland

39. Yuan, L., Huang, X.-Y., Liu, Z.-Y., Zhang, F., Zhu, X.-L., Yu, J.-Y., Ji, X., Xu, Y.-P., Li, G., Li, C., Wang, H.-J., Deng, Y.-Q., Wu, M., Cheng, M.-L., Ye, Q., Xie, D.-Y., Li, X.-F., Wang, X., Shi, W., Hu, B., Shi, P.-Y., Xu, Z., and Qin, C.-F. (2017) A single mutation in the prM protein of Zika virus contributes to fetal microcephaly. *Science*. **358**, 933–936

40. Brasil, P., Vasconcelos, Z., Kerin, T., Gabaglia, C. R., Ribeiro, I. P., Bonaldo, M. C., Damasceno, L., Pone, M. V., Pone, S., Zin, A., Tsui, I., Adachi, K., Pereira, J. P., Gaw, S. L., Carvalho, L., Cunha, D. C., Guida, L., Rocha, M., Cherry, J. D., Wang, L., Aliyari, S., Cheng, G., Foo, S.-S., Chen, W., Jung, J., Brickley, E., Moreira, M. E. L., and Nielsen-Saines, K. (2020) Zika virus vertical transmission in children with confirmed antenatal exposure. *Nat. Commun.* **11**, 3510

41. Paz-Bailey, G., Rosenberg, E. S., Doyle, K., Munoz-Jordan, J., Santiago, G. A., Klein, L., Perez-Padilla, J., Medina, F. A., Waterman, S. H., Adams, L. E., Lozier, M. J., Bertrán-Pasarell, J., Garcia Gubern, C., Alvarado, L. I., and Sharp, T. M. (2018) Persistence of Zika Virus in Body Fluids — Final Report. *N. Engl. J. Med.* **379**, 1234–1243

42. D'Ortenzio, E., Matheron, S., de Lamballerie, X., Hubert, B., Piorkowski, G., Maquart, M.,

Descamps, D., Damond, F., Yazdanpanah, Y., and Leparc-Goffart, I. (2016) Evidence of Sexual Transmission of Zika Virus. *N. Engl. J. Med.* **374**, 2195–2198

43. Wang, T., Li, P., Zhang, Y., Liu, Y., Tan, Z., Sun, J., Ke, X., Miao, Y., Luo, D., Hu, Q., Xu, F., Wang, H., and Zheng, Z. (2020) In vivo imaging of Zika virus reveals dynamics of viral invasion in immune-sheltered tissues and vertical propagation during pregnancy. *Theranostics*. **10**, 6430–6447
44. Gurung, S., Nadeau, H., Maxted, M., Peregrine, J., Reuter, D., Norris, A., Edwards, R., Hyatt, K., Singleton, K., Papin, J. F., and Myers, D. A. (2020) Maternal Zika Virus (ZIKV) Infection following Vaginal Inoculation with ZIKV-Infected Semen in Timed-Pregnant Olive Baboons. *J. Virol.* **94**, e00058-20
45. Ciota, A. T. (2017) West Nile virus and its vectors. *Curr. Opin. Insect Sci.* **22**, 28–36
46. Murgue, B., Zeller, H., and Deubel, V. (2002) The ecology and epidemiology of West Nile virus in Africa, Europe and Asia. *Curr. Top. Microbiol. Immunol.* **267**, 195–221
47. Roehrig, J. T., Layton, M., Smith, P., Campbell, G. L., Nasci, R., and Lanciotti, R. S. (2002) The Emergence of West Nile Virus in North America: Ecology, Epidemiology, and Surveillance. *Curr. Top. Microbiol. Immunol.* **267**, 223–240
48. Suthar, M. S., Diamond, M. S., and Gale Jr, M. (2013) West Nile virus infection and immunity. *Nat. Rev. Microbiol.* **11**, 115–128
49. Petersen, L. R. (2019) Epidemiology of West Nile Virus in the United States: Implications for Arbovirology and Public Health. *J. Med. Entomol.* **56**, 1456–1462
50. Diaz, A., Coffey, L. L., Burkett-Cadena, N., and Day, J. F. (2018) Reemergence of St. Louis Encephalitis Virus in the Americas. *Emerg. Infect. Dis.* **24**, 2150–2157
51. Luby, J. P., Sulkin, S. E., and Sanford, J. P. (1969) The Epidemiology of St. Louis Encephalitis: A Review. *Annu. Rev. Med.* **20**, 329–349
52. Salimi, H., Cain, M. D., and Klein, R. S. (2016) Encephalitic Arboviruses: Emergence, Clinical Presentation, and Neuropathogenesis. *Neurotherapeutics*. **13**, 514–534

53. Monath, T. P. (2001) Yellow fever: an update. *Lancet Infect. Dis.* **1**, 11–20

54. Kamgang, B., Vazeille, M., Yougang, A. P., Tedjou, A. N., Wilson-Bahun, T. A., Mousson, L., Wondji, C. S., and Failloux, A.-B. (2019) Potential of Aedes albopictus and Aedes aegypti (Diptera: Culicidae) to transmit yellow fever virus in urban areas in Central Africa. *Emerg. Microbes Infect.* **8**, 1636–1641

55. Monath, T. P., and Barrett, A. D. T. (2003) Pathogenesis and Pathophysiology of Yellow Fever. in *Advances in Virus Research*, pp. 343–395, **60**, 343–395

56. Beasley, D. W. C., McAuley, A. J., and Bente, D. A. (2015) Yellow fever virus: genetic and phenotypic diversity and implications for detection, prevention and therapy. *Antiviral Res.* **115**, 48–70

57. Mousson, L., Dauga, C., Garrigues, T., Schaffner, F., Vazeille, M., and Failloux, A.-B. (2005) Phylogeography of Aedes (Stegomyia) aegypti (L.) and Aedes (Stegomyia) albopictus (Skuse) (Diptera: Culicidae) based on mitochondrial DNA variations. *Genet. Res.* **86**, 1

58. Acosta, E. G., Castilla, V., and Damonte, E. B. (2008) Functional entry of dengue virus into Aedes albopictus mosquito cells is dependent on clathrin-mediated endocytosis. *J. Gen. Virol.* **89**, 474–484

59. World Health Organization (2009) *Dengue: guidelines for diagnosis, treatment, prevention, and control*, WHO/HTM/NTD/DEN/2009.1

60. Muller, D. A., Depelsenaire, A. C. I., and Young, P. R. (2017) Clinical and Laboratory Diagnosis of Dengue Virus Infection. *J. Infect. Dis.* **215**, S89–S95

61. Pang, X., Zhang, R., and Cheng, G. (2017) Progress towards understanding the pathogenesis of dengue hemorrhagic fever. *Virol. Sin.* **32**, 16–22

62. Martina, B. E. E., Koraka, P., and Osterhaus, A. D. M. E. (2009) Dengue Virus Pathogenesis: an Integrated View. *Clin. Microbiol. Rev.* **22**, 564–581

63. Halstead, S. B. (1970) Observations related to pathogensis of dengue hemorrhagic fever.

VI. Hypotheses and discussion. *Yale J. Biol. Med.* **42**, 350–62

64. Halstead, S. B., Mahalingam, S., Marovich, M. A., Ubol, S., and Mosser, D. M. (2010) Intrinsic antibody-dependent enhancement of microbial infection in macrophages: disease regulation by immune complexes. *Lancet Infect. Dis.* **10**, 712–722

65. Halstead, S. B. (2017) Biologic Evidence Required for Zika Disease Enhancement by Dengue Antibodies. *Emerg. Infect. Dis.* **23**, 569–573

66. Halstead, S. B. (2014) Dengue Antibody-Dependent Enhancement: Knowns and Unknowns. *Microbiol. Spectr.* **2**, 1–18

67. Haslwanter, D., Blaas, D., Heinz, F. X., and Stiasny, K. (2017) A novel mechanism of antibody-mediated enhancement of flavivirus infection. *PLOS Pathog.* **13**, e1006643

68. Moulton, S. L., Mulligan, J., Srikiatkhachorn, A., Kalayanarooj, S., Grudic, G. Z., Green, S., Gibbons, R. V, Muniz, G. W., Hinojosa-Laborde, C., Rothman, A. L., Thomas, S. J., and Convertino, V. A. (2016) State-of-the-art monitoring in treatment of dengue shock syndrome: a case series. *J. Med. Case Rep.* **10**, 233

69. World Health Organization (2020) *Dengue and severe dengue Key Facts*, Geneva, Switzerland

70. Bardina, S. V., Bunduc, P., Tripathi, S., Duehr, J., Frere, J. J., Brown, J. A., Nachbagauer, R., Foster, G. A., Krysztof, D., Tortorella, D., Stramer, S. L., García-Sastre, A., Krammer, F., and Lim, J. K. (2017) Enhancement of Zika virus pathogenesis by preexisting antiflavivirus immunity. *Science*. **356**, 175–180

71. Maslow, J. N. (2019) Zika Vaccine Development—Current Progress and Challenges for the Future. *Trop. Med. Infect. Dis.* **4**, 104

72. Barrett, A. D. T. (2017) Yellow fever live attenuated vaccine: A very successful live attenuated vaccine but still we have problems controlling the disease. *Vaccine*. **35**, 5951–5955

73. Thisyakorn, U., and Thisyakorn, C. (2014) Latest developments and future directions in

dengue vaccines. *Ther. Adv. Vaccines*. **2**, 3–9

74. Noble, C. G., Chen, Y. L., Dong, H., Gu, F., Lim, S. P., Schul, W., Wang, Q. Y., and Shi, P. Y. (2010) Strategies for development of dengue virus inhibitors. *Antiviral Res.* **85**, 450–462

75. Guo, C., Zhou, Z., Wen, Z., Liu, Y., Zeng, C., Xiao, D., Ou, M., Han, Y., Huang, S., Liu, D., Ye, X., Zou, X., Wu, J., Wang, H., Zeng, E. Y., Jing, C., and Yang, G. (2017) Global Epidemiology of Dengue Outbreaks in 1990–2015: A Systematic Review and Meta-Analysis. *Front. Cell. Infect. Microbiol.* **7**, 1–11

76. Bos, S., Gadea, G., and Despres, P. (2018) Dengue: a growing threat requiring vaccine development for disease prevention. *Pathog. Glob. Health*. **112**, 294–305

77. Girard, Y. A., Klingler, K. A., and Higgs, S. (2004) West Nile Virus Dissemination and Tissue Tropisms in Orally Infected Culex pipiens quinquefasciatus. *Vector-Borne Zoonotic Dis.* **4**, 109–122

78. Salazar, M. I., Richardson, J. H., Sánchez-Vargas, I., Olson, K. E., and Beaty, B. J. (2007) Dengue virus type 2: replication and tropisms in orally infected Aedes aegypti mosquitoes. *BMC Microbiol.* **7**, 9

79. Chamberlain, R. W., and Sudia, W. D. (1961) Mechanism of Transmission of Viruses by Mosquitoes. *Annu. Rev. Entomol.* **6**, 371–390

80. Lequime, S., Fontaine, A., Ar Gouilh, M., Moltini-Conclois, I., and Lambrechts, L. (2016) Genetic Drift, Purifying Selection and Vector Genotype Shape Dengue Virus Intra-host Genetic Diversity in Mosquitoes. *PLoS Genet.* **12**, 1–24

81. Lambrechts, L., and Lequime, S. (2016) Evolutionary dynamics of dengue virus populations within the mosquito vector. *Curr. Opin. Virol.* **21**, 47–53

82. Black IV, W. C., Bennett, K. E., Gorrochótegui-Escalante, N., Barillas-Mury, C. V., Fernández-Salas, I., Muñoz, M. D. L., Farfán-Alé, J. A., Olson, K. E., and Beaty, B. J. (2002) Flavivirus susceptibility in Aedes aegypti. *Arch. Med. Res.* **33**, 379–388

83. Franz, A., Kantor, A., Passarelli, A., and Clem, R. (2015) Tissue Barriers to Arbovirus Infection in Mosquitoes. *Viruses*. **7**, 3741–3767

84. Gubler, D. J., Nalim, S., Tan, R., Saipan, H., and Saroso, J. S. (1979) Variation in Susceptibility to Oral Infection with Dengue Viruses among Geographic Strains of Aedes Aegypti *. *Am. J. Trop. Med. Hyg.* **28**, 1045–1052

85. Bosio, C. F., Beaty, B. J., and Black IV, W. C. (1998) Quantitative genetics of vector competence for dengue-2 virus in Aedes aegypti. *Am. J. Trop. Med. Hyg.* **59**, 965–970

86. Mercado-Curiel, R. F., Black, W. C., and Muñoz, M. de L. (2008) A dengue receptor as possible genetic marker of vector competence in Aedes aegypti. *BMC Microbiol.* **8**, 118

87. Smith, D. R. (2012) An update on mosquito cell expressed dengue virus receptor proteins. *Insect Mol. Biol.* **21**, 1–7

88. Bennett, K. E., Flick, D., Fleming, K. H., Jochim, R., Beaty, B. J., and Black IV, W. C. (2005) Quantitative trait loci that control dengue-2 virus dissemination in the mosquito Aedes aegypti. *Genetics*. **170**, 185–194

89. Weaver, S. C. (1986) Electron Microscopic Analysis of Infection Patterns for Venezuelan Equine Encephalomyelitis Virus in the Vector Mosquito, Culex (Melanoconion) Taeniopus. *Am. J. Trop. Med. Hyg.* **35**, 624–631

90. Parikh, G. R., Oliver, J. D., and Bartholomay, L. C. (2009) A haemocyte tropism for an arbovirus. *J. Gen. Virol.* **90**, 292–296

91. Hardy, J. L., Houk, E. J., Kramer, L. D., and Reeves, W. C. (1983) Intrinsic Factors Affecting Vector Competence of Mosquitoes for Arboviruses. *Annu. Rev. Entomol.* **28**, 229–262

92. Raquin, V., and Lambrechts, L. (2017) Dengue virus replicates and accumulates in Aedes aegypti salivary glands. *Virology*. **507**, 75–81

93. Sriurairatna, S., and Bhamarapravati, N. (1977) Replication of Dengue-2 Virus in Aedes albopictus Mosquitoes. *Am. J. Trop. Med. Hyg.* **26**, 1199–1205

94. Brinton, M. A., and Basu, M. (2015) Functions of the 3′ and 5′ genome RNA regions of members of the genus Flavivirus. *Virus Res.* **206**, 108–119

95. Li, X. D., Shan, C., Deng, C. L., Ye, H. Q., Shi, P. Y., Yuan, Z. M., Gong, P., and Zhang, B. (2014) The Interface between Methyltransferase and Polymerase of NS5 Is Essential for Flavivirus Replication. *PLoS Negl. Trop. Dis.* **8**, 1–11

96. Ng, W. C., Soto-Acosta, R., Bradrick, S. S., Garcia-Blanco, M. A., and Ooi, E. E. (2017) The 5' and 3' Untranslated Regions of the Flaviviral Genome. *Viruses*. **9**, 137

97. Alvarez, D. E., De Lella Ezcurra, A. L., Fucito, S., and Gamarnik, A. V. (2005) Role of RNA structures present at the 3'UTR of dengue virus on translation, RNA synthesis, and viral replication. *Virology*. **339**, 200–12

98. Li, W., and Brinton, M. A. (2001) The 3' stem loop of the West Nile virus genomic RNA can suppress translation of chimeric mRNAs. *Virology*. **287**, 49–61

99. Holden, K. L., and Harris, E. (2004) Enhancement of dengue virus translation: role of the 3' untranslated region and the terminal 3' stem-loop domain. *Virology*. **329**, 119–33

100. Holden, K. L., Stein, D. A., Pierson, T. C., Ahmed, A. A., Clyde, K., Iversen, P. L., and Harris, E. (2006) Inhibition of dengue virus translation and RNA synthesis by a morpholino oligomer targeted to the top of the terminal 3' stem-loop structure. *Virology*. **344**, 439–52

101. Wei, Y., Qin, C., Jiang, T., Li, X., Zhao, H., Liu, Z., Deng, Y., Liu, R., Chen, S., Yu, M., and Qin, E. (2009) Translational regulation by the 3′ untranslated region of the dengue type 2 virus genome. *Am. J. Trop. Med. Hyg.* **81**, 817–824

102. Yu, L., and Markoff, L. (2005) The Topology of Bulges in the Long Stem of the Flavivirus 3′ Stem-Loop Is a Major Determinant of RNA Replication Competence. *J. Virol.* **79**, 2309–2324

103. Cahour, A., Pletnev, A., Vazielle-Falcoz, M., Rosen, L., and Lai, C. J. (1995) Growth-restricted dengue virus mutants containing deletions in the 5' noncoding region of the

RNA genome. *Virology*. **207**, 68–76

104. Cleaves, G. R., and Dubin, D. T. (1979) Methylation status of intracellular dengue type 2 40 S RNA. *Virology*. **96**, 159–165

105. Villordo, S. M., Carballeda, J. M., Filomatori, C. V., and Gamarnik, A. V. (2016) RNA Structure Duplications and Flavivirus Host Adaptation. *Trends Microbiol.* **24**, 270–283

106. Göertz, G. P., Abbo, S. R., Fros, J. J., and Pijlman, G. P. (2018) Functional RNA during Zika virus infection. *Virus Res.* **254**, 41–53

107. Coutard, B., Barral, K., Lichière, J., Selisko, B., Martin, B., Aouadi, W., Lombardia, M. O., Debart, F., Vasseur, J.-J., Guillemot, J. C., Canard, B., and Decroly, E. (2017) Zika Virus Methyltransferase: Structure and Functions for Drug Design Perspectives. *J. Virol.* **91**, e02202-16

108. Dong, H., Fink, K., Züst, R., Lim, S. P., Qin, C.-F., and Shi, P.-Y. (2014) Flavivirus RNA methylation. *J. Gen. Virol.* **95**, 763–778

109. Kuhn, R. J., Zhang, W., Rossmann, M. G., Pletnev, S. V., Corver, J., Lenches, E., Jones, C. T., Mukhopadhyay, S., Chipman, P. R., Strauss, E. G., Baker, T. S., and Strauss, J. H. (2002) Structure of dengue virus: implications for flavivirus organization, maturation, and fusion. *Cell*. **108**, 717–25

110. Sirohi, D., Chen, Z., Sun, L., Klose, T., Pierson, T. C., Rossmann, M. G., and Kuhn, R. J. (2016) The 3.8 A resolution cryo-EM structure of Zika virus. *Science*. **352**, 467–470

111. Mukhopadhyay, S., Kim, B.-S., Chipman, P. R., Rossmann, M. G., and Kuhn, R. J. (2003) Structure of West Nile virus. *Science*. **302**, 248

112. Fibriansah, G., Tan, J. L., Smith, S. A., de Alwis, R., Ng, T.-S., Kostyuchenko, V. A., Jadi, R. S., Kukkaro, P., de Silva, A. M., Crowe, J. E., and Lok, S.-M. (2015) A highly potent human antibody neutralizes dengue virus serotype 3 by binding across three surface proteins. *Nat. Commun.* **6**, 6341

113. Zhang, X., Ge, P., Yu, X., Brannan, J. M., Bi, G., Zhang, Q., Schein, S., and Zhou, Z. H.

(2013) Cryo-EM structure of the mature dengue virus at 3.5-Å resolution. *Nat. Struct. Mol. Biol.* **20**, 105–110

114. Wang, X., Li, S.-H., Zhu, L., Nian, Q.-G., Yuan, S., Gao, Q., Hu, Z., Ye, Q., Li, X.-F., Xie, D.-Y., Shaw, N., Wang, J., Walter, T. S., Huiskonen, J. T., Fry, E. E., Qin, C.-F., Stuart, D. I., and Rao, Z. (2017) Near-atomic structure of Japanese encephalitis virus reveals critical determinants of virulence and stability. *Nat. Commun.* **8**, 14

115. Modis, Y., Ogata, S., Clements, D., and Harrison, S. C. (2003) A ligand-binding pocket in the dengue virus envelope glycoprotein. *Proc. Natl. Acad. Sci.* **100**, 6986–6991

116. Modis, Y., Ogata, S., Clements, D., and Harrison, S. C. (2005) Variable Surface Epitopes in the Crystal Structure of Dengue Virus Type 3 Envelope Glycoprotein. *J. Virol.* **79**, 1223–1231

117. Kostyuchenko, V. A., Chew, P. L., Ng, T.-S., and Lok, S.-M. (2014) Near-Atomic Resolution Cryo-Electron Microscopic Structure of Dengue Serotype 4 Virus. *J. Virol.* **88**, 477–482

118. Kostyuchenko, V. A., Lim, E. X. Y., Zhang, S., Fibriansah, G., Ng, T.-S., Ooi, J. S. G., Shi, J., and Lok, S.-M. (2016) Structure of the thermally stable Zika virus. *Nature*. **533**, 425–428

119. Sirohi, D., and Kuhn, R. J. (2017) Zika Virus Structure, Maturation, and Receptors. *J. Infect. Dis.* **216**, S935–S944

120. Kostyuchenko, V. A., Zhang, Q., Tan, J. L., Ng, T.-S., and Lok, S.-M. (2013) Immature and Mature Dengue Serotype 1 Virus Structures Provide Insight into the Maturation Process. *J. Virol.* **87**, 7700–7707

121. Zhang, Y., Zhang, W., Ogata, S., Clements, D., Strauss, J. H., Baker, T. S., Kuhn, R. J., and Rossmann, M. G. (2004) Conformational Changes of the Flavivirus E Glycoprotein. *Structure*. **12**, 1607–1618

122. Li, L., Lok, S.-M., Yu, I.-M., Zhang, Y., Kuhn, R. J., Chen, J., and Rossmann, M. G.

(2008) The flavivirus precursor membrane-envelope protein complex: structure and maturation. *Science*. **319**, 1830–4

123. Modis, Y., Ogata, S., Clements, D., and Harrison, S. C. (2004) Structure of the dengue virus envelope protein after membrane fusion. *Nature*. **427**, 313–319

124. Pierson, T. C., and Diamond, M. S. (2014) Vaccine Development as a Means to Control Dengue Virus Pathogenesis: Do We Know Enough? *Annu. Rev. Virol.* **1**, 375–398

125. Cruz-Oliveira, C., Freire, J. M., Conceição, T. M., Higa, L. M., Castanho, M. A. R. B., and Da Poian, A. T. (2015) Receptors and routes of dengue virus entry into the host cells. *FEMS Microbiol. Rev.* **39**, 155–170

126. Wang, P., Hu, K., Luo, S., Zhang, M., Deng, X., Li, C., Jin, W., Hu, B., He, S., Li, M., Du, T., Xiao, G., Zhang, B., Liu, Y., and Hu, Q. (2016) DC-SIGN as an attachment factor mediates Japanese encephalitis virus infection of human dendritic cells via interaction with a single high-mannose residue of viral E glycoprotein. *Virology*. **488**, 108–119

127. Chen, Y., Maguire, T., Hileman, R. E., Fromm, J. R., Esko, J. D., Linhardt, R. J., and Marks, R. M. (1997) Dengue virus infectivity depends on envelope protein binding to target cell heparan sulfate. *Nat. Med.* **3**, 866–871

128. Byk, L. A., Iglesias, N. G., De Maio, F. A., Gebhard, L. G., Rossi, M., and Gamarnik, A. V. (2016) Dengue Virus Genome Uncoating Requires Ubiquitination. *MBio*. **7**, 1–10

129. Welsch, S., Miller, S., Romero-Brey, I., Merz, A., Bleck, C. K. E., Walther, P., Fuller, S. D., Antony, C., Krijnse-Locker, J., and Bartenschlager, R. (2009) Composition and Three-Dimensional Architecture of the Dengue Virus Replication and Assembly Sites. *Cell Host Microbe*. **5**, 365–375

130. Saeedi, B. J., and Geiss, B. J. (2013) Regulation of flavivirus RNA synthesis and capping. *Wiley Interdiscip. Rev. RNA*. **4**, 723–35

131. Pierson, T. C., and Diamond, M. S. (2014) Vaccine Development as a Means to Control Dengue Virus Pathogenesis: Do We Know Enough? *Annu. Rev. Virol.* **1**, 375–398

132. Perera, R., and Kuhn, R. J. (2008) Structural proteomics of dengue virus. *Curr. Opin. Microbiol.* **11**, 369–377

133. Yu, L., Takeda, K., and Gao, Y. (2017) Characterization of virus-specific vesicles assembled by West Nile virus non-structural proteins. *Virology*. **506**, 130–140

134. den Boon, J. A., and Ahlquist, P. (2010) Organelle-Like Membrane Compartmentalization of Positive-Strand RNA Virus Replication Factories. *Annu. Rev. Microbiol.* **64**, 241–256

135. Arakawa, M., and Morita, E. (2019) Flavivirus Replication Organelle Biogenesis in the Endoplasmic Reticulum: Comparison with Other Single-Stranded Positive-Sense RNA Viruses. *Int. J. Mol. Sci.* **20**, 2336

136. Falgout, B., Pethel, M., Zhang, Y. M., and Lai, C. J. (1991) Both nonstructural proteins NS2B and NS3 are required for the proteolytic processing of dengue virus nonstructural proteins. *J. Virol.* **65**, 2467–2475

137. Clum, S., Ebner, K. E., and Padmanabhan, R. (1997) Cotranslational membrane insertion of the serine proteinase precursor NS2B-NS3(Pro) of dengue virus type 2 is required for efficient in vitro processing and is mediated through the hydrophobic regions of NS2B. *J. Biol. Chem.* **272**, 30715–30723

138. Yusof, R., Clum, S., Wetzel, M., Murthy, H. M. K., and Padmanabhan, R. (2000) Purified NS2B/NS3 serine protease of dengue virus type 2 exhibits cofactor NS2B dependence for cleavage of substrates with dibasic amino acids in vitro. *J. Biol. Chem.* **275**, 9963–9969

139. Chambers, T. J., Weir, R. C., Grakoui, A., McCourt, D. W., Bazan, J. F., Fletterick, R. J., and Rice, C. M. (1990) Evidence that the N-terminal domain of nonstructural protein NS3 from yellow fever virus is a serine protease responsible for site-specific cleavages in the viral polyprotein. *Proc. Natl. Acad. Sci.* **87**, 8898–8902

140. Li, H., Clum, S., You, S., Ebner, K. E., and Padmanabhan, R. (1999) The serine protease and RNA-stimulated nucleoside triphosphatase and RNA helicase functional domains of

dengue virus type 2 NS3 converge within a region of 20 amino acids. *J. Virol.* **73**, 3108–3116

141. Bartelma, G., and Padmanabhan, R. (2002) Expression, Purification, and Characterization of the RNA 5'-Triphosphatase Activity of Dengue Virus Type 2 Nonstructural Protein 3. *Virology*. **299**, 122–132

142. Benarroch, D., Selisko, B., Locatelli, G. A., Maga, G., Romette, J.-L., and Canard, B. (2004) The RNA helicase, nucleotide 5'-triphosphatase, and RNA 5'-triphosphatase activities of Dengue virus protein NS3 are Mg2+-dependent and require a functional Walker B motif in the helicase catalytic core. *Virology*. **328**, 208–18

143. Matusan, A. E., Pryor, M. J., Davidson, A. D., and Wright, P. J. (2001) Mutagenesis of the Dengue Virus Type 2 NS3 Protein within and outside Helicase Motifs: Effects on Enzyme Activity and Virus Replication. *J. Virol.* **75**, 9633–9643

144. Wengler, G., and Wengler, G. (1993) The NS 3 Nonstructural Protein of Flaviviruses Contains an RNA Triphosphatase Activity. *Virology*. **197**, 265–273

145. Wang, C.-C., Huang, Z.-S., Chiang, P.-L., Chen, C.-T., and Wu, H.-N. (2009) Analysis of the nucleoside triphosphatase, RNA triphosphatase, and unwinding activities of the helicase domain of dengue virus NS3 protein. *FEBS Lett.* **583**, 691–6

146. Xu, T., Sampath, A., Chao, A., Wen, D., Nanao, M., Chene, P., Vasudevan, S. G., and Lescar, J. (2005) Structure of the Dengue Virus Helicase/Nucleoside Triphosphatase Catalytic Domain at a Resolution of 2.4 A. *J. Virol.* **79**, 10278–10288

147. Issur, M., Geiss, B. J., Bougie, I., Picard-Jean, F., Despins, S., Mayette, J., Hobdey, S. E., and Bisaillon, M. (2009) The flavivirus NS5 protein is a true RNA guanylyltransferase that catalyzes a two-step reaction to form the RNA cap structure. *RNA*. **15**, 2340–2350

148. Egloff, M. P., Benarroch, D., Selisko, B., Romette, J. L., and Canard, B. (2002) An RNA cap (nucleoside-2'-O-)-methyltransferase in the flavivirus RNA polymerase NS5: Crystal structure and functional characterization. *EMBO J.* **21**, 2757–2768

149. Ray, D., Shah, A., Tilgner, M., Guo, Y., Zhao, Y., Dong, H., Deas, T. S., Zhou, Y., Li, H., and Shi, P.-Y. (2006) West Nile virus 5'-cap structure is formed by sequential guanine N-7 and ribose 2'-O methylations by nonstructural protein 5. *J. Virol.* **80**, 8362–70

150. Guyatt, K. J., Westaway, E. G., and Khromykh, A. A. (2001) Expression and purification of enzymatically active recombinant RNA-dependent RNA polymerase (NS5) of the flavivirus Kunjin. *J. Virol. Methods*. **92**, 37–44

151. Tan, B. H., Fu, J., Sugrue, R. J., Yap, E. H., Chan, Y. C., and Tan, Y. H. (1996) Recombinant dengue type 1 virus NS5 protein expressed in Escherichia coli exhibits RNA-dependent RNA polymerase activity. *Virology*. **216**, 317–25

152. Chu, P. W., and Westaway, E. G. (1985) Replication strategy of Kunjin virus: evidence for recycling role of replicative form RNA as template in semiconservative and asymmetric replication. *Virology*. **140**, 68–79

153. Yu, L., Takeda, K., and Markoff, L. (2013) Protein–protein interactions among West Nile non-structural proteins and transmembrane complex formation in mammalian cells. *Virology*. **446**, 365–377

154. Miller, S., Kastner, S., Krijnse-Locker, J., Bühler, S., and Bartenschlager, R. (2007) The Non-structural Protein 4A of Dengue Virus Is an Integral Membrane Protein Inducing Membrane Alterations in a 2K-regulated Manner. *J. Biol. Chem.* **282**, 8873–8882

155. Westaway, E. G., Mackenzie, J. M., Kenney, M. T., Jones, M. K., and Khromykh, A. A. (1997) Ultrastructure of Kunjin virus-infected cells: colocalization of NS1 and NS3 with double-stranded RNA, and of NS2B with NS3, in virus-induced membrane structures. *J. Virol.* **71**, 6650–6661

156. Mackenzie, J. M., Khromykh, A. a, Jones, M. K., and Westaway, E. G. (1998) Subcellular Localization and Some Biochemical Properties of the Flavivirus Kunjin Nonstructural Proteins NS2A and NS4A. *Virology*. **245**, 203–215

157. Preugschat, F., Yao, C. W., and Strauss, J. H. (1990) In vitro processing of dengue virus

type 2 nonstructural proteins NS2A, NS2B, and NS3. *J. Virol.* **64**, 4364–4374

158. Westaway, E. G., Mackenzie, J. M., and Khromykh, A. A. (2002) Replication and Gene Function in Kunjin Virus. in *Current Topics in Microbiology and Immunology* (Mackenzie, J. S., Barrett, A. D. T., and Deubel, V. eds), pp. 323–351, Springer Berlin Heidelberg, **267**, 323–351

159. Filomatori, C. V., Iglesias, N. G., Villordo, S. M., Alvarez, D. E., and Gamarnik, A. V. (2011) RNA sequences and structures required for the recruitment and activity of the dengue virus polymerase. *J. Biol. Chem.* **286**, 6929–6939

160. Lindenbach, B. D., Heinz-Jurgen, T., and Rice, C. M. (2007) Flaviviridae: The Viruses and Their Replication. in *Fields Virology*, 5th Ed. (Knipe, D. M., and Howley, P. M. eds), pp. 1101–1152, Lippincott-Raven Publishers, Philadelphia

161. You, S., Falgout, B., Markoff, L., and Padmanabhan, R. (2001) In Vitro RNA Synthesis from Exogenous Dengue Viral RNA Templates Requires Long Range Interactions between 5′- and 3′-Terminal Regions That Influence RNA Structure. *J. Biol. Chem.* **276**, 15581–15591

162. Filomatori, C. V., Lodeiro, M. F., Alvarez, D. E., Samsa, M. M., Pietrasanta, L., and Gamarnik, A. V. (2006) A 5' RNA element promotes dengue virus RNA synthesis on a circular genome. *Genes Dev.* **20**, 2238–49

163. Iglesias, N. G., Filomatori, C. V., and Gamarnik, A. V. (2011) The F1 Motif of Dengue Virus Polymerase NS5 Is Involved in Promoter-Dependent RNA Synthesis. *J. Virol.* **85**, 5745–5756

164. Friebe, P., Peña, J., Pohl, M. O. F., and Harris, E. (2012) Composition of the sequence downstream of the dengue virus 5′ cyclization sequence (dCS) affects viral RNA replication. *Virology*. **422**, 346–356

165. Friebe, P., and Harris, E. (2010) Interplay of RNA Elements in the Dengue Virus 5′ and 3′ Ends Required for Viral RNA Replication. *J. Virol.* **84**, 6103–6118

166. Davis, W. G., Basu, M., Elrod, E. J., Germann, M. W., and Brinton, M. A. (2013) Identification of cis-Acting Nucleotides and a Structural Feature in West Nile Virus 3'-Terminus RNA That Facilitate Viral Minus Strand RNA Synthesis. *J. Virol.* **87**, 7622–7636

167. Lim, S. P., Noble, C. G., and Shi, P.-Y. (2015) The dengue virus NS5 protein as a target for drug discovery. *Antiviral Res.* **119**, 57–67

168. Luo, D., Xu, T., Watson, R. P., Scherer-Becker, D., Sampath, A., Jahnke, W., Yeong, S. S., Wang, C. H., Lim, S. P., Strongin, A., Vasudevan, S. G., and Lescar, J. (2008) Insights into RNA unwinding and ATP hydrolysis by the flavivirus NS3 protein. *EMBO J.* **27**, 3209–19

169. Luo, D., Vasudevan, S. G., and Lescar, J. (2015) The flavivirus NS2B-NS3 protease-helicase as a target for antiviral drug development. *Antiviral Res.* **118**, 148–58

170. Fairman-Williams, M. E., Guenther, U. P., and Jankowsky, E. (2010) SF1 and SF2 helicases: Family matters. *Curr. Opin. Struct. Biol.* **20**, 313–324

171. Wu, J., Bera, A. K., Kuhn, R. J., and Smith, J. L. (2005) Structure of the Flavivirus Helicase: Implications for Catalytic Activity, Protein Interactions, and Proteolytic Processing. *J. Virol.* **79**, 10268–10277

172. Geiss, B. J., Thompson, A. A., Andrews, A. J., Sons, R. L., Gari, H. H., Keenan, S. M., and Peersen, O. B. (2009) Analysis of Flavivirus NS5 Methyltransferase Cap Binding. *J. Mol. Biol.* **385**, 1643–1654

173. Lin, C., Amberg, S. M., Chambers, T. J., and Rice, C. M. (1993) Cleavage at a novel site in the NS4A region by the yellow fever virus NS2B-3 proteinase is a prerequisite for processing at the downstream 4A/4B signalase site. *J. Virol.* **67**, 2327–2335

174. Chambers, T. J., Grakoui, A., and Rice, C. M. (1991) Processing of the yellow fever virus nonstructural polyprotein: a catalytically active NS3 proteinase domain and NS2B are required for cleavages at dibasic sites. *J. Virol.* **65**, 6042–6050

175. Wengler, G., and Wengler, G. (1991) The carboxy-terminal part of the NS 3 protein of the

West Nile flavivirus can be isolated as a soluble protein after proteolytic cleavage and represents an RNA-stimulated NTPase. *Virology*. **184**, 707–15

176. Singleton, M. R., Dillingham, M. S., and Wigley, D. B. (2007) Structure and Mechanism of Helicases and Nucleic Acid Translocases. *Annu. Rev. Biochem.* **76**, 23–50

177. Teraoka, Y., Morino, S., Tomoo, K., and Ishida, T. (1996) Mutation of the Cysteine Residues in Human Initiation Factor 4E: Effects on mRNA Cap Binding Ability. *Biochem. Biophys. Res. Commun.* **228**, 704–708

178. Tanner, N. K., Cordin, O., Banroques, J., Doère, M., and Linder, P. (2003) The Q motif: a newly identified motif in DEAD box helicases may regulate ATP binding and hydrolysis. *Mol. Cell*. **11**, 127–38

179. Korolev, S., Lohman, T. M., Waksman, G., Yao, N., and Weber, P. C. (1998) Comparisons between the structures of HCV and Rep helicases reveal structural similarities between SF1 and SF2 super-families of helicases. *Protein Sci.* **7**, 605–610

180. Mahdi, A. A. (2003) A model for dsDNA translocation revealed by a structural motif common to RecG and Mfd proteins. *EMBO J.* **22**, 724–734

181. Pérez-Villa, A., Darvas, M., and Bussi, G. (2015) ATP dependent NS3 helicase interaction with RNA: Insights from molecular simulations. *Nucleic Acids Res.* **43**, 8725–8734

182. Swarbrick, C. M. D., Basavannacharya, C., Chan, K. W. K., Chan, S.-A., Singh, D., Wei, N., Phoo, W. W., Luo, D., Lescar, J., and Vasudevan, S. G. (2017) NS3 helicase from dengue virus specifically recognizes viral RNA sequence to ensure optimal replication. *Nucleic Acids Res.* **45**, 12904–12920

183. Mastrangelo, E., Milani, M., Bollati, M., Selisko, B., Peyrane, F., Pandini, V., Sorrentino, G., Canard, B., Konarev, P. V, Svergun, D. I., de Lamballerie, X., Coutard, B., Khromykh, A. a, and Bolognesi, M. (2007) Crystal Structure and Activity of Kunjin Virus NS3 Helicase; Protease and Helicase Domain Assembly in the Full Length NS3 Protein. *J.*

Mol. Biol. **372**, 444–455

184. Appleby, T. C., Anderson, R., Fedorova, O., Pyle, A. M., Wang, R., Liu, X., Brendza, K. M., and Somoza, J. R. (2011) Visualizing ATP-dependent RNA translocation by the NS3 helicase from HCV. *J. Mol. Biol.* **405**, 1139–1153

185. Dumont, S., Cheng, W., Serebrov, V., Beran, R. K., Tinoco, I., Pyle, A. M., and Bustamante, C. (2006) RNA translocation and unwinding mechanism of HCV NS3 helicase and its coordination by ATP. *Nature*. **439**, 105–8

186. Gu, M., and Rice, C. M. (2010) Three conformational snapshots of the hepatitis C virus NS3 helicase reveal a ratchet translocation mechanism. *Proc. Natl. Acad. Sci. U. S. A.* **107**, 521–8

187. Myong, S., Bruno, M. M., Pyle, A. M., and Ha, T. (2007) Spring-loaded mechanism of DNA unwinding by hepatitis C virus NS3 helicase. *Science*. **317**, 513–6

188. Kwong, A. D., Kim, J. L., and Lin, C. (2000) Structure and Function of Hepatitis C virus NS3 helicase. *Curr. Top. Microbiol. Immunol.* **242**, 171–196

189. Saraste, M., Sibbald, P. R., and Wittinghofer, A. (1990) The P-loop — a common motif in ATP- and GTP-binding proteins. *Trends Biochem. Sci.* **15**, 430–434

190. Caruthers, J. M., and McKay, D. B. (2002) Helicase structure and mechanism. *Curr. Opin. Struct. Biol.* **12**, 123–133

191. Kadaré, G., and Haenni, A.-L. (1997) Virus-Encoded RNA Helicases. *J. Virol.* **71**, 2583–2590

192. Subramanya, H. S., Bird, L. E., Brannigan, J. A., and Wigley, D. B. (1996) Crystal structure of a DExx box DNA helicase. *Nature*. **384**, 379–383

193. Yao, N., Hesson, T., Cable, M., Hong, Z., Kwong, A. D., Le, H. V., and Weber, P. C. (1997) Structure of the hepatitis C virus RNA helicase domain. *Nat. Struct. Biol.* **4**, 463–467

194. Tai, C., Pan, W., Liaw, S., Yang, U., Hwang, L., and Chen, D. (2001) Structure-Based

Mutational Analysis of the Hepatitis C Virus NS3 Helicase. *Society*. **75**, 8289–8297

195. Heilek, G. M., and Peterson, M. G. (1997) A point mutation abolishes the helicase but not the nucleoside triphosphatase activity of hepatitis C virus NS3 protein. *J. Virol.* **71**, 6264–6266

196. Levin, M. K., and Patel, S. S. (1999) The helicase from hepatitis C virus is active as an oligomer. *J. Biol. Chem.* **274**, 31839–31846

197. Min, K. H., Sung, Y. C., Choi, S. Y., and Ahn, B. Y. (1999) Functional interactions between conserved motifs of the hepatitis C virus RNA helicase protein NS3. *Virus Genes*. **19**, 33–43

198. Wardell, A. D., Errington, W., Ciaramella, G., Merson, J., and McGarvey, M. J. (1999) Characterization and mutational analysis of the helicase and NTPase activities of hepatitis C virus full-length NS3 protein. *J. Gen. Virol.* **80**, 701–709

199. Sampath, A., Xu, T., Chao, A., Luo, D., Lescar, J., and Vasudevan, S. G. (2006) Structure-based mutational analysis of the NS3 helicase from dengue virus. *J. Virol.* **80**, 6686–90

200. Kim, D. W., Kim, J., Gwack, Y., Han, J. H., and Choe, J. (1997) Mutational analysis of the hepatitis C virus RNA helicase. *J. Virol.* **71**, 9400–9

201. Lin, C., and Kim, J. L. (1999) Structure-based mutagenesis study of hepatitis C virus NS3 helicase. *J. Virol.* **73**, 8798–807

202. Lam, A. M. I., Keeney, D., and Frick, D. N. (2003) Two Novel Conserved Motifs in the Hepatitis C Virus NS3 Protein Critical for Helicase Action. *J. Biol. Chem.* **278**, 44514–44524

203. Davidson, R. B., Hendrix, J., Geiss, B. J., and McCullagh, M. (2018) Allostery in the dengue virus NS3 helicase: Insights into the NTPase cycle from molecular simulations. *PLoS Comput. Biol.* **14**, e1006103

204. Pierson, T. C., Sánchez, M. D., Puffer, B. A., Ahmed, A. A., Geiss, B. J., Valentine, L. E.,

Altamura, L. A., Diamond, M. S., and Doms, R. W. (2006) A rapid and quantitative assay for measuring antibody-mediated neutralization of West Nile virus infection. *Virology*. **346**, 53–65

205. Condit, R. C. (2013) Principles of Virology. in *Fields Virology*, 6th Ed. (Knipe, D. M., and Howley, P. M. eds), pp. 21–51, Lippincott Williams & Wilkins, Philadelphia
206. Hanson, A. M., Hernandez, J. J., Shadrick, W. R., and Frick, D. N. (2012) Identification and analysis of inhibitors targeting the hepatitis C virus NS3 helicase. *Methods Enzymol.* **511**, 463–83
207. Sweeney, N. L., Hanson, A. M., Mukherjee, S., Ndjomou, J., Geiss, B. J., Steel, J. J., Frankowski, K. J., Li, K., Schoenen, F. J., and Frick, D. N. (2015) Benzothiazole and Pyrrolone Flavivirus Inhibitors Targeting the Viral Helicase. *ACS Infect. Dis.* **1**, 140–148
208. Maier, J. A., Martinez, C., Kasavajhala, K., Wickstrom, L., Hauser, K. E., and Simmerling, C. (2015) ff14SB: Improving the Accuracy of Protein Side Chain and Backbone Parameters from ff99SB. *J. Chem. Theory Comput.* **11**, 3696–3713
209. Case, D. A., Ben-Shalom, I. Y., Brozell, S. R., Cerutti, D. S., Cheatham, T. E. I., Cruzeiro, V. W. D., Darden, T. A., Duke, R. E., Ghoreishi, D., Gilson, M. K., Gohlke, H., Goetz, A. W., Greene, D., Harris, R., Homeyer, N., Izadi, S., Kovalenko, A., Kurtzman, T., Lee, T. S., LeGrand, S., Li, P., Lin, C., Liu, J., Luchko, T., Luo, R., Mermelstein, D. J., Merz, K. M., Miao, Y., Monard, G., Nguyen, C., Nguyen, H., Omelyan, I., Onufriev, A., Pan, F., Qi, R., Roe, D. R., Roitberg, A., Sagui, C., Schott-Verdugo, S., Shen, J., Simmerling, C. L., Smith, J., Salomon-Ferrer, R., Swails, J., Walker, R. C., Wang, J., Wei, H., Wolf, R. M., Wu, X., Xiao, L., York, D. M., and Kollman, P. A. (2018) *AMBER 2018*, University of California, San Francisco
210. Brooks, B. R., Brooks, C. L., Mackerell, A. D., Nilsson, L., Petrella, R. J., Roux, B., Won, Y., Archontis, G., Bartels, C., Boresch, S., Caflisch, A., Caves, L., Cui, Q., Dinner, A. R., Feig, M., Fischer, S., Gao, J., Hodoscek, M., Im, W., Kuczera, K., Lazaridis, T., Ma, J.,

Ovchinnikov, V., Paci, E., Pastor, R. W., Post, C. B., Pu, J. Z., Schaefer, M., Tidor, B., Venable, R. M., Woodcock, H. L., Wu, X., Yang, W., York, D. M., and Karplus, M. (2009) CHARMM: The biomolecular simulation program. *J. Comput. Chem.* **30**, 1545–1614

211. MacKerell, A. D., Bashford, D., Bellott, M., Dunbrack, R. L., Evanseck, J. D., Field, M. J., Fischer, S., Gao, J., Guo, H., Ha, S., Joseph-McCarthy, D., Kuchnir, L., Kuczera, K., Lau, F. T. K., Mattos, C., Michnick, S., Ngo, T., Nguyen, D. T., Prodhom, B., Reiher, W. E., Roux, B., Schlenkrich, M., Smith, J. C., Stote, R., Straub, J., Watanabe, M., Wiórkiewicz-Kuczera, J., Yin, D., and Karplus, M. (1998) All-Atom Empirical Potential for Molecular Modeling and Dynamics Studies of Proteins †. *J. Phys. Chem. B*. **102**, 3586–3616
212. Hess, B., Kutzner, C., van der Spoel, D., and Lindahl, E. (2008) GROMACS 4: Algorithms for Highly Efficient, Load-Balanced, and Scalable Molecular Simulation. *J. Chem. Theory Comput.* **4**, 435–447
213. Jorgensen, W. L., and Tirado-Rives, J. (1988) The OPLS [optimized potentials for liquid simulations] potential functions for proteins, energy minimizations for crystals of cyclic peptides and crambin. *J. Am. Chem. Soc.* **110**, 1657–1666
214. Robertson, M. J., Tirado-Rives, J., and Jorgensen, W. L. (2015) Improved Peptide and Protein Torsional Energetics with the OPLS-AA Force Field. *J. Chem. Theory Comput.* **11**, 3499–3509
215. Phillips, J. C., Braun, R., Wang, W., Gumbart, J., Tajkhorshid, E., Villa, E., Chipot, C., Skeel, R. D., Kalé, L., and Schulten, K. (2005) Scalable molecular dynamics with NAMD. *J. Comput. Chem.* **26**, 1781–1802
216. Ponder, J. W., and Case, D. A. (2003) Force Fields for Protein Simulations. in *Advances in Protein Chemistry*, pp. 27–85, **66**, 27–85
217. Du Pont, K. E., Davidson, R. B., McCullagh, M., and Geiss, B. J. (2020) Motif V regulates energy transduction between the flavivirus NS3 ATPase and RNA-binding cleft. *J. Biol. Chem.* **295**, 1551–1564

218. Henchal, E. A., and Putnak, J. R. (1990) The dengue viruses. *Clin. Microbiol. Rev.* **3**, 376–396

219. Luo, D., Xu, T., Hunke, C., Grüber, G., Vasudevan, S. G., and Lescar, J. (2008) Crystal structure of the NS3 protease-helicase from dengue virus. *J. Virol.* **82**, 173–83

220. Noueiry, A. O., Olivo, P. D., Slomczynska, U., Zhou, Y., Buscher, B., Geiss, B., Engle, M., Roth, R. M., Chung, K. M., Samuel, M., and Diamond, M. S. (2007) Identification of Novel Small-Molecule Inhibitors of West Nile Virus Infection. *J. Virol.* **81**, 11992–12004

221. Low, J. G. H., Ooi, E. E., and Vasudevan, S. G. (2017) Current Status of Dengue Therapeutics Research and Development. *J. Infect. Dis.* **215**, S96–S102

222. Brand, C., Bisaillon, M., and Geiss, B. J. (2017) Organization of the Flavivirus RNA replicase complex. *Wiley Interdiscip. Rev. RNA*. **8**, e1437

223. Heck, A. M., and Wilusz, J. (2018) The Interplay between the RNA Decay and Translation Machinery in Eukaryotes. *Cold Spring Harb. Perspect. Biol.* **10**, a032839

224. Cross, S. T., Michalski, D., Miller, M. R., and Wilusz, J. (2019) RNA regulatory processes in RNA virus biology. *Wiley Interdiscip. Rev. RNA*. 10.1002/wrna.1536

225. Byrd, A. K., and Raney, K. D. (2012) Superfamily 2 helicases. *Front. Biosci. (Landmark Ed.* **17**, 2070–88

226. Gorbalenya, A. E., and Koonin, E. V. (1993) Helicases: amino acid sequence comparisons and structure-function relationships. *Curr. Opin. Struct. Biol.* **3**, 419–429

227. Story, R. M., and Steitz, T. A. (1992) Structure of the recA protein-ADP complex. *Nature*. **355**, 374–6

228. Warrener, P., Tamura, J. K., and Collett, M. S. (1993) RNA-stimulated NTPase activity associated with yellow fever virus NS3 protein expressed in bacteria. *J. Virol.* **67**, 989–96

229. Mastrangelo, E., Bolognesi, M., and Milani, M. (2012) Flaviviral helicase: insights into the mechanism of action of a motor protein. *Biochem. Biophys. Res. Commun.* **417**, 84–7

230. Banroques, J., Cordin, O., Doere, M., Linder, P., and Tanner, N. K. (2008) A Conserved

Phenylalanine of Motif IV in Superfamily 2 Helicases Is Required for Cooperative, ATP-Dependent Binding of RNA Substrates in DEAD-Box Proteins. *Mol. Cell. Biol.* **28**, 3359–3371

231. Teramoto, T., Boonyasuppayakorn, S., Handley, M., Choi, K. H., and Padmanabhan, R. (2014) Substitution of NS5 N-terminal Domain of Dengue Virus Type 2 RNA with Type 4 Domain Caused Impaired Replication and Emergence of Adaptive Mutants with Enhanced Fitness. *J. Biol. Chem.* **289**, 22385–22400
232. Yap, T. L., Xu, T., Chen, Y.-L., Malet, H., Egloff, M.-P., Canard, B., Vasudevan, S. G., and Lescar, J. (2007) Crystal Structure of the Dengue Virus RNA-Dependent RNA Polymerase Catalytic Domain at 1.85-Angstrom Resolution. *J. Virol.* **81**, 4753–4765
233. Selisko, B., Papageorgiou, N., Ferron, F., and Canard, B. (2018) Structural and Functional Basis of the Fidelity of Nucleotide Selection by Flavivirus RNA-Dependent RNA Polymerases. *Viruses*. **10**, 59
234. Ashour, J., Laurent-Rolle, M., Shi, P.-Y., and García-Sastre, A. (2009) NS5 of dengue virus mediates STAT2 binding and degradation. *J. Virol.* **83**, 5408–18
235. Henderson, B. R., Saeedi, B. J., Campagnola, G., and Geiss, B. J. (2011) Analysis of RNA binding by the dengue virus NS5 RNA capping enzyme. *PLoS One*. **6**, e25795
236. Sweeney, N. L., Shadrick, W. R., Mukherjee, S., Li, K., Frankowski, K. J., Schoenen, F. J., and Frick, D. N. (2013) Primuline derivatives that mimic RNA to stimulate hepatitis C virus NS3 helicase-catalyzed ATP hydrolysis. *J. Biol. Chem.* **288**, 19949–19957
237. R Core Team (2014) *R: A Language and Environment for Statistical Computing*, Vienna, Austria
238. Gullberg, R. C., Jordan Steel, J., Moon, S. L., Soltani, E., and Geiss, B. J. (2015) Oxidative stress influences positive strand RNA virus genome synthesis and capping. *Virology*. **475**, 219–29
239. Hunter, J. D. (2007) Matplotlib: A 2D Graphics Environment. *Comput. Sci. Eng.* **9**, 90–95

240. Meagher, K. L., Redman, L. T., and Carlson, H. A. (2003) Development of polyphosphate parameters for use with the AMBER force field. *J. Comput. Chem.* **24**, 1016–25

241. Gowers, R., Linke, M., Barnoud, J., Reddy, T., Melo, M., Seyler, S., Domański, J., Dotson, D., Buchoux, S., Kenney, I., and Beckstein, O. (2016) MDAnalysis: A Python Package for the Rapid Analysis of Molecular Dynamics Simulations. in *Proceedings of the 15th Python in Science Conference*, pp. 98–105, 10.25080/Majora-629e541a-00e

242. Michaud-Agrawal, N., Denning, E. J., Woolf, T. B., and Beckstein, O. (2011) MDAnalysis: A toolkit for the analysis of molecular dynamics simulations. *J. Comput. Chem.* **32**, 2319–2327

243. Humphrey, W., Dalke, A., and Schulten, K. (1996) VMD: visual molecular dynamics. *J. Mol. Graph.* **14**, 33–8, 27–8

244. Du Pont, K. E., Sexton, N. R., McCullagh, M., Ebel, G. D., and Geiss, B. J. (2020) A Hyperactive Kunjin Virus NS3 Helicase Mutant Demonstrates Increased Dissemination and Mortality in Mosquitoes. *J. Virol.* **94**, e01021-20

245. Frost, M. J., Zhang, J., Edmonds, J. H., Prow, N. A., Gu, X., Davis, R., Hornitzky, C., Arzey, K. E., Finlaison, D., Hick, P., Read, A., Hobson-Peters, J., May, F. J., Doggett, S. L., Haniotis, J., Russell, R. C., Hall, R. A., Khromykh, A. A., and Kirkland, P. D. (2012) Characterization of Virulent West Nile Virus Kunjin Strain, Australia, 2011. *Emerg. Infect. Dis.* **18**, 792–800

246. Gray, T. J., Burrow, J. N., Markey, P. G., Whelan, P. I., Jackson, J., Smith, D. W., and Currie, B. J. (2011) West nile virus (Kunjin subtype) disease in the northern territory of Australia--a case of encephalitis and review of all reported cases. *Am. J. Trop. Med. Hyg.* **85**, 952–6

247. Solomon, T. (2004) Flavivirus Encephalitis. *N. Engl. J. Med.* **351**, 370–378

248. Weaver, S. C., and K, R. W. (2010) Present and Future Arboriral Threaths. *Antiviral Res.* **85**, 1–36

249. Byas, A. D., and Ebel, G. D. (2020) Comparative Pathology of West Nile Virus in Humans and Non-Human Animals. *Pathogens*. **9**, 48

250. Petersen, L. R., Carson, P. J., Biggerstaff, B. J., Custer, B., Borchardt, S. M., and Busch, M. P. (2013) Estimated cumulative incidence of West Nile virus infection in US adults, 1999-2010. *Epidemiol. Infect.* **141**, 591–5

251. Busch, M. P., Wright, D. J., Custer, B., Tobler, L. H., Stramer, S. L., Kleinman, S. H., Prince, H. E., Bianco, C., Foster, G., Petersen, L. R., Nemo, G., and Glynn, S. A. (2006) West Nile virus infections projected from blood donor screening data, United States, 2003. *Emerg. Infect. Dis.* **12**, 395–402

252. Flynn, L. M., Coelen, R. J., and Mackenzie, J. S. (1989) Kunjin Virus Isolates of Australia Are Genetically Homogeneous. *J. Gen. Virol.* **70**, 2819–2824

253. Grubaugh, N. D., and Ebel, G. D. (2016) Dynamics of West Nile virus evolution in mosquito vectors. *Curr. Opin. Virol.* **21**, 132–138

254. Scherret, J. H., Poidinger, M., Mackenzie, J. S., Broom, A. K., Deubel, V., Lipkin, W. I., Briese, T., Gould, E. A., and Hall, R. A. (2001) The Relationships between West Nile and Kunjin Viruses. *Emerg. Infect. Dis.* **7**, 697–705

255. Hall, R. A., Scherret, J. H., and Mackenzie, J. S. (2001) Kunjin virus: an Australian variant of West Nile? *Ann. N. Y. Acad. Sci.* **951**, 153–60

256. Coia, G., Parker, M. D., Speight, G., Byrne, M. E., and Westaway, E. G. (1988) Nucleotide and Complete Amino Acid Sequences of Kunjin Virus: Definitive Gene Order and Characteristics of the Virus-specified Proteins. *J. Gen. Virol.* **69**, 1–21

257. Liu, W. J., Sedlak, P. L., Kondratieva, N., and Khromykh, A. A. (2002) Complementation analysis of the flavivirus Kunjin NS3 and NS5 proteins defines the minimal regions essential for formation of a replication complex and shows a requirement of NS3 in cis for virus assembly. *J. Virol.* **76**, 10766–75

258. Neufeldt, C. J., Cortese, M., Acosta, E. G., and Bartenschlager, R. (2018) Rewiring

cellular networks by members of the Flaviviridae family. *Nat. Rev. Microbiol.* **16**, 125–142

259. Wengler, G., and Wengler, G. (1993) The NS 3 Nonstructural Protein of Flaviviruses Contains an RNA Triphosphatase Activity. *Virology*. **197**, 265–273

260. Daniel F. Gilbert, O. F. (2017) *Cell Viability Assays* (Gilbert, D. F., and Friedrich, O. eds), Methods in Molecular Biology, Springer New York, New York, NY, 10.1007/978-1-4939-6960-9

261. O'Brien, J., Wilson, I., Orton, T., and Pognan, F. (2000) Investigation of the Alamar Blue (resazurin) fluorescent dye for the assessment of mammalian cell cytotoxicity. *Eur. J. Biochem.* **267**, 5421–5426

262. Rampersad, S. N. (2012) Multiple Applications of Alamar Blue as an Indicator of Metabolic Function and Cellular Health in Cell Viability Bioassays. *Sensors*. **12**, 12347–12360

263. Kay, B. H., Fanning, I. D., and Carley, J. G. (1982) Vector competence of Culex pipiens quinquefasciatus for Murray Valley encephalitis, Kunjin, and Ross River viruses from Australia. *Am. J. Trop. Med. Hyg.* **31**, 844–848

264. Huang, H., Zhang, X., Li, S., Liu, N., Lian, W., McDowell, E., Zhou, P., Zhao, C., Guo, H., Zhang, C., Yang, C., Wen, G., Dong, X., Lu, L., Ma, N., Dong, W., Dou, Q. P., Wang, X., and Liu, J. (2010) Physiological levels of ATP negatively regulate proteasome function. *Cell Res.* **20**, 1372–85

265. Latta, M., Künstle, G., Leist, M., and Wendel, A. (2000) Metabolic Depletion of Atp by Fructose Inversely Controls Cd95- and Tumor Necrosis Factor Receptor 1–Mediated Hepatic Apoptosis. *J. Exp. Med.* **191**, 1975–1986

266. Eguchi, Y., Shimizu, S., and Tsujimoto, Y. (1997) Intracellular ATP levels determine cell death fate by apoptosis or necrosis. *Cancer Res.* **57**, 1835–40

267. Leist, M., Single, B., Castoldi, A. F., Kühnle, S., and Nicotera, P. (1997) Intracellular adenosine triphosphate (ATP) concentration: a switch in the decision between apoptosis

and necrosis. *J. Exp. Med.* **185**, 1481–6

268. Liu, J., Zheng, H., Tang, M., Ryu, Y.-C., and Wang, X. (2008) A therapeutic dose of doxorubicin activates ubiquitin-proteasome system-mediated proteolysis by acting on both the ubiquitination apparatus and proteasome. *Am. J. Physiol. Heart Circ. Physiol.* **295**, H2541-50

269. Kwong, J. Q., Henning, M. S., Starkov, A. A., and Manfredi, G. (2007) The mitochondrial respiratory chain is a modulator of apoptosis. *J. Cell Biol.* **179**, 1163–77

270. Patkar, C. G., and Kuhn, R. J. (2008) Yellow Fever Virus NS3 Plays an Essential Role in Virus Assembly Independent of Its Known Enzymatic Functions. *J. Virol.* **82**, 3342–3352

271. Samuel, G. H., Adelman, Z. N., and Myles, K. M. (2018) Antiviral Immunity and Virus-Mediated Antagonism in Disease Vector Mosquitoes. *Trends Microbiol.* **26**, 447–461

272. Rückert, C., and Ebel, G. D. (2018) How Do Virus-Mosquito Interactions Lead to Viral Emergence? *Trends Parasitol.* **34**, 310–321

273. Meola, M. A., Moudy, R. M., Morin, L.-L. L., Ebel, G. D., and Kramer, L. D. (2007) A Newly Emergent Genotype of West Nile Virus Is Transmitted Earlier and More Efficiently by Culex Mosquitoes. *Am. J. Trop. Med. Hyg.* **77**, 365–370

274. Robison, A., Young, M. C., Byas, A. D., Rückert, C., and Ebel, G. D. (2020) Comparison of Chikungunya Virus and Zika Virus Replication and Transmission Dynamics in Aedes aegypti Mosquitoes. *Am. J. Trop. Med. Hyg.* 10.4269/ajtmh.20-0143

275. Wang, H., Gort, T., Boyle, D. L., and Clem, R. J. (2012) Effects of Manipulating Apoptosis on Sindbis Virus Infection of Aedes aegypti Mosquitoes. *J. Virol.* **86**, 6546–6554

276. Kelly, E. M., Moon, D. C., and Bowers, D. F. (2012) Apoptosis in mosquito salivary glands: Sindbis virus-associated and tissue homeostasis. *J. Gen. Virol.* **93**, 2419–2424

277. Liu, Q., and Clem, R. J. (2011) Defining the core apoptosis pathway in the mosquito disease vector Aedes aegypti: the roles of iap1, ark, dronc, and effector caspases. *Apoptosis*. **16**, 105–113

278. O'Neill, K., Olson, B. J. S. C., Huang, N., Unis, D., and Clem, R. J. (2015) Rapid selection against arbovirus-induced apoptosis during infection of a mosquito vector. *Proc. Natl. Acad. Sci. U. S. A.* **112**, E1152-61

279. Khromykh, A. A., and Westaway, E. G. (1994) Completion of Kunjin virus RNA sequence and recovery of an infectious RNA transcribed from stably cloned full-length cDNA. *J. Virol.* **68**, 4580–8

280. Khromykh, A. A., Sedlak, P. L., Guyatt, K. J., Hall, R. A., and Westaway, E. G. (1999) Efficient trans-complementation of the flavivirus kunjin NS5 protein but not of the NS1 protein requires its coexpression with other components of the viral replicase. *J. Virol.* **73**, 10272–80

281. Ciota, A. T., Chin, P. A., and Kramer, L. D. (2013) The effect of hybridization of Culex pipiens complex mosquitoes on transmission of West Nile virus. *Parasit. Vectors*. **6**, 305

282. Weger-Lucarelli, J., Duggal, N. K., Bullard-Feibelman, K., Veselinovic, M., Romo, H., Nguyen, C., Rückert, C., Brault, A. C., Bowen, R. A., Stenglein, M., Geiss, B. J., and Ebel, G. D. (2017) Development and Characterization of Recombinant Virus Generated from a New World Zika Virus Infectious Clone. *J. Virol.* **91**, e01765-16

283. Garcia-Luna, S. M., Weger-Lucarelli, J., Rückert, C., Murrieta, R. A., Young, M. C., Byas, A. D., Fauver, J. R., Perera, R., Flores-Suarez, A. E., Ponce-Garcia, G., Rodriguez, A. D., Ebel, G. D., and Black, W. C. (2018) Variation in competence for ZIKV transmission by Aedes aegypti and Aedes albopictus in Mexico. *PLoS Negl. Trop. Dis.* **12**, e0006599

284. Wu, B., Buxbaum, A. R., Katz, Z. B., Yoon, Y. J., and Singer, R. H. (2015) Quantifying Protein-mRNA Interactions in Single Live Cells. *Cell*. **162**, 211–220

APPENDIX A – CHAPTER 3 SUPPLEMENTAL INFORMATION

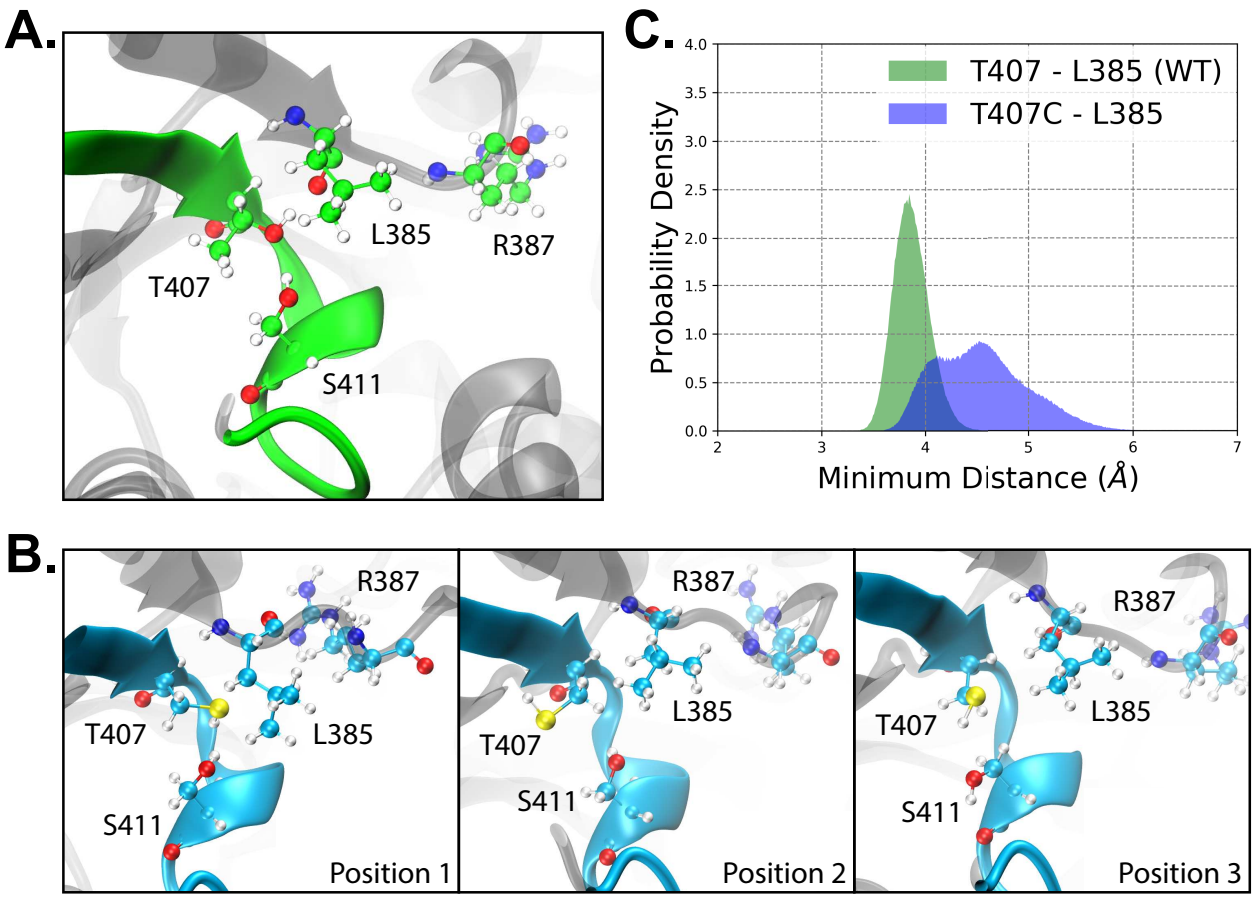

Figure A.1. Methyl group in the T407 sidechain stabilizes T407 interactions with L385. A) The methyl group stabilizes the structure of T407 in the WT simulations. B) Without the methyl group, the sulfur group of T407C fluctuates frequently throughout the T407C simulations. C) The minimum distance was calculated between the L387 sidechain and either the hydroxyl group (threonine sidechain) or the thiol group (cysteine sidechain) at position 407 for each replicate of the WT and the T407C simulations. The probability density of the average minimum distance was then determined for WT and T407C simulations.

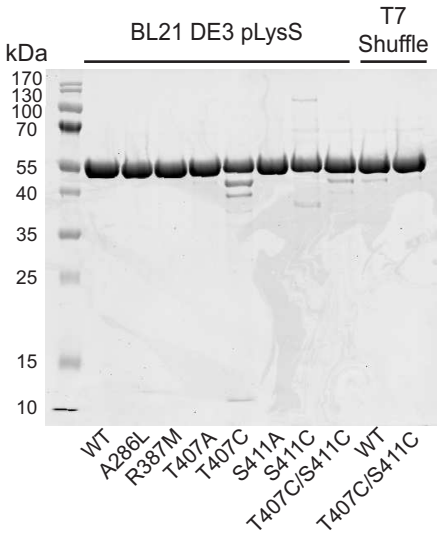

Figure A.2. Confirmation purified NS3 helicase variants. Recombinant NS3 helicase variants were purified and confirmed on SDS-PAGE. We noted that T407C degraded over time but it was full-length when used in assays.

Table A.1. Flavivirus sequence variability at positions 404, 405, 406, 407, and 411. Flavivirus sequences were analyzed to determine the consensus sequence at motif V positions 404, 405, 406, 407, and 411. The percentage of finding the consensus or another residue instead of the consensus are reported for each position for each flavivirus.

Virus	Number of Sequences	404 Consensus	F404(%)	Y404(%)	L404(%)	405 Consensus	V405(%)	L405(%)	I405(%)	406 Consensus	V406(%)	D406(%)	G406(%)	I406(%)	L406(%)	407 Consensus	T407(%)	A407(%)	S407(%)	411 Consensus	S411(%)	A411(%)
Karshi Virus	1	**F**	100.0	-	-	**V**	100.0	-	-	**V**	100.0	-	-	-	-	**T**	100.0	-	-	**S**	100.0	-
Powassan	22	**F**	100.0	-	-	**V**	100.0	-	-	**V**	100.0	-	-	-	-	**T**	100.0	-	-	**S**	100.0	-
MMLV	3	**F**	100.0	-	-	**I**	-	-	100.0	**L**	-	-	-	-	100.0	**T**	100.0	-	-	**S**	100.0	-
Rio Bravo	3	**F**	100.0	-	-	**I**	-	-	100.0	**L**	-	-	-	-	100.0	**T**	100.0	-	-	**S**	100.0	-
Modoc	3	**F**	100.0	-	-	**I**	-	-	100.0	**L**	-	-	-	-	100.0	**T**	100.0	-	-	**S**	100.0	-
Apoi	2	**F**	100.0	-	-	**I**	-	-	100.0	**L**	-	-	-	-	100.0	**T**	100.0	-	-	**S**	100.0	-
JEV	321	**F**	100.0	-	-	**V**	100.0	-	-	**I**	0.9	-	-	99.1	-	**T**	100.0	-	-	**S**	100.0	-
Usutu	138	**F**	100.0	-	-	**V**	100.0	-	-	**I**	0.7	-	-	99.3	-	**T**	100.0	-	-	**S**	100.0	-
WNV	2008	**F**	100.0	-	-	**V**	100.0	-	-	**I**	0.6	-	-	99.4	-	**T**	100.0	-	-	**S**	100.0	-
Kunjin	44	**F**	100.0	-	-	**V**	100.0	-	-	**V**	100.0	-	-	-	-	**T**	100.0	-	-	**S**	100.0	-
Bagaza	12	**F**	100.0	-	-	**V**	100.0	-	-	**I**	-	-	-	100.0	-	**T**	100.0	-	-	**S**	100.0	-
Ilheus	1	**F**	100.0	-	-	**V**	100.0	-	-	**I**	-	-	-	100.0	-	**T**	100.0	-	-	**S**	100.0	-
Kedougou	1	**F**	100.0	-	-	**V**	100.0	-	-	**I**	-	-	-	100.0	-	**T**	100.0	-	-	**S**	100.0	-
Zika	659	**F**	100.0	-	-	**V**	100.0	-	-	**I**	85.6	-	-	14.4	-	**T**	100.0	-	-	**S**	100.0	-
Bussuquara	1	**F**	100.0	-	-	**V**	100.0	-	-	**V**	100.0	-	-	-	-	**T**	100.0	-	-	**S**	100.0	-
DENV1	1948	**Y**	0.1	99.9	-	**V**	100.0	-	-	**V**	99.9	-	0.1	-	-	**T**	100.0	-	-	**S**	100.0	-
DENV2	1524	**F**	100.0	-	-	**V**	100.0	-	-	**V**	99.8	0.1	-	0.1	-	**T**	100.0	-	-	**S**	100.0	-
DENV3	1112	**F**	100.0	-	-	**V**	99.9	0.1	-	**V**	99.9	-	0.1	-	-	**T**	99.8	0.2	-	**S**	100.0	-
DENV4	241	**F**	100.0	-	-	**V**	100.0	-	-	**V**	100.0	-	-	-	-	**T**	100.0	-	-	**S**	100.0	-
Kokobera	1	**F**	100.0	-	-	**V**	100.0	-	-	**I**	-	-	-	100.0	-	**T**	100.0	-	-	**S**	100.0	-
YFV	105	**F**	100.0	-	-	**I**	-	-	100.0	**L**	-	-	-	-	100.0	**A**	-	100.0	-	**A**	-	100.0
Sepik	1	**F**	100.0	-	-	**I**	-	-	100.0	**L**	-	-	-	-	100.0	**A**	-	100.0	-	**A**	-	100.0
Entebbe Bat	1	**F**	100.0	-	-	**I**	-	-	100.0	**L**	-	-	-	-	100.0	**T**	100.0	-	-	**A**	-	100.0
Cell fusing agent	35	**L**	-	-	100.0	**V**	100.0	-	-	**I**	-	-	-	100.0	-	**S**	-	-	100.0	**S**	100.0	-
Kamiti River	2	**L**	-	-	100.0	**V**	100.0	-	-	**V**	100.0	-	-	-	-	**S**	-	-	100.0	**S**	100.0	-
Culex	32	**F**	100.0	-	-	**I**	-	-	100.0	**V**	100.0	-	-	-	-	**S**	-	-	100.0	**S**	100.0	-

Table A.2. ATP substrate inhibition of ATPase activity. The ATPase activity exhibited substrate inhibition at high concentrations of ATP. As a result of substrate inhibition, the data was fit to the substrate inhibition equation. The inhibition constant (K_i) was reported for each NS3 helicase variant.

Substrate Inhibition of ATPase Activity

NS3h variant	K_i (μM)
WT	888.2 ± 247.7
A286L	570.5 ± 377.4
R387M	745.7 ± 371.1
T407A	1442.1 ± 727.5
T407C	587.6 ± 177.8
S411A	695.5 ± 404.4
S411C	775.8 ± 166.9
T407C/S411C	1157.8 ± 480.1
WT reduced†	534.3 ± 110.5
WT oxidized‡	297.3 ± 133.0
T407C/S411C reduced†	729.0 ± 148.4
T407C/S411C oxidized‡	532.7 ± 137.3